TARGETED DELIVERY OF DASATINIB FOR ACCELERATED BONE FRACTURE REPAIR

by

Mingding Wang

A Dissertation

Submitted to the Faculty of Purdue University

In Partial Fulfillment of the Requirements for the degree of

Doctor of Philosophy

Department of Chemistry

West Lafayette, Indiana

May 2019

THE PURDUE UNIVERSITY GRADUATE SCHOOL
STATEMENT OF COMMITTEE APPROVAL

Dr. Philip S. Low, Chair
Department of Chemistry
Dr. Mingji Dai
Department of Chemistry
Dr. Chengde Mao
Department of Chemistry
Dr. Christopher Uyeda
Department of Chemistry

Approved by:

Dr. Christine Hrycyna
Head of the Graduate Program

In dedication to my parents, for their unconditional love, support, and belief through the highs and lows.

ACKNOWLEDGMENTS

First and foremost, I would like to dedicate my most sincere gratitude to my research advisor, Dr. Philip Low. All of my accomplishments in Purdue, including the doctorate I am finally obtaining, would not have been possible without Dr. Low's continuous guidance, patience, and support. I have learned from him not specific techniques for specific tasks, but the way to think critically, logically, and creatively when facing any problems. This intellectual habit is certainly going to benefit me for the rest of my entire career. Also, I would like to thank my committee members Dr. Mingji Dai and Dr. Chengde Mao, for their invaluable help and advice on both my studies and my career.

And of course, I am particularly grateful to my parents and family for their unconditional love and support, and their understanding when I have been unable to go home for more than five years. I want to say thank you to my girlfriend Danyang Chen, for all of your support, encouragement, and company over the years. I would not have joined the Low lab without you, and I would not have graduated from the Low lab without you.

Last but not least, I would like to acknowledge my fellow lab members for being not only colleagues but friends, and for their selfless help and company throughout my Ph.D. years. I want to thank Dr. Chris Galliford for sharing with me his expertise in organic synthesis, sharp scientific instincts, and awkward British TV shows. Many thanks to Xin Liu, Weichuan Luo, Boning Zhang, Dr. Jyoti Roy, and Dr. Mark Li for turning the lab into a family where I can find company and warmth. Thanks to Dr. Qingshou Chen, Dr. Pengcheng Lv, Dr. Guo Li, Dr. Isaac Marks, Dr. Yong Gu Lee, Dr. Yingwen Hu, Estela Puchulu-Campanella, Dr. Madduri Srinivasarao, Dr. Suilan Zheng, Dr. Bingbing Wang, Dr. Ian Wang, and Dr. Daniel Sheik for always being by my side when I needed their

assistance. I would like to give my special thanks to bone group members Dr. Stewart Low and Jeff Nielsen, whose expertise in bone biology and dedication to the bone project have always inspired and motivated me to do better. I want to thank Patti Cauble for her tireless work to make sure everything, big or small, goes smoothly in the lab. I would not even want to imagine what the lab would be like without her! I would also like to share my gratitude to Pam Lachnik for her precious help with the microCT facility, and to Karson Putt for his ultra-valuable professional opinions and unrivaled sarcasm.

TABLE OF CONTENTS

LIST OF FIGURES 11
LIST OF ABBREVIATIONS 14
ABSTRACT 16
CHAPTER 1. INTRODUCTION 18
1.1 Physiology of Bone 18
1.1.1 Bone Composition and Organization 18
1.1.2 Cells Involved in Bone Homeostasis 19
1.1.2.1 Osteoblasts 20
1.1.2.2 Osteoclasts 22
1.1.2.3 Osteocytes 23
1.1.3 Bone Problems and Pathologies 24
1.2 Bone Fracture Repair 25
1.2.1 Types of Bone Fracture 25
1.2.2 Natural Process of Fracture Repair 25
1.2.3 Need for Improvements in the Treatment of Bone Fractures 26
1.2.3.1 Problems with Antiresorptive Drugs 27
1.2.3.2 Problems with Derivatives of Parathyroid Hormone 28
1.2.3.3 Problems with BMPs 28
1.3 The Role of Src Kinase in Bone Metabolism 29
1.4 Targeted Delivery of Bone-Anabolic Agents to Accelerate Fracture Repair 30
1.4.1 Leading Drugs to the Right Places: Targeted Drug Delivery 30
1.4.2 Bone-Fracture-Specific Targeting Ligands 30
1.5 Summary of Our Hypothesis 33
1.6 References 34
CHAPTER 2. IN VITRO EVALUATION OF THE EFFECT OF DASATINIB TREATMENT ON OSTEOBLASTS 43
2.1 Introduction 43
2.1.1 The Effect of Src Inhibition on Bone Cells 43
2.1.2 Dasatinib, a Potent Src Inhibitor 43

2.1.3 Genes Selected for the Evaluation of Dasatinib's Effects on Osteoblasts .. 44
2.2 Materials and Methods 45
2.2.1 Culture of a Murine Pre-Osteoblastic Cell Line, MC3T3-E1 45
2.2.2 Real-Time Quantitative PCR 46
2.2.3 Quantitation of Alkaline Phosphatase Activity 47
2.3 Results 47
2.3.1 Expression of Osteogenesis-Related Genes in Response to Dasatinib Treatment 47
2.4 Discussion 50
2.5 References 52
CHAPTER 3. SYNTHESIS AND CHARACTERIZATION OF THE DASATINIB-ASPARTIC$_{10}$ CONJUGATE (DAC) AND ASPARTIC$_{10}$-S0456 DYE CONJUGATE .. 55
3.1 Introduction 55
3.2 Materials and Methods 56
3.2.1 Materials 56
3.2.2 Synthesis of D$_{10}$-Cys 56
3.2.3 Synthesis of 2-(4-(6-((5-((2-chloro-6-methylphenyl)carbamoyl)thiazol-2-yl)amino)-2-methylpyrimidin-4-yl)piperazin-1-yl)ethyl 3-(2,5-dioxo-2,5-dihydro-1H-pyrrol-1-yl)propanoate (Dasatinib-Maleimide) 58
3.2.4 Synthesis of Dasatinib-Aspartic$_{10}$ Conjugate (DAC) 59
3.2.5 Synthesis of S0456-Maleimide 60
3.2.6 Synthesis of D$_{10}$-S0456 Conjugate 61
3.3 Characterization of Intermediates and Products 62
3.3.1 Mass Spectrometry 62
3.3.2 HPLC Chromatograms 63
3.4 Discussion 64
3.4.1 Synthesis of DAC 64
3.4.2 Synthesis of D$_{10}$-S0456 Dye Conjugate 64
3.5 References 65

CHAPTER 4. IN VIVO EVALUATION OF THE BONE-FRACTURE TARGETING CAPABILITY OF ASPARTIC$_{10}$ AND DAC'S EFFICACY FOR THE ACCELERATION OF BONE-FRACTURE REPAIR 66
4.1 Introduction 66
4.2 Materials and Methods 67
4.2.1 Animal Husbandry and Femoral Fracture Induction 67
4.2.2 Drug Formulation and Injection Schedule 68
4.2.3 Microcomputed Tomography 68
4.2.4 Four-Point Bending Test 69
4.2.5 Quantification of Aspartic$_{10}$-S0456 Conjugate in Bone 70
4.2.6 Statistical Analyses 70
4.3 Results 71
4.3.1 Fracture-Specificity of Aspartic$_{10}$-S0456 Dye Conjugate 71
4.3.2 Fracture-Healing Efficacy of DAC With Daily Dosage 72
4.3.3 Fracture-Healing Efficacy of DAC With Dosage at Lower Dosing Frequencies 73
4.3.3.1 Bone Properties at the Fracture Site 74
4.3.3.2 Mouse Body Weight Change 75
4.3.4 The Time Course of DAC-Stimulated Bone Fracture Healing 75
4.3.4.1 Bone Density at the Fracture Callus and Mechanical Strength of the Healed Femurs 77
4.3.4.2 Mouse Body Weight Change 79
4.3.4.3 Analysis of Healthy Contralateral Femurs 79
4.4 Discussion 80
4.5 References 84
CHAPTER 5. FURTHER OPTIMIZATION OF THE DOSING SCHEDULE OF DAC 87
5.1 Introduction 87
5.1.1 DAC's Proposed Function at Different Stages of Fracture Repair 87
5.1.2 Tweaking the Drug Release Rate and Retention Kinetics of DAC at Fracture Site 89

5.2 Materials and Methods 90
5.2.1 Materials 90
5.2.2 Synthesis of Dasatinib Protected Ester Slow-Release Conjugate (MW0346) 90
5.2.3 Synthesis of D-Aspartic$_{10}$-S0456 Conjugate 91
5.2.4 Synthesis of D-Aspartic$_{10}$-Dasatinib Conjugate 93
5.2.5 Kinetics of Conjugate Hydrolysis and Drug Release 93
5.2.6 Drug Formulation and Injection Schedule 94
5.3 Results 95
5.3.1 Optimizing the Dosing Schedule for DAC 95
5.3.1.1 Choosing the Best Dosage Starting Point 95
5.3.1.2 Increasing Dosage with Different Dosing Schedules 97
5.3.1.3 Selection of the Optimal Dosing Window 100
5.3.2 Hydrolysis and Retention Kinetics of DAC and Slow-Release Conjugate 102
5.3.2.1 Hydrolysis Kinetics of DAC at Different pHs 102
5.3.2.2 Hydrolysis Kinetics of DAC at pH 7 in the Presence of Hydroxyapatite 104
5.3.2.3 Hydrolysis Kinetics of Slow-Release Conjugate MW0346 at pH 7 105
5.3.3 Retention Kinetics of L- and D-Aspartic$_{10}$ at the Fracture Site 106
5.3.4 In Vivo Evaluation of Slow-Release Conjugate MW0346 and DD$_{10}$-Dasatinib Conjugates 108
5.3.4.1 Fracture-Repair Efficacy of MW0346 Conjugate 109
5.3.4.2 Fracture-Repair Efficacy of DD$_{10}$-Dasatinib Conjugate 111
5.4 Discussion 112
5.5 References 115
CHAPTER 6. IN VITRO AND IN VIVO EVALUATION OF OTHER SMALL MOLECULES TO FACILITATE FRACTURE REPAIR 118
6.1 Introduction 118
6.1.1 Src Kinase Inhibitor E738 118
6.1.2 GSK-3β Inhibitors 119

6.1.3 Small Molecules that Stimulate Sphingosine-1-Phosphate Receptor 1 (S1PR1) 121
6.2 Materials and Methods 122
6.2.1 Materials 122
6.2.2 Synthesis of MW0260 and D_{10}-MW0260 Conjugate 123
6.2.3 Synthesis of D_{10}-E738 Conjugate 125
6.2.4 Synthesis of D_{10}-DOP Conjugate 127
6.2.5 Synthesis of D_{10}-Ozanimod Conjugate 128
6.3 Results 129
6.3.1 Bone-Fracture-Healing Efficacy of GSK-3β Inhibitors CHIR-98014 and MW0260 129
6.3.1.1 Effect of CHIR-98014 Treatment on MC3T3-E1 Cells 129
6.3.1.2 In Vivo Evaluation of D_{10}-MW0260 Conjugate 130
6.3.2 Bone-Fracture-Healing Efficacy of Src Kinase Inhibitor E738 131
6.3.2.1 Effect of E738 Treatment on MC3T3-E1 Cells 131
6.3.2.2 In Vivo Evaluation of D_{10}-E738 Conjugate 133
6.3.3 Bone-Fracture-Healing Efficacy of S1PR1-Stimulating Agents 134
6.3.3.1 Effect of Ozanimod (S1PR1 Agonist) Treatment on MC3T3-E1 Cells 135
6.3.3.2 In Vivo Evaluation of D_{10}-Ozanimod Conjugate 136
6.3.3.3 In Vivo Evaluation of D_{10}-DOP Conjugate (S1P Lyase Inhibitor) 137
6.4 Discussion 138
6.5 References 141
CHAPTER 7. CONCLUSIONS AND FUTURE DIRECTIONS 145
7.1 Conclusions 145
7.2 Future Directions 147
7.3 References 149
VITA 151
PUBLICATION 152

LIST OF FIGURES

Fig. 1.1 Structure and Organization of Long Bone. 19

Fig. 1.2 Depiction of Osteoblasts and Osteocytes. 20

Fig. 1.3 Depiction of an Osteoclast. 22

Fig. 1.4 The Four Stages of Fracture Repair. 26

Fig. 1.5 SPECT/CT Image of Fracture-Bearing Mice Receiving Free (Left) or Targeted (Right) Versions of ^{125}I-6BIO. 32

Fig. 2.1 Dasatinib Stimulates Expression of Multiple Osteogenic Genes. 48

Fig. 3.1 Synthesis for DAC. 58

Fig. 3.2 Synthesis of D_{10}-S0456 Conjugate. 60

Fig. 3.3 HPLC Chromatogram for DAC. 63

Fig. 3.4 HPLC Chromatogram for D_{10}-S0456 Conjugate. 63

Fig. 4.1 Quantification of D_{10}-S0456 in Fracture-Bearing Mice. 71

Fig. 4.2 DAC Increases Bone Density and Volume While Reducing Trabecular Spacing at the Fracture Site. 72

Fig. 4.3 DAC Stimulates Bone Growth at Lower Dosing Frequencies. 74

Fig. 4.4 Efficacy of DAC Declines as Dosing Frequency Lowers. 75

Fig. 4.5 DAC Accelerates Fracture Repair and Return to Normal Mechanical Strength. 76

Fig. 4.6 DAC Accelerates Return to Normal Mechanical Strength. 77

Fig. 4.7 DAC Accelerates Fracture Repair and Return to Normal Morphology. 78

Fig. 4.8 DAC Causes No Detectable Changes in Healthy Contralateral Femurs. 80

Fig. 5.1 Synthesis of Dasatinib Protected Ester Slow-Release Conjugate (MW0346). ... 90

Fig. 5.2 Synthesis of DD_{10}-S0456. 92

Fig. 5.3 Synthesis of D-D_{10}-Dasatinib. 93

Fig. 5.4 Determining the Optimal Dosing Starting Point for DAC. 95

Fig. 5.5 Fracture Callus Comparison Between Doses During Week 2 and Week 3..... 96

Fig. 5.6 High Dosage with Q.A.D. Dosing Schedule Induces Toxicity. 98

Fig. 5.7 High Dosage with W3 Dosing Schedule Retains Efficacy and Circumvents Toxicity. 98

Fig. 5.8 Finding the Optimal Dosing Window of DAC..... 100

Fig. 5.9 DAC Hydrolysis Curves at pH 7 and pH 4. 103

Fig. 5.10 DAC Absorption and Hydrolysis Curves at pH 7 with HAp. 104

Fig. 5.11 Slow Release Conjugate MW0346 Degrades Slower at pH 7..... 105

Fig. 5.12 DD_{10} Remains Undamaged at the Fracture Site Longer Than D_{10}..... 107

Fig. 5.13 Slow-Release Conjugate MW0346 Increases Bone Density and Volume in Mice. 109

Fig. 5.14 Comparison of Bone Density and Bone Volume Between MW0346 and DAC with Different Dosing Schedules. 110

Fig. 5.15 DD_{10}-Dasatinib Conjugate Failed to Accelerate Fracture Healing. 112

Fig. 6.1 Structures of Indirubin Derivative Src Inhibitors E804 and E738. 119

Fig. 6.2 Phosphorylation by GSK3 Marks β-Catenin for Degradation Via Proteolysis. 120

Fig. 6.3 The Role of S1PR1 and S1PR2 in Osteoblast Precursors and Osteoblasts. 121

Fig. 6.4 Synthesis of MW0260. 124

Fig. 6.5 Synthesis of D_{10}-MW0260 Conjugate. 125

Fig. 6.6 Synthesis of D_{10}-MW0260 Conjugate. 126

Fig. 6.7 Synthesis of D_{10}-DOP Conjugate. 127

Fig. 6.8 Synthesis of D_{10}-Ozanimod Conjugate..... 128

Fig. 6.9 GSK-3β Inhibitor CHIR-98014 Stimulates ALP Activity. 129

Fig. 6.10 D_{10}-MW0260 Conjugate Did Not Promote Bone Fracture Repair in Vivo. ... 130

Fig. 6.11 E738 Treatment Upregulates Multiple Osteogenic Genes *in Vitro*. 131

Fig. 6.12 E738 Treatment Promotes ALP Activity in Mouse Osteoblasts. 132

Fig. 6.13 D_{10}-E738 Conjugate Increases Callus Density and Bone Volume. 134

Fig. 6.14 Ozanimod Promotes ALP Activity in Mouse Osteoblasts. 135

Fig. 6.15 D_{10}-Ozanimod Moderately Accelerate Bone Fracture Repair in Vivo. 136

Fig. 6.16 D_{10}-DOP Accelerates Bone Fracture Repair. 138

LIST OF ABBREVIATIONS

6BIO	6-Bromoindirubin oxime
Ac_2O	Acetic anhydride
$AlCl_3$	Aluminum chloride
ALP	Alkaline phosphatase
BTK	Bruton's tyrosine kinase
CML	Chronic myeloid leukemia
Col1A1	Type-I collagen alpha 1
DCM	Dichlorormethane
DIPEA	Diisopropylethylamine
DMAP	4-Dimethylaminopyridine
DMF	Dimethylformamide
DMSO	Dimethyl sulfoxide
DOP	4-Deoxypyridoxine
EDT	Ethanedithiol
EDTA	ethylenediaminetetraacetic acid
Et_2O	Dimethyl ether
EtOAc	Ethyl acetate
Fmoc	Fluorenylmethoxycarbonyl
GAPDH	Glyceraldehyde 3-phosphate dehydrogenase
GSK-3β	Glycogen Synthase Kinase 3β
HAp	Hydroxyapatite
HI-FBS	Heat-inactivated fetal bovine serum
HPLC	High-performance liquid chromatography
IC_{50}	Half maximal inhibitory concentration
MeI	Methyl iodide
MeOH	Methanol
NaH	Sodium hydride
NMR	Nuclear magnetic resonance

OPG	Osteoprotegerin
OPN	Osteopontin
Osx	Osterix
PBS	Phosphate-buffered saline
PDGFR	Platelet-derived growth factor receptor
PyBOP	Benzotriazol-1-yl-oxytripyrrolidinophosphonium hexafluorophosphate
Q.A.D.	Every other day
RANK	Receptor activator of nuclear factor κB
S1PR1	Sphingosine-1-Phosphate Receptor 1
SPPS	Solid-phase peptide synthesis
TBAF	Tetrabutylammonium fluoride
TBDPSCl	tert-Butyl(chloro)diphenylsilane
TEA	Triethylamine
TFA	Trifluoroacetic acid
THF	Tetrahydrofuran
TIPS	Triisopropylsilane
TMG	Tetramethylguanidine

ABSTRACT

Author: Wang, Mingding. PhD
Institution: Purdue University
Degree Received: May 2019
Title: Targeted Delivery of Dasatinib for Accelerated Bone Fracture Healing.
Committee Chair: Philip S. Low

Approximately 6.3 million bone fractures occur annually in the USA, resulting in considerable morbidity, deterioration in quality of life, loss of productivity and wages, and sometimes death (e.g. hip fractures). Although anabolic and antiresorptive agents have been introduced for treatment of osteoporosis, no systemically-administered drug has been developed to accelerate the fracture healing process. To address this need, we have undertaken to target a bone anabolic agent selectively to fracture surfaces in order to concentrate the drug's healing power directly on the fracture site. We report here that conjugation of dasatinib to a bone fracture-homing oligopeptide via a releasable linker reduces fractured femur healing times in mice by ~60% without causing overt off-target toxicity or remodeling of nontraumatized bones. Thus, achievement of healthy bone density, normal bone volume, and healthy bone mechanical properties at the fracture site is realized after only 3-4 weeks in dasatinib-targeted mice, but requires ~8 weeks in PBS-treated controls. Moreover, optimizations have been implemented to the dosing regimen and releasing mechanisms of this targeted-dasatinib therapy, which has enabled us to cut the total doses by half, reduce the risk of premature release in circulation, and still improve upon the therapeutic efficacy. These efforts might reduce the burden associated with frequent doses on patients with broken bones and lower potential toxicity brought by drug degradation in the blood stream. In addition to dasatinib, a few other small molecules have also been targeted to fracture surfaces and identified as prospective therapeutic agents for

the acceleration of fracture repair. In conclusion, in this dissertation, we have successfully targeted dasatinib to bone fracture surfaces, which can significantly accelerate the healing process at dasatinib concentrations that are known to be safe in oncological applications. A modular synthetic method has also been developed to allow for easy conversion of a bone-anabolic warhead into a fracture-targeted version for improved fracture repair.

CHAPTER 1. INTRODUCTION

1.1 Physiology of Bone

1.1.1 Bone Composition and Organization

Bone is one of the most important and versatile organs in the human body. Beside its primary function of providing mechanical support and protection, bone also plays essential roles in mineral homeostasis and hematopoiesis.[1] Bone is not a dead stick of mineral; instead, it is a highly dynamic organ undergoing catabolism and anabolism constantly, with multiple highly-differentiated cell types performing various physiological functions. The adult bone consists of 50-70% mineral, 20-40% organic matrix, 5-10% water and 1-5% lipids.[2] About 90% of the organic matrix is made up of type I collagen, with the remaining 10% being noncollagenous proteins. During bone formation, collagen is first deposited in a highly organized manner with heavy cross-linkage, followed by the formation of bone mineral within the collagen network.[1] The major mineral component of the bone is hydroxyapatite (HAp) with a chemical formula of $Ca_{10}(PO_4)_6(OH)_2$, which is regularly broken down and freshly deposited.

Macroscopically, bone is organized in two distinct forms: cortical bone and cancellous bone (Fig. 1.1). Cortical bone is dense and compact, delivering the majority of structural support and protection; on the other hand, cancellous bone is porous, composing of small plates and rods of bone (trabecular bone) that take up only 25-30% of its total tissue volume.[1] Cortical bone forms most of the shafts and diaphyses of long bones, while trabecular bone is primarily located in the metaphyses of bone and mineralized fracture calluses.[1,3] Trabecular bone still provides crucial mechanical support, especially in a fracture callus (see Section 1.2.2). The mechanical properties of cancellous bone is highly

dependent on the density, interconnectivity, and thickness of trabeculae that it is comprised of.[1,2] A membrane called periosteum covers the outside of the bone, and the hollow cavity inside the bone (intramedullary cavity) is filled with bone marrow, endowing the bone with the capacity to influence hematopoietic homeostasis.

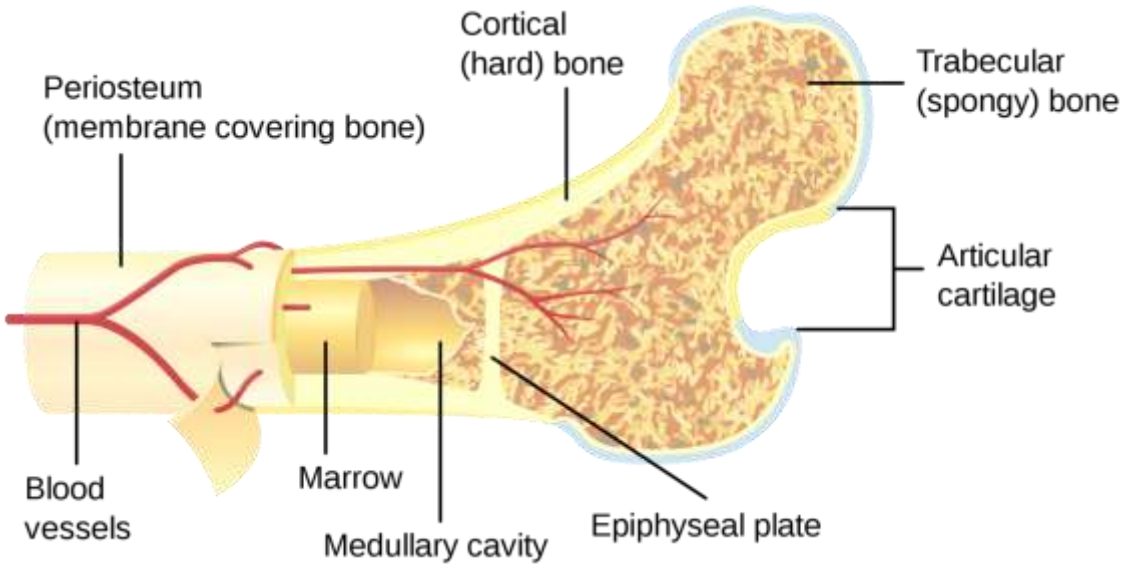

Fig. 1.1 Structure and Organization of Long Bone.
Diagram originally created by Pbroks13 [CC BY 3.0 (https://creativecommons.org/licenses/by/3.0)] and modified for use.

1.1.2 Cells Involved in Bone Homeostasis

Physiological functions of bone, including its anabolic and catabolic activities, response to mechanical loading, and mineral homeostasis, rely on bone cells. There are three major types of bone cells: osteoclasts, osteoblasts, and osteocyte, all of which contribute to bone metabolism highly specifically. In the attempt to alter the homeostasis of bone (e.g. to accelerate the rate of fracture healing), understanding and manipulating the physiological functions of those cells is essential, making them important targets for therapeutics agents.

1.1.2.1 Osteoblasts

Being the only cell that synthesizes and deposits newly-formed bone, osteoblasts are one of the most important bone cells.[4] Osteoblasts are highly-differentiated, single-nucleated cells of the mesenchymal lineage that are capable of producing crosslinked networks of collagen (majorly type I) and other noncollagenous proteins such as osteopontin to form a highly organized organic matrix of bone, namely osteoid.[14–195] Subsequently, HAp is produced by osteoblasts and deposited into the osteoid to form mineralized bone tissue.[4]

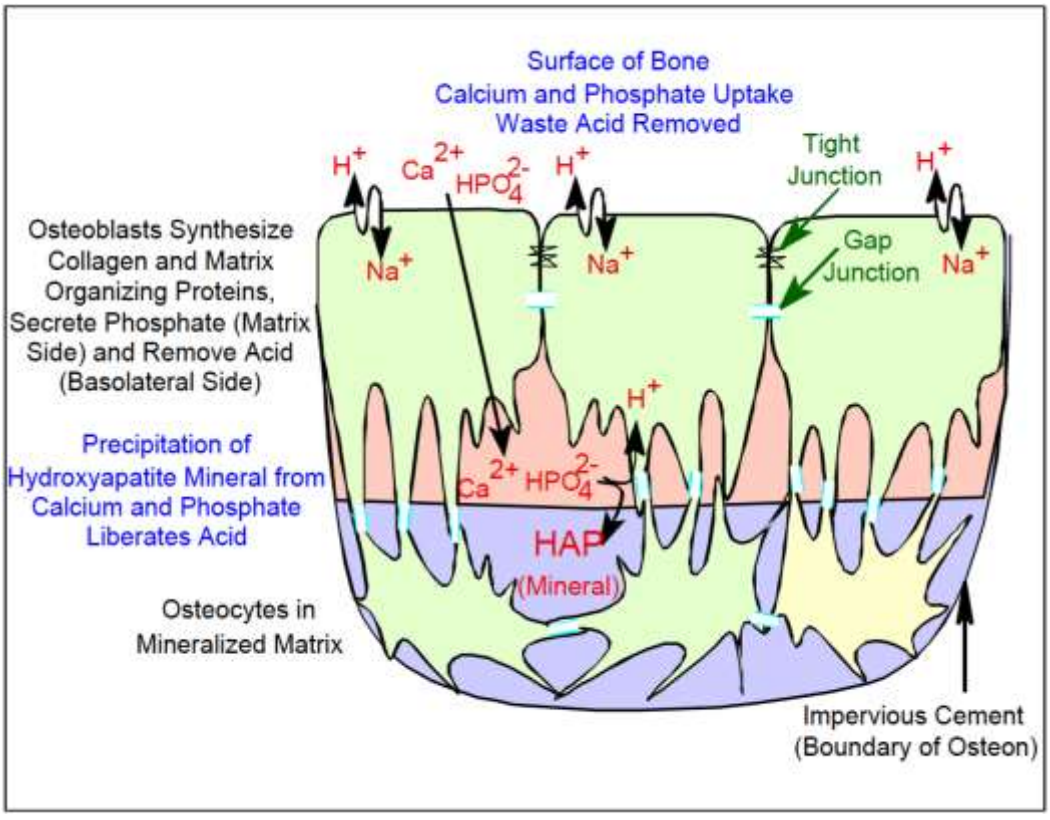

Fig. 1.2 Depiction of Osteoblasts and Osteocytes.
Diagram originally created by Physio Muse [CC BY-SA 3.0 (https://creativecommons.org/licenses/by-sa/3.0/)] and modified for use.

Bone morphogenetic proteins (BMPs) and Wnts activate the two major pathways that promote osteoblast differentiation.[6] The binding of BMPs to type I and type II BMP receptors triggers the BMP signaling pathway and activates Smad transcription factors 1, 5, and 8, which would enter the osteoblast nucleus after forming complexes with Smad4. This complex promotes the transcription of key factors such as RUNX2 and Osx as well as various osteoblastogenesis genes, which in turn stimulates the proliferation and differentiation of osteoblasts.[7–10] The bone-anabolic efficacy of BMPs has drawn forth two FDA-approved drugs for fracture repair: BMP-2 (Infuse®, Medtronic) and BMP-7 (OP-1®, Stryker Biotech), both of which are locally- and surgically-applied therapeutics for long bone fractures.[11–13]

The Wnt pathway has been known to play important roles in cell proliferation, differentiation, and apoptosis in many tissues.[14,15] Binding of Wnts to the frizzled (FZD) family receptors or low-density lipoprotein receptor protein 5/6 (LRP5/6) activates the Wnt signaling pathway, leading to the accumulation of β-catenin in the cytoplasm, which would later translocate into the nucleus. β-catenin stimulates Tcf/LEF-mediated transcription in the nucleus, which leads to proliferation, differentiation, and survival of osteoblasts.[15–17] Given the central role that Wnt pathway plays in osteoblast function, it is not surprising to see a plethora of research efforts put into stimulation of the pathway by suppressing the physiological inhibitory factors of the pathway in order to promote osteoblast differentiation and activity. Several mechanisms are involved in the inhibition of Wnt pathway. The intracellular enzyme glycogen synthase kinase 3 (GSK3) phosphorylates β-catenin, which serves as a signal for the degradation of β-catenin and prevents its nucleus translocation, suppressing the activation of Wnt pathway.[18,19] Thus, many GSK3 inhibitors,

both known and newly-developed, have been studied for their potential as bone-anabolic agents[20–25]. Meanwhile, several endogenous factors that antagonizes and hinders the binding between Wnts and FZDs or LRP5/6 have been discovered, such as secreted frizzled-related proteins (sFRPs), dickkopf-1 (Dkk-1), Wnt-inhibitory factor-1 (WIF-1), sclerostin, etc.[26] Positive results of enhanced bone formation by inhibition of extracellular Wnt inhibitors have been reported, utilizing either neutralizing antibodies (Dkk-1 and sclerostin) or small-molecule inhibitors (sFRP-1).[27–29]

1.1.2.2 Osteoclasts

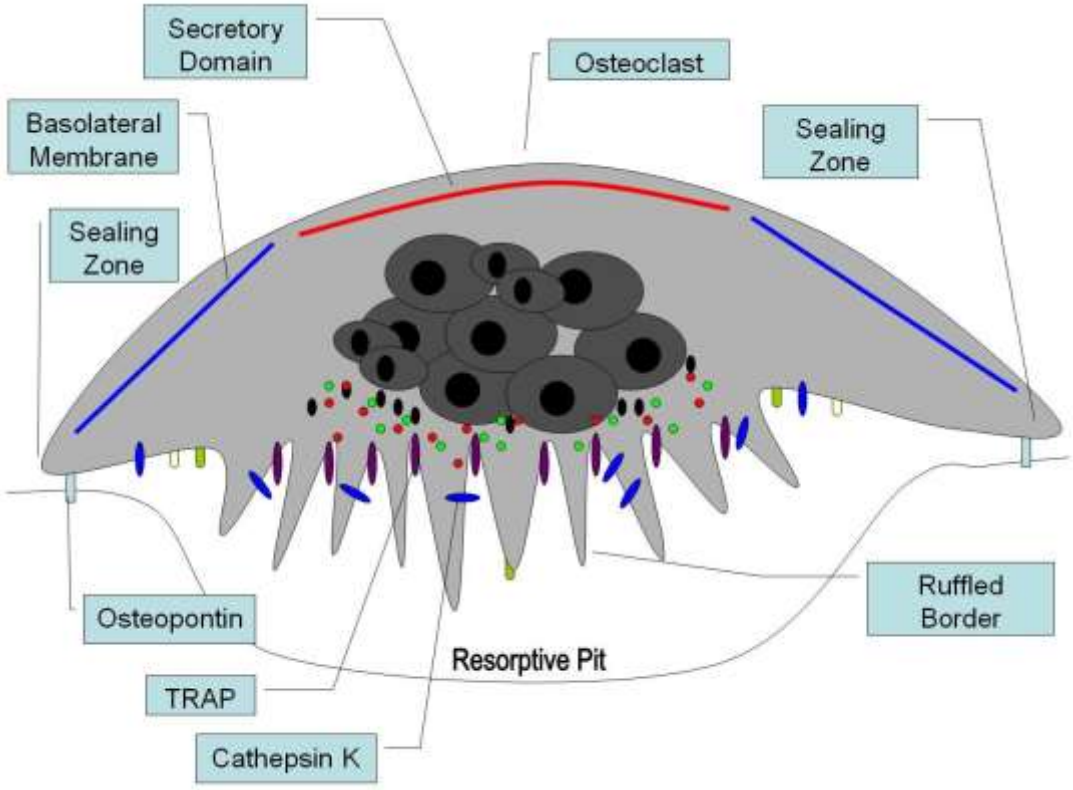

Fig. 1.3 Depiction of an Osteoclast.
Diagram originally created by Cellpath [CC BY-SA 3.0 (http://creativecommons.org/licenses/by-sa/3.0/)] and modified for use.

Osteoclasts are the major cell type involved in bone resorption, the catabolic activity of bone homeostasis. Osteoclasts are multinucleated cells of the monocyte lineage, which is formed by the *in-situ* proliferation and fusion of precursor cells recruited to the bone surface.[30] A mature osteoclast adheres to bone, creates a sealing zone, and forms a resorptive pit under the cell (Fig. 1.3). Osteoclast-mediated bone resorption begins with the acidification of the resorptive pit by proton pumps to dissolve the bone mineral, followed by the secretion of various enzymes (e.g. cathepsin K and matrix metalloproteinases) to break down the organic matrix of bone.[4,30,31]

The most important pathway to regulate the differentiation and function of osteoclasts is the RANKL/RANK pathway.[32] RANK is a type I transmembrane protein expressed on the cell surface of osteoclasts, which regulates osteoclast differentiation and activation.[33] RANK ligand, or RANKL, is a type II membrane protein belonging to the tumor necrosis factor (TNF) superfamily expressed on osteoblast and osteocyte surface, and serves as the endogenous ligand for RANK.[34] The binding of RANKL to RANK on the surface of osteoclasts and its precursor cells functions as the signal for osteoclastogenesis[35]. The ability to express RANKL has enabled osteoblasts to initiate and regulate the activity of osteoclasts, and in turn, bone resorption.[36]

1.1.2.3 Osteocytes

Osteocytes are terminally-differentiated osteoblasts embedded in the bone matrix (Fig. 1.2).[37] Osteocytes make up more than 90% of bone cells, making them the most abundant cell type in bone tissue.[4,38] Canaliculi, which are dendritic processes formed by osteocytes, extend to all directions and form an osteocyte network for communication and exchange of materials such as proteins (see Fig. 1.1).[4,39] Osteocytes are important

regulators of bone homeostasis by secreting factors that influence osteoblast and osteoclast activity (e.g. OPG, RANKL, sclerostin, etc.).[40] Additionally, osteocytes are in charge of bone's response to mechanical load; they sense mechanical signals and react by directing bone modeling to counteract the mechanical load.[41] Moreover, osteocytes play an important endocrine role: when unusual changes in plasma hormone levels are detected, osteocytes would regulate bone formation and resorption in response to those changes.[42]

1.1.3 Bone Problems and Pathologies

When one or more processes in bone homeostasis fail, bone pathologies would develop. Common pathologies arising from altered bone homeostasis include osteoporosis (more active bone resorption than bone formation[43]), Paget's Disease (bone turnover malfunction[44]), and osteogenesis imperfecta (impaired osteoid production[45]). Healthy bone can also fall victim to mechanical impact or bacterial infection, leading to bone fracture or osteomyelitis.[46]

Among all bone pathologies, osteoporosis and bone fracture are the most common.[47] Since osteoporosis is a major risk factor of bone fracture, the two pathologies are tightly related.[48] In the US, approximately 44 million people have low bone density with 10 million already suffering from osteoporosis, implying that a large proportion of the population will have increased likelihood for fractures[49]. Unfortunately, although many osteoporosis therapies have been developed, there is still a void for an effective, convenient, and safe bone fracture repair therapy (see Section 1.2.3).

1.2 Bone Fracture Repair

1.2.1 Types of Bone Fracture

Bone fractures occur when there is a break in the bone.[50] Differentiated by the character and cause, bone fractures can be classified as simple fracture, comminuted fracture, and stress fracture. When bone is broken into two fragments, it is defined as a simple fracture, while comminuted fracture describes a situation where bone is shattered into several pieces. Stress fracture is characterized by an accumulation of microdamage caused by the exposure to continuous and repeated force.[50]

1.2.2 Natural Process of Fracture Repair

The process of fracture repair can be divided into four stages: inflammatory response, soft callus formation, hard callus formation, and bone remodeling (Fig. 1.4).[50] The inflammatory stage occurs immediately following the trauma, and lasts for as long as 7 days. During this stage, a hypoxic hematoma forms around the fracture wound site with an influx of inflammation-responder cells (e.g. macrophages, leukocytes, etc.).[51] These recruited cells begin to participate in angiogenesis and fibrogenesis, resulting in the formation of a fibrocartilage callus that bridges the fractured ends of bone, namely the soft callus.[52] This stage usually peaks on day 7-10 in rodent models.[50] Following that, the soft callus is gradually replace with cancellous/trabecular bone, bridging the bone ends with a mineralized bony structure called hard callus, which leads to the progressive restoration of the mechanical strength of the broken bone.[53] During this stage, osteoblasts are highly active, and osteoblast markers such as alkaline phosphatase (ALP) and type I collagen are significantly upregulated.[50] The peak of this stage is around day 14 in rodent models. The last stage of fracture repair, bone remodeling, occurs from week 3-4 and may last for

several months to several years before completion.[53] During this stage, trabecular bone in the fracture callus is gradually remodeled into cortical bone while the callus restores to the original shape of the bone, although the reshaping might never fully complete.[50] Osteoclasts and osteoblasts are both actively involved in the bone remodeling process, where osteoclasts resorbs the trabecular bone in the fracture callus while osteoblasts build new cortical bone.[54] Inhibition of osteoclast activity with antiresorptives (such as bisphosphonates) during this stage would impair the removal of trabecular bone tissue and formation of compact bone.[50]

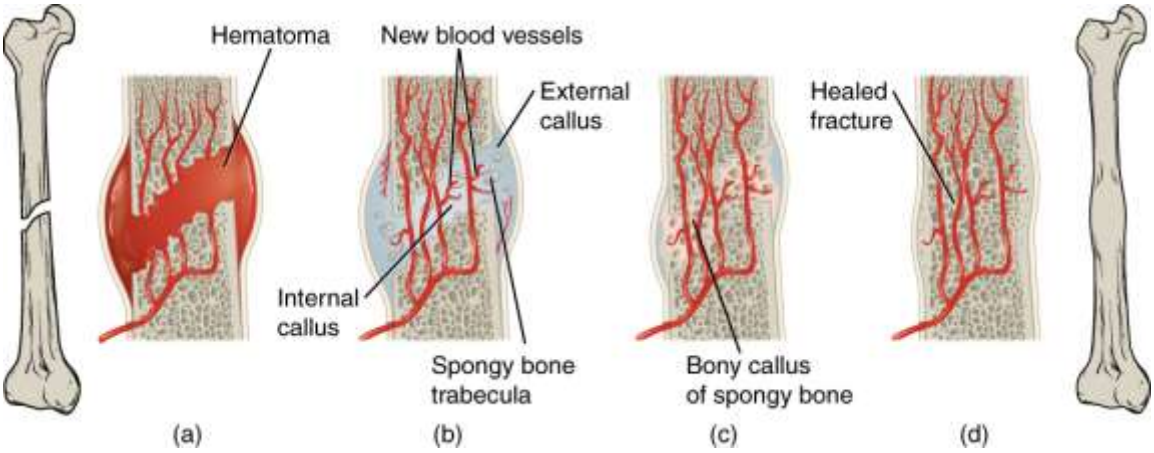

Fig. 1.4 The Four Stages of Fracture Repair.
(a) Inflammatory stage; (b) soft callus formation; (c) hard callus formation; (d) bone remodeling. Diagram adapted from *Anatomy and Physiology*[55] [CC BY 4.0 (https://creativecommons.org/licenses/by/4.0/)]

1.2.3 Need for Improvements in the Treatment of Bone Fractures

Bone fracture has long been one of the least desirable ailments for human beings, and it is causing major problems in the US and around the world. Approximately 6 million bone fractures occur each year in the USA[55], resulting in 3.5 million visits to the emergency room and 887,679 longer term hospitalizations (data source: National Ambulatory Medical

Care Survey and the American Academy of Orthopaedic Surgeons). With 61 million older Americans estimated to suffer from osteoporosis[56], this number of fractures is expected to increase, especially as the population continues to age. Costs associated with hip fracture repairs were estimated at $21 billion in 2009[57], and lost wages due to fracture-related absence from work have added substantially to these costs[58]. Morbidities deriving from loss of motility, pain, anxiety, and depression can also erode a patient's quality of life[59,60]. Most importantly, many fractures trigger more serious pathologies, with complications deriving from hip fractures leading to 75,000 deaths/year in the USA[61,62]. Clearly, strategies that might accelerate and/or improve bone fracture repair could mitigate many problems facing an aging and physically active population.

Despite the burdens bone fractures have been and will be laying on the aging population from all over the world, the current therapeutic solutions for bone fracture has yet to catch up with the growing demand. Antiresorptive drugs and anabolic drugs are the two major classes of drugs that are currently available for the expansion of bone mass, each with its own disadvantages to be used for the improvement of bone fracture repair.

1.2.3.1 Problems with Antiresorptive Drugs

Examples of antiresorptive include various bisphosphonates (alendronate, zoledronic acid, etc.), estrogen therapy, and RANKL antibody (Denosumab). Those agents increase bone mass by inhibiting the function of osteoclasts, resulting in a decrease in bone resorption. Bisphosphonates suppress bone resorption by suppressing osteoclast activity[63], while estrogen prevents bone loss by disrupting the initiation of osteoclastogenesis and inducing osteoclast apoptosis[64]. RANKL antibody neutralizes RANKL and inhibits the binding between RANKL and RANK, which hinders the differentiation from

hematopoietic precursor cells into osteoclasts[65]. Since osteoporosis is caused by an imbalance between bone formation and resorption, those antiresorptive drugs work well for osteoporosis by inhibition of bone resorption. However, they have not been employed to accelerate fracture healing since they do not promote the formation of new bone, which is essential in the process of fracture healing. Additionally, bisphosphonates inhibit angiogenesis, which together with their resorption-hindering ability, might impede bone turnover essential for fracture repair[66,67]. Furthermore, as mentioned about in Section 1.2.2, inhibition of bone resorption is detrimental to the last stage of fracture healing, which is an undesirable feature for a drug intended to enhance fracture repair.

1.2.3.2 Problems with Derivatives of Parathyroid Hormone

Problems also exists for a class of parathyroid-hormone-related bone-anabolic agents. Recombinant human parathyroid hormone 1-34 (Forteo®, Eli Lilly), abaloparatide (Tymlos®, Radius Health), and parathyroid hormone related protein (PTHrP) can all activate osteoblasts and thereby induce bone mineralization[68,69], but their abilities to improve fracture repair in human have not proven statistically significant[70], even at concentrations that promoted hypercalcemia and the consequent pain, nausea, confusion and fatigue[71–73]. In fact, since PTH can induce osteoclastogenesis and may cause either a net gain or a net loss of bone material depending on the dosing regimen[68,71], there are reports of conflicting results on Forteo's ability to improve fracture healing[69,74].

1.2.3.3 Problems with BMPs

BMP-2 and BMP-7 are the only FDA approved anabolic drugs for fractures; however, they must be applied topically for fractures in which the fracture surface is exposed during surgery or spinal fusion, severely restricting their use.[75] Both clinically approved BMPs

have also been continuously plagued by safety concerns such as vertebral osteolysis and ectopic bone growth, leading to the withdrawal of BMP-7/OP-1® from the market in August 2014.[76–79]

Clearly, a major need exists for a systemically administered drug that will accelerate fracture repair without promoting turnover of undamaged bones or causing other unwanted side effects such as hypercalcemia. From our perspective, a bone anabolic agent that would concentrate at the fracture site, promote osteoblast activity without overt inhibition of bone resorption, and clear rapidly from unaffected sites should satisfy the above requirements.

1.3 The Role of Src Kinase in Bone Metabolism

In the search for a novel bone-anabolic agent that avoids the above-mentioned drawbacks, Src inhibition has drawn our attention as a potential strategy that meets our criteria. Indeed, studies with *Src*-knockout mouse models have shown that although Src kinase is ubiquitously expressed in tissues[80], the only major consequence of Src gene knockout appears to be osteopetrosis (excess formation of bone)[81,82], suggesting that Src kinase plays a critical role in bone turnover and formation[83]. However, it was unclear whether this effect has been a result of promoted bone formation or suppressed bone resorption. Since the role that Src plays in osteoclastogenesis has been extensively studied and documented,[1,84,85] the prevailing opinion has been that Src inhibition would merely act as an antiresorptive.[86,87]

Despite the dogma, multiple recently reports have studied and discussed the effect of Src inhibition on bone-anabolism (see Section 2.1), giving us the initiative to explore the possibilities of using Src inhibitors as bone-anabolic agents for accelerated fracture repair.

Dasatinib, a potent Src inhibitor with a safety profile that has stood up to the test with human patients for over a decade,[88] is our top candidate.

1.4 Targeted Delivery of Bone-Anabolic Agents to Accelerate Fracture Repair

1.4.1 Leading Drugs to the Right Places: Targeted Drug Delivery

Traditional drug discovery designs drug molecules that interfere with one or more key processes during disease development. Given that the majority of these processes are not constrained to diseased tissue, those drug molecules are, in turn, non-specific in terms of toxicity. Hence, many effective drugs fail due to side effects originating from their interaction with normal, healthy cells and tissues.[89] This concern brings into our sight a new class of drug conjugates that combine a drug payload with a disease-tissue-specific ligand.[90] This new class of targeted drug conjugates would accumulate specifically at the disease site, release the drug payload, and achieve improved therapeutic efficacy as well as reduced systemic toxicity.[91] Apparently, a therapy to accelerate bone fracture healing would benefit significantly from targeted drug delivery, which enables concentration of the bone-anabolic efficacy of the drug and reduction of the potential for systemic toxicity (e.g. abnormal ectopic bone growth, hypercalcemia, etc.). The key to a successful targeted drug for bone fracture repair is finding a good targeting ligand with high specificity for a bone fracture.

1.4.2 Bone-Fracture-Specific Targeting Ligands

To achieve fracture-specific targeting, a HAp-binding moiety should work well since crystalline HAp is exposed in the case of a fracture, whereas it is fully covered with the periosteum in healthy bones.[92] HAp-specific bone targeting ability has been in existence

for quite some time: technetium-99m-methylene diphosphonate (^{99m}Tc-MDP) was developed in the 1970s, and has been widely used in bone scintillation scans for almost four decades.[93,94] Besides bisphosphonates, other HAp-targeting moieties such as calcium phosphate nanomaterials/scaffolds and oligo-acidic peptides are all potential choices as targeting ligands. However, despite bisphosphonates' strong HAp binding characteristics, they cause an imbalance in the fracture repair process by potently inhibiting osteoclastogenesis,[95] which is undesirable for a fracture healing drug as discussed before. Plus, their excessively long half-life in bone[96] and teeth[97] may increase the risk of side-effects. Calcium phosphate nanomaterials/scaffolds are similar in composition to bone and have demonstrated potential as bone-specific delivery systems, but they have been difficult to be reproducibly synthesized with well-defined morphologies and have therefore not yet progressed into the clinic.[95]

A superior strategy for fracture targeting involves targeting moieties consisting of strings of acidic amino acids, such as aspartic acid and glutamic acid.[98] Oligomers of aspartic acid and glutamic acid are compositionally similar to motifs of bone sialoprotein (BSP) and proteins in the small integrin-binding ligand, N-linked glycoprotein (SIBLING) family, which are naturally occurring bone homing peptides with strong affinity for HAp.[99,100] Additionally, their peptidic nature allows them to be readily biodegraded following completion of their targeting function.[101] Consequently, oligomers of aspartic acid and glutamic acid are burdened by few if any unwanted side effects when used for fracture targeting. The biodistribution profile of aspartic acid octapeptide, in particular, was impressive with high uptake in fractured bone, high fractured-to-healthy bone ratio, and limited uptake in other tissues.[100,102] As shown in Fig. 1.5, an ^{125}I-labeled,

oligoaspartic-acid-targeted small molecule 6BIO would concentrate specifically at the fracture site of a mouse 24 h post injection, while the free, untargeted version had mostly been excreted with only small quantities distributed in a scattered fashion in the mouse body.[100] Hexamers, octamers and decamers of oligoaspartic acids have all been reported to localize efficiently to bone fracture surfaces and clear rapidly from the plasma *in vivo*, with increasing targeting ability with increasing length of the peptide.[98,103] For those reasons, aspartic acid decapeptide has been chosen for our fracture-targeting purposes.

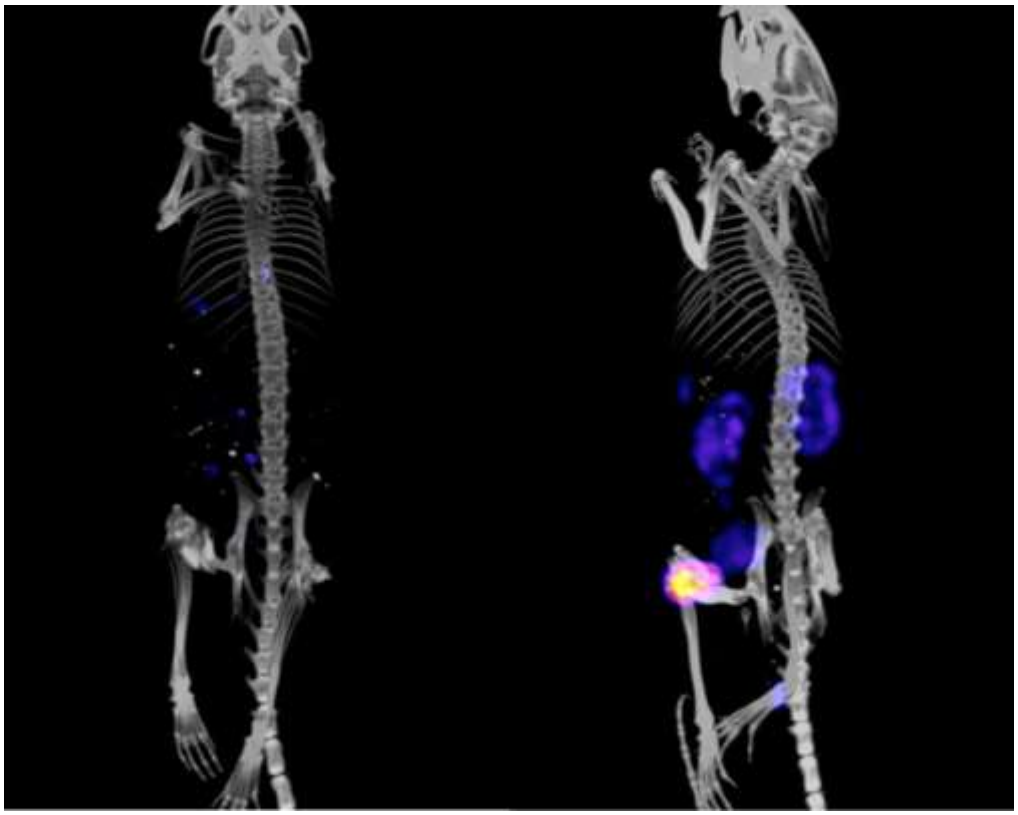

Fig. 1.5 SPECT/CT Image of Fracture-Bearing Mice Receiving Free (Left) or Targeted (Right) Versions of ^{125}I-6BIO.
The small amount of remaining free ^{125}I-6BIO was randomly distributed in the mouse body, while a considerable quantity of targeted ^{125}I-6BIO had accumulated at the fracture site. Images were taken 24 hours after injection of the radiolabeled compounds. Reprinted (adapted) with permission from [100]. Copyright © 2015, American Chemical Society.

1.5 Summary of Our Hypothesis

Since osteoblasts play essential roles in both bone formation, regulation of the activity of osteoblasts is the key to manipulation of the fracture repair process. Given that Src inhibition could promote the activity and differentiation of osteoblasts *in vivo*, we hypothesize that accumulation of a potent Src inhibitor at the fracture site should stimulate new bone formation, which might in turn facilitate the healing of a fracture. To test our hypothesis, we would need to first verify the ability of a Src inhibitor to stimulate osteoblast differentiation and function *in vitro*. If the inhibitor does facilitate osteoblastogenesis, we would implement a mouse fracture model and concentrate the inhibitor at the fracture surface to test its bone fracture healing efficacy. Src inhibitor dasatinib is chosen to be tested owing to its potency and safety, and a deca-aspartic acid will be used as the fracture-targeting ligand for specific delivery to the fracture site. Since dasatinib needs to be released from the targeting moiety to work, the two parts would be joined by a hydrolysable ester linker.

If a fracture-targeted version of dasatinib should turn out to be a potent bone-anabolic agent that could facilitate bone fracture repair, this finding may have significant clinical implications. Complications derived from prolonged immobility could be alleviated, and patients could be able to return to their normal lives sooner. Moreover, we would also attempt to reduce the dosing frequency of the targeted drug to further cater to the need of patients bearing bone fractures. Finally, more bone-anabolic small molecules would be delivered to bone fracture with the same targeting ligand to examine their ability to facilitate fracture healing.

1.6 References

(1) Burr, D. B.; Akkus, O. Bone Morphology and Organization. In *Basic and Applied Bone Biology*; Elsevier, 2014; pp 3–25.

(2) Low, S. A.; Kopeček, J. Targeting Polymer Therapeutics to Bone. *Adv. Drug Deliv. Rev.* **2012**, *64* (12), 1189–1204.

(3) Henry, G. A.; Cole, R. Fracture Healing and Complications in Dogs. In *Textbook of Veterinary Diagnostic Radiology*; Elsevier, 2018; pp 366–389.

(4) Bellido, T.; Plotkin, L. I.; Bruzzaniti, A. Bone Cells. In *Basic and Applied Bone Biology*; Elsevier, 2014; pp 27–45.

(5) Blair, H. C.; Larrouture, Q. C.; Li, Y.; Lin, H.; Beer-Stoltz, D.; Liu, L.; Tuan, R. S.; Robinson, L. J.; Schlesinger, P. H.; Nelson, D. J. Osteoblast Differentiation and Bone Matrix Formation In Vivo and In Vitro. *Tissue Eng. Part B Rev.* **2017**, *23* (3), 268–280.

(6) Plotkin, L. I.; Bivi, N. Local Regulation of Bone Cell Function. In *Basic and Applied Bone Biology*; Elsevier, 2014; pp 47–73.

(7) Celil, A. B.; Campbell, P. G. BMP-2 and Insulin-like Growth Factor-I Mediate Osterix (Osx) Expression in Human Mesenchymal Stem Cells via the MAPK and Protein Kinase D Signaling Pathways. *J. Biol. Chem.* **2005**, *280* (36), 31353–31359.

(8) Chen, G.; Deng, C.; Li, Y.-P. TGF-β and BMP Signaling in Osteoblast Differentiation and Bone Formation. *Int. J. Biol. Sci.* **2012**, *8* (2), 272–288.

(9) Lee, K.-S.; Kim, H.-J.; Li, Q.-L.; Chi, X.-Z.; Ueta, C.; Komori, T.; Wozney, J. M.; Kim, E.-G.; Choi, J.-Y.; Ryoo, H.-M.; et al. Runx2 Is a Common Target of Transforming Growth Factor Beta 1 and Bone Morphogenetic Protein 2, and Cooperation between Runx2 and Smad5 Induces Osteoblast-Specific Gene Expression in the Pluripotent Mesenchymal Precursor Cell Line C2C12. *Mol. Cell. Biol.* **2000**, *20* (23), 8783–8792.

(10) Yamaguchi, A.; Sakamoto, K.; Minamizato, T.; Katsube, K.; Nakanishi, S. Regulation of Osteoblast Differentiation Mediated by BMP, Notch, and CCN3/NOV. *Jpn. Dent. Sci. Rev.* **2008**, *44* (1), 48–56.

(11) Conway, J. D.; Shabtai, L.; Bauernschub, A.; Specht, S. C. BMP-7 versus BMP-2 for the Treatment of Long Bone Nonunion. *Orthopedics* **2014**, *37* (12), e1049-1057.

(12) White, A. P.; Vaccaro, A. R.; Hall, J. A.; Whang, P. G.; Friel, B. C.; McKee, M. D. Clinical Applications of BMP-7/OP-1 in Fractures, Nonunions and Spinal Fusion. *Int. Orthop.* **2007**, *31* (6), 735–741.

(13) McKay, W. F.; Peckham, S. M.; Badura, J. M. A Comprehensive Clinical Review of Recombinant Human Bone Morphogenetic Protein-2 (INFUSE Bone Graft). *Int. Orthop.* **2007**, *31* (6), 729–734.

(14) Goessling, W.; North, T. E.; Loewer, S.; Lord, A. M.; Lee, S.; Stoick-Cooper, C. L.; Weidinger, G.; Puder, M.; Daley, G. Q.; Moon, R. T.; et al. Genetic Interaction of PGE2 and Wnt Signaling Regulates Developmental Specification of Stem Cells and Regeneration. *Cell* **2009**, *136* (6), 1136–1147.

(15) Logan, C. Y.; Nusse, R. The Wnt Signaling Pathway in Development and Disease. *Annu. Rev. Cell Dev. Biol.* **2004**, *20*, 781–810.

(16) Komiya, Y.; Habas, R. Wnt Signal Transduction Pathways. *Organogenesis* **2008**, *4* (2), 68–75.

(17) Yavropoulou, M. P.; Yovos, J. G. The Role of the Wnt Signaling Pathway in Osteoblast Commitment and Differentiation. *Horm. Athens Greece* **2007**, *6* (4), 279–294.

(18) Wu, D.; Pan, W. GSK3: A Multifaceted Kinase in Wnt Signaling. *Trends Biochem. Sci.* **2010**, *35* (3), 161–168.

(19) Metcalfe, C.; Bienz, M. Inhibition of GSK3 by Wnt Signalling - Two Contrasting Models. *J. Cell Sci.* **2011**, *124* (21), 3537–3544.

(20) Atilla-Gokcumen, G. E.; Pagano, N.; Streu, C.; Maksimoska, J.; Filippakopoulos, P.; Knapp, S.; Meggers, E. Extremely Tight Binding of a Ruthenium Complex to Glycogen Synthase Kinase 3. *ChemBioChem* **2008**, *9* (18), 2933–2936.

(21) Gaisina, I. N.; Gallier, F.; Ougolkov, A. V.; Kim, K. H.; Kurome, T.; Guo, S.; Holzle, D.; Luchini, D. N.; Blond, S. Y.; Billadeau, D. D.; et al. From a Natural Product Lead to the Identification of Potent and Selective Benzofuran-3-Yl-(Indol-3-Yl)Maleimides as Glycogen Synthase Kinase 3β Inhibitors That Suppress Proliferation and Survival of Pancreatic Cancer Cells. *J. Med. Chem.* **2009**, *52* (7), 1853–1863.

(22) Kulkarni, N. H.; Onyia, J. E.; Zeng, Q.; Tian, X.; Liu, M.; Halladay, D. L.; Frolik, C. A.; Engler, T.; Wei, T.; Kriauciunas, A.; et al. Orally Bioavailable GSK-3α/β Dual Inhibitor Increases Markers of Cellular Differentiation In Vitro and Bone Mass In Vivo. *J. Bone Miner. Res.* **2006**, *21* (6), 910–920.

(23) Kramer, T.; Schmidt, B.; Lo Monte, F. Small-Molecule Inhibitors of GSK-3: Structural Insights and Their Application to Alzheimer's Disease Models. *Int. J. Alzheimers Dis.* **2012**, *2012*, 1–32.

(24) Naujok, O.; Lentes, J.; Diekmann, U.; Davenport, C.; Lenzen, S. Cytotoxicity and Activation of the Wnt/Beta-Catenin Pathway in Mouse Embryonic Stem Cells Treated with Four GSK3 Inhibitors. **2014**, *7*, 273.

(25) Schoeman, M. A. E.; Moester, M. J. C.; Oostlander, A. E.; Kaijzel, E. L.; Valstar, E. R.; Nelissen, R. G. H. H.; Löwik, C. W. G. M.; Rooij, K. E. d. Inhibition of GSK3β Stimulates BMP Signaling and Decreases *SOST* Expression Which Results in Enhanced Osteoblast Differentiation: G SK3B I NHIBITION D ECREASES S OST E XPRESSION. *J. Cell. Biochem.* **2015**, *116* (12), 2938–2946.

(26) Cruciat, C.-M.; Niehrs, C. Secreted and Transmembrane Wnt Inhibitors and Activators. *Cold Spring Harb. Perspect. Biol.* **2013**, *5* (3), a015081–a015081.

(27) Bodine, P. V. N.; Stauffer, B.; Ponce-de-Leon, H.; Bhat, R. A.; Mangine, A.; Seestaller-Wehr, L. M.; Moran, R. A.; Billiard, J.; Fukayama, S.; Komm, B. S.; et al. A Small Molecule Inhibitor of the Wnt Antagonist Secreted Frizzled-Related Protein-1 Stimulates Bone Formation. *Bone* **2009**, *44* (6), 1063–1068.

(28) McClung, M. R. Sclerostin Antibodies in Osteoporosis: Latest Evidence and Therapeutic Potential. *Ther. Adv. Musculoskelet. Dis.* **2017**, *9* (10), 263–270.

(29) Florio, M.; Gunasekaran, K.; Stolina, M.; Li, X.; Liu, L.; Tipton, B.; Salimi-Moosavi, H.; Asuncion, F. J.; Li, C.; Sun, B.; et al. A Bispecific Antibody Targeting Sclerostin and DKK-1 Promotes Bone Mass Accrual and Fracture Repair. *Nat. Commun.* **2016**, *7* (1).

(30) Nijweide, P. J.; Burger, E. H.; Feyen, J. H. Cells of Bone: Proliferation, Differentiation, and Hormonal Regulation. *Physiol. Rev.* **1986**, *66* (4), 855–886.

(31) Stenbeck, G. Formation and Function of the Ruffled Border in Osteoclasts. *Semin. Cell Dev. Biol.* **2002**, *13* (4), 285–292.

(32) Lowe, C.; Yoneda, T.; Boyce, B. F.; Chen, H.; Mundy, G. R.; Soriano, P. Osteopetrosis in Src-Deficient Mice Is Due to an Autonomous Defect of Osteoclasts. *Proc. Natl. Acad. Sci. U. S. A.* **1993**, *90* (10), 4485–4489.

(33) Naito, A.; Azuma, S.; Tanaka, S.; Miyazaki, T.; Takaki, S.; Takatsu, K.; Nakao, K.; Nakamura, K.; Katsuki, M.; Yamamoto, T.; et al. Severe Osteopetrosis, Defective Interleukin-1 Signalling and Lymph Node Organogenesis in TRAF6-Deficient Mice. *Genes Cells Devoted Mol. Cell. Mech.* **1999**, *4* (6), 353–362.

(34) Hanada, R.; Hanada, T.; Sigl, V.; Schramek, D.; Penninger, J. M. RANKL/RANK-beyond Bones. *J. Mol. Med. Berl. Ger.* **2011**, *89* (7), 647–656.

(35) Boyce, B. F.; Xing, L. The RANKL/RANK/OPG Pathway. *Curr. Osteoporos. Rep.* **2007**, *5* (3), 98–104.

(36) Katagiri, T.; Takahashi, N. Regulatory Mechanisms of Osteoblast and Osteoclast Differentiation. *Oral Dis.* **2002**, *8* (3), 147–159.

(37) Aarden, E. M.; Burger, E. H.; Nijweide, P. J. Function of Osteocytes in Bone. *J. Cell. Biochem.* **1994**, *55* (3), 287–299.

(38) Buenzli, P. R.; Sims, N. A. Quantifying the Osteocyte Network in the Human Skeleton. *Bone* **2015**, *75*, 144–150.

(39) Bonewald, L. F. The Amazing Osteocyte. *J. Bone Miner. Res. Off. J. Am. Soc. Bone Miner. Res.* **2011**, *26* (2), 229–238.

(40) Knothe Tate, M. L.; Adamson, J. R.; Tami, A. E.; Bauer, T. W. The Osteocyte. *Int. J. Biochem. Cell Biol.* **2004**, *36* (1), 1–8.

(41) Bonewald, L. F. Mechanosensation and Transduction in Osteocytes. *BoneKEy Osteovision* **2006**, *3* (10), 7–15.

(42) Dallas, S. L.; Prideaux, M.; Bonewald, L. F. The Osteocyte: An Endocrine Cell ... and More. *Endocr. Rev.* **2013**, *34* (5), 658–690.

(43) Raisz, L. G. Pathogenesis of Osteoporosis: Concepts, Conflicts, and Prospects. *J. Clin. Invest.* **2005**, *115* (12), 3318–3325.

(44) Paul Tuck, S.; Layfield, R.; Walker, J.; Mekkayil, B.; Francis, R. Adult Paget's Disease of Bone: A Review. *Rheumatol. Oxf. Engl.* **2017**, *56* (12), 2050–2059.

(45) Forlino, A.; Cabral, W. A.; Barnes, A. M.; Marini, J. C. New Perspectives on Osteogenesis Imperfecta. *Nat. Rev. Endocrinol.* **2011**, *7* (9), 540–557.

(46) Schmitt, S. K. Osteomyelitis. *Infect. Dis. Clin. North Am.* **2017**, *31* (2), 325–338.

(47) *Prevention and Management of Osteoporosis: Report of a WHO Scientific Group ; [WHO Scientific Group Meeting on Prevention and Management of Osteoporosis, Geneva, 7 - 10 April]*; Scientific Group Meeting on Prevention and Management of Osteoporosis, Weltgesundheitsorganisation, Eds.; WHO Technical Report Series; World Health Organization: Geneva, 2003.

(48) Assessment of Fracture Risk and Its Application to Screening for Postmenopausal Osteoporosis. Report of a WHO Study Group. *World Health Organ. Tech. Rep. Ser.* **1994**, *843*, 1–129.

(49) Wright, N. C.; Looker, A. C.; Saag, K. G.; Curtis, J. R.; Delzell, E. S.; Randall, S.; Dawson-Hughes, B. The Recent Prevalence of Osteoporosis and Low Bone Mass in the United States Based on Bone Mineral Density at the Femoral Neck or Lumbar Spine. *J. Bone Miner. Res. Off. J. Am. Soc. Bone Miner. Res.* **2014**, *29* (11), 2520–2526.

(50) Li, J.; Stocum, D. L. Fracture Healing. In *Basic and Applied Bone Biology*; Elsevier, 2014; pp 205–223.

(51) Loi, F.; Córdova, L. A.; Pajarinen, J.; Lin, T.; Yao, Z.; Goodman, S. B. Inflammation, Fracture and Bone Repair. *Bone* **2016**, *86*, 119–130.

(52) Kisseleva, T.; Brenner, D. A. Mechanisms of Fibrogenesis. *Exp. Biol. Med. Maywood NJ* **2008**, *233* (2), 109–122.

(53) Marsell, R.; Einhorn, T. A. The Biology of Fracture Healing. *Injury* **2011**, *42* (6), 551–555.

(54) Schindeler, A.; McDonald, M. M.; Bokko, P.; Little, D. G. Bone Remodeling during Fracture Repair: The Cellular Picture. *Semin. Cell Dev. Biol.* **2008**, *19* (5), 459–466.

(55) Betts, J. G.; DeSaix, P.; Johnson, E.; Johnson, J. E.; Korol, O.; Kruse, D. H.; Poe, B.; Wise, J. A.; Womble, M.; Young, K. A. *Anatomy and Physiology*; 2017.

(56) Office of the Surgeon General (US). *Bone Health and Osteoporosis: A Report of the Surgeon General*; Reports of the Surgeon General; Office of the Surgeon General (US): Rockville (MD), 2004.

(57) Bartl, R.; Frisch, B.; Bartl, C. *Osteoporosis: Diagnosis, Prevention, Therapy*, 2nd rev. ed.; Springer: Berlin, 2009.

(58) Gu, Q.; Koenig, L.; Mather, R. C.; Tongue, J. Surgery for Hip Fracture Yields Societal Benefits That Exceed the Direct Medical Costs. *Clin. Orthop. Relat. Res.* **2014**, *472* (11), 3536–3546.

(59) Holm, A. G. V.; Lurås, H.; Randsborg, P.-H. The Economic Burden of Outpatient Appointments Following Paediatric Fractures. *Injury* **2016**, *47* (7), 1410–1413.

(60) Keene, G. S.; Parker, M. J.; Pryor, G. A. Mortality and Morbidity after Hip Fractures. *BMJ* **1993**, *307* (6914), 1248–1250.

(61) Adachi, J. D.; Adami, S.; Gehlbach, S.; Anderson, F. A.; Boonen, S.; Chapurlat, R. D.; Compston, J. E.; Cooper, C.; Delmas, P.; Díez-Pérez, A.; et al. Impact of Prevalent Fractures on Quality of Life: Baseline Results from the Global Longitudinal Study of Osteoporosis in Women. *Mayo Clin. Proc.* **2010**, *85* (9), 806–813.

(62) Bentler, S. E.; Liu, L.; Obrizan, M.; Cook, E. A.; Wright, K. B.; Geweke, J. F.; Chrischilles, E. A.; Pavlik, C. E.; Wallace, R. B.; Ohsfeldt, R. L.; et al. The Aftermath of Hip Fracture: Discharge Placement, Functional Status Change, and Mortality. *Am. J. Epidemiol.* **2009**, *170* (10), 1290–1299.

(63) Braithwaite, R. S.; Col, N. F.; Wong, J. B. Estimating Hip Fracture Morbidity, Mortality and Costs. *J. Am. Geriatr. Soc.* **2003**, *51* (3), 364–370.

(64) Lee, D.; Heo, D. N.; Kim, H.-J.; Ko, W.-K.; Lee, S. J.; Heo, M.; Bang, J. B.; Lee, J. B.; Hwang, D.-S.; Do, S. H.; et al. Inhibition of Osteoclast Differentiation and Bone Resorption by Bisphosphonate-Conjugated Gold Nanoparticles. *Sci. Rep.* **2016**, *6* (1), 27336.

(65) Fitzpatrick, L. A. Estrogen Therapy for Postmenopausal Osteoporosis. *Arq. Bras. Endocrinol. Metabol.* **2006**, *50* (4), 705–719.

(66) Deeks, E. D. Denosumab: A Review in Postmenopausal Osteoporosis. *Drugs Aging* **2018**, *35* (2), 163–173.

(67) Fournier, P.; Boissier, S.; Filleur, S.; Guglielmi, J.; Cabon, F.; Colombel, M.; Clézardin, P. Bisphosphonates Inhibit Angiogenesis in Vitro and Testosterone-Stimulated Vascular Regrowth in the Ventral Prostate in Castrated Rats. *Cancer Res.* **2002**, *62* (22), 6538–6544.

(68) Giraudo, E.; Inoue, M.; Hanahan, D. An Amino-Bisphosphonate Targets MMP-9-Expressing Macrophages and Angiogenesis to Impair Cervical Carcinogenesis. *J. Clin. Invest.* **2004**, *114* (5), 623–633.

(69) Kroll, M. H. Parathyroid Hormone Temporal Effects on Bone Formation and Resorption. *Bull. Math. Biol.* **2000**, *62* (1), 163–188.

(70) Babu, S.; Sandiford, N. A.; Vrahas, M. Use of Teriparatide to Improve Fracture Healing: What Is the Evidence? *World J. Orthop.* **2015**, *6* (6), 457–461.

(71) Shi, Z.; Zhou, H.; Pan, B.; Lu, L.; Liu, J.; Kang, Y.; Yao, X.; Feng, S. Effectiveness of Teriparatide on Fracture Healing: A Systematic Review and Meta-Analysis. *PLOS ONE* **2016**, *11* (12), e0168691.

(72) Zhao, W.; Byrne, M. H.; Boyce, B. F.; Krane, S. M. Bone Resorption Induced by Parathyroid Hormone Is Strikingly Diminished in Collagenase-Resistant Mutant Mice. *J. Clin. Invest.* **1999**, *103* (4), 517–524.

(73) Karatoprak, C.; Kayatas, K.; Kilicaslan, H.; Yolbas, S.; Yazimci, N. A.; Gümüskemer, T.; Demirtunç, R. Severe Hypercalcemia Due to Teriparatide. *Indian J. Pharmacol.* **2012**, *44* (2), 270–271.

(74) Neer, R. M.; Arnaud, C. D.; Zanchetta, J. R.; Prince, R.; Gaich, G. A.; Reginster, J. Y.; Hodsman, A. B.; Eriksen, E. F.; Ish-Shalom, S.; Genant, H. K.; et al. Effect of Parathyroid Hormone (1-34) on Fractures and Bone Mineral Density in Postmenopausal Women with Osteoporosis. *N. Engl. J. Med.* **2001**, *344* (19), 1434–1441.

(75) Johansson, T. PTH 1-34 (Teriparatide) May Not Improve Healing in Proximal Humerus Fractures. A Randomized, Controlled Study of 40 Patients. *Acta Orthop.* **2016**, *87* (1), 79–82.

(76) Bishop, G. B.; Einhorn, T. A. Current and Future Clinical Applications of Bone Morphogenetic Proteins in Orthopaedic Trauma Surgery. *Int. Orthop.* **2007**, *31* (6), 721–727.

(77) Sreekumar, V.; Aspera-Werz, R. H.; Tendulkar, G.; Reumann, M. K.; Freude, T.; Breitkopf-Heinlein, K.; Dooley, S.; Pscherer, S.; Ochs, B. G.; Flesch, I.; et al. BMP9 a Possible Alternative Drug for the Recently Withdrawn BMP7? New Perspectives for (Re-)Implementation by Personalized Medicine. *Arch. Toxicol.* **2017**, *91* (3), 1353–1366.

(78) Lissenberg-Thunnissen, S. N.; de Gorter, D. J. J.; Sier, C. F. M.; Schipper, I. B. Use and Efficacy of Bone Morphogenetic Proteins in Fracture Healing. *Int. Orthop.* **2011**, *35* (9), 1271–1280.

(79) Shimer, A. L.; Öner, F. C.; Vaccaro, A. R. Spinal Reconstruction and Bone Morphogenetic Proteins: Open Questions. *Injury* **2009**, *40*, S32–S38.

(80) Govender, S.; Csimma, C.; Genant, H. K.; Valentin-Opran, A.; Amit, Y.; Arbel, R.; Aro, H.; Atar, D.; Bishay, M.; Börner, M. G.; et al. Recombinant Human Bone Morphogenetic Protein-2 for Treatment of Open Tibial Fractures: A Prospective, Controlled, Randomized Study of Four Hundred and Fifty Patients. *J. Bone Joint Surg. Am.* **2002**, *84-A* (12), 2123–2134.

(81) Peruzzi, B.; Rucci, N.; Teti, A. *Protein Kinases*; Da Silva Xavier, G., Ed.; InTech, 2012.

(82) Soriano, P.; Montgomery, C.; Geske, R.; Bradley, A. Targeted Disruption of the C-Src Proto-Oncogene Leads to Osteopetrosis in Mice. *Cell* **1991**, *64* (4), 693–702.

(83) Boyce, B. F.; Yoneda, T.; Lowe, C.; Soriano, P.; Mundy, G. R. Requirement of Pp60c-Src Expression for Osteoclasts to Form Ruffled Borders and Resorb Bone in Mice. *J. Clin. Invest.* **1992**, *90* (4), 1622–1627.

(84) Marzia, M.; Sims, N. A.; Voit, S.; Migliaccio, S.; Taranta, A.; Bernardini, S.; Faraggiana, T.; Yoneda, T.; Mundy, G. R.; Boyce, B. F.; et al. Decreased C-Src Expression Enhances Osteoblast Differentiation and Bone Formation. *J. Cell Biol.* **2000**, *151* (2), 311–320.

(85) Miyazaki, T.; Sanjay, A.; Neff, L.; Tanaka, S.; Horne, W. C.; Baron, R. Src Kinase Activity Is Essential for Osteoclast Function. *J. Biol. Chem.* **2004**, *279* (17), 17660–17666.

(86) Miyazaki, T.; Tanaka, S.; Sanjay, A.; Baron, R. The Role of C-Src Kinase in the Regulation of Osteoclast Function. *Mod. Rheumatol.* **2006**, *16* (2), 68–74.

(87) Vandyke, K.; Dewar, A. L.; Diamond, P.; Fitter, S.; Schultz, C. G.; Sims, N. A.; Zannettino, A. C. The Tyrosine Kinase Inhibitor Dasatinib Dysregulates Bone Remodeling through Inhibition of Osteoclasts in Vivo. *J. Bone Miner. Res.* **2010**, *25* (8), 1759–1770.

(88) Brownlow, N.; Mol, C.; Hayford, C.; Ghaem-Maghami, S.; Dibb, N. J. Dasatinib Is a Potent Inhibitor of Tumour-Associated Macrophages, Osteoclasts and the FMS Receptor. *Leukemia* **2009**, *23* (3), 590–594.

(89) Korashy, H. M.; Rahman, A. F. M. M.; Kassem, M. G. Dasatinib. In *Profiles of Drug Substances, Excipients and Related Methodology*; Elsevier, 2014; Vol. 39, pp 205–237.

(90) Srinivasarao, M.; Low, P. S. Ligand-Targeted Drug Delivery. *Chem. Rev.* **2017**, *117* (19), 12133–12164.

(91) Srinivasarao, M.; Galliford, C. V.; Low, P. S. Principles in the Design of Ligand-Targeted Cancer Therapeutics and Imaging Agents. *Nat. Rev. Drug Discov.* **2015**, *14* (3), 203–219.

(92) Xia, W.; Low, P. S. Folate-Targeted Therapies for Cancer. *J. Med. Chem.* **2010**, *53* (19), 6811–6824.

(93) *Bio-Targets and Drug Delivery Approaches*; Maiti, S., Sen, K. K., Eds.; Taylor & Francis: Boca Raton, 2017.

(94) Subramanian, G.; McAfee, J. G.; Blair, R. J.; Kallfelz, F. A.; Thomas, F. D. Technetium-99m-Methylene Diphosphonate--a Superior Agent for Skeletal Imaging: Comparison with Other Technetium Complexes. *J. Nucl. Med. Off. Publ. Soc. Nucl. Med.* **1975**, *16* (8), 744–755.

(95) Thrall, J. H. Technetium-99m Labeled Agents for Skeletal Imaging. *CRC Crit. Rev. Clin. Radiol. Nucl. Med.* **1976**, *8* (1), 1–31.

(96) Stapleton, M.; Sawamoto, K.; Alméciga-Díaz, C.; Mackenzie, W.; Mason, R.; Orii, T.; Tomatsu, S. Development of Bone Targeting Drugs. *Int. J. Mol. Sci.* **2017**, *18* (7), 1345.

(97) Lin, J. H. Bisphosphonates: A Review of Their Pharmacokinetic Properties. *Bone* **1996**, *18* (2), 75–85.

(98) Botelho, M. G.; Chan, A. W. K.; Newsome, P. R. H.; McGrath, C. P.; Lam, W. Y. H. A Randomized Controlled Trial of Home Bleaching of Tetracycline-Stained Teeth. *J. Dent.* **2017**, *67*, 29–35.

(99) Sekido, T.; Sakura, N.; Higashi, Y.; Miya, K.; Nitta, Y.; Nomura, M.; Sawanishi, H.; Morito, K.; Masamune, Y.; Kasugai, S.; et al. Novel Drug Delivery System to Bone Using Acidic Oligopeptide: Pharmacokinetic Characteristics and Pharmacological Potential. *J. Drug Target.* **2001**, *9* (2), 111–121.

(100) Minamizaki, T.; Yoshiko, Y. The Bioactive Acidic Serine- and Aspartate-Rich Motif Peptide. *Curr. Protein Pept. Sci.* **2015**, *16* (3), 196–202.

(101) Low, S. A.; Galliford, C. V.; Yang, J.; Low, P. S.; Kopeček, J. Biodistribution of Fracture-Targeted GSK3β Inhibitor-Loaded Micelles for Improved Fracture Healing. *Biomacromolecules* **2015**, *16* (10), 3145–3153.

(102) Kasugai, S.; Fujisawa, R.; Waki, Y.; Miyamoto, K.; Ohya, K. Selective Drug Delivery System to Bone: Small Peptide (Asp)6 Conjugation. *J. Bone Miner. Res. Off. J. Am. Soc. Bone Miner. Res.* **2000**, *15* (5), 936–943.

(103) Low, S. A.; Galliford, C. V.; Jones-Hall, Y. L.; Roy, J.; Yang, J.; Low, P. S.; Kopeček, J. Healing Efficacy of Fracture-Targeted GSK3β Inhibitor-Loaded Micelles for Improved Fracture Repair. *Nanomed.* **2017**, *12* (3), 185–193.

(104) Yokogawa, K.; Miya, K.; Sekido, T.; Higashi, Y.; Nomura, M.; Fujisawa, R.; Morito, K.; Masamune, Y.; Waki, Y.; Kasugai, S.; et al. Selective Delivery of Estradiol to Bone by Aspartic Acid Oligopeptide and Its Effects on Ovariectomized Mice. *Endocrinology* **2001**, *142* (3), 1228–1233.

CHAPTER 2. IN VITRO EVALUATION OF THE EFFECT OF DASATINIB TREATMENT ON OSTEOBLASTS

2.1 Introduction

2.1.1 The Effect of Src Inhibition on Bone Cells

As discussed in Chapter 1, the potential that Src inhibition might be a good bone-anabolic strategy for has driven us to examine the efficacy of Src inhibition on fracture healing. The essential role Src plays in osteoclast activity has long been well-documented;[1,2] however, it would be premature to conclude that the increased bone formation in *Src*-knockout mice is a result of an impaired bone resorption process. Although the potent Src inhibitor dasatinib inhibited both the formation and activity of osteoclasts *in vitro*[3], reports in the literature claimed that the number of osteoclasts derived from *Src*-KO mice were actually increased, measuring more than twice that in wild-type (WT) mice[4,5]. Also, a marked increase in both osteoblast number and activity was observed *in vivo* on *Src*-KO mice[5]. These results confirmed that the osteopetrosis phenotype of *Src*-KO mice was not a result of reduced osteoclast formation, but rather of boosted osteoblast activity as well as reduced osteoclast function. These observations suggest that instead of being merely anti-resorptive as traditionally believed, Src inhibition might actually be bone-anabolic by stimulating osteoblast differentiation and function. This has made Src inhibition a promising bone-anabolic strategy for our purpose of accelerating bone fracture repair.

2.1.2 Dasatinib, a Potent Src Inhibitor

Dasatinib is a small-molecule Src kinase inhibitor with an IC_{50} of 0.8 nM. It has been developed by Bristol-Myers-Squibb for the primary indication of CML and approved by

the FDA in 2006. Our initial speculation that dasatinib might be a potential drug for fracture repair has been reinforced by multiple reports of dasatinib being a potential bone-modifying agent.[3,6–8] However, results from those reports are not only conflicting and confusing, but are mainly focused on the effect of dasatinib on osteoclasts, presumably owing to the dogma that Src pathway is only involved in osteoclastogenesis. Due to the limited documentation of the direct effect of Src inhibition on osteoblasts and the conflicting results of whether Src inhibition is anti-resorptive, we have undertaken to elucidate the relationship between Src inhibition by dasatinib and osteoblastic function and differentiation.

In this Chapter, we are studying a murine pre-osteoblastic cell line (MC3T3-E1) cultured in mineralization media containing different concentrations of dasatinib to evaluate the effect of the Src kinase inhibitor, dasatinib, on osteoblast differentiation and function *in vitro*.

2.1.3 Genes Selected for the Evaluation of Dasatinib's Effects on Osteoblasts

In order to fully assess the interaction between dasatinib and osteoblasts, expression of essential genes involved in osteoblast differentiation and function need to be analyzed with and without exposure to dasatinib. Representatives of three classes of genes were selected for this evaluation: a) genes necessary for the differentiation of osteoblasts from mesenchymal precursors, e.g. RUNX2, and Osx[9,10]; b) genes for intracellular enzymes and extracellular matrix proteins indicative of osteoblastic function, e.g. ALP, COL1A1, and OPN[11,12]; c) genes for factors that regulate osteogenesis, e.g. RANKL, and OPG[13,14]. The formation and differentiation of osteoblasts from mesenchymal precursors are regulated by multiple transcription factors, with RUNX2 and Osx being two of the most important

ones.[15] RUNX2 and Osx are critical for the maturation of osteoblasts, and a lack of either genes would lead to a cartilaginous skeleton caused by impaired mineralization, and even perinatal lethality.[10,16] ALP hydrolyzes organic monophosphates and inorganic pyrophosphates to produce inorganic phosphates, which promotes mineralization of hard tissue[17]. Type-I collagen is the most abundant protein in the organic scaffold in bone that mineralization takes place, and plays an important role in the tensile strength of the bone[12,18]. The distribution of OPN is rich on cell-matrix and matrix-matrix interfaces in bone; it facilitates the attachment of bone cells to bone matrix as well as increases the physical strength of the bone tissue[11,19]. The binding of RANKL to RANK on osteoclasts promotes osteoclastogenesis, while OPG functions as the decoy receptor for RANKL by binding to RANKL and inhibiting its interaction with RANK. Osteoblasts express RANKL to stimulate bone resorption as they mature to keep a tight regulation between bone formation and resorption[14]. At the meantime, a housekeeping gene, GAPD, was used as the reference gene.

In addition to the target genes mentioned above, the enzymatic activity of intracellular ALP was measured with a colorimetric enzyme kinetic assay. ALP activity has been widely used as a reliable marker for osteoblast differentiation.[20]

2.2 Materials and Methods

2.2.1 Culture of a Murine Pre-Osteoblastic Cell Line, MC3T3-E1

A murine pre-osteoblast cell line (MC3T3-E1) was purchased from American Type Culture Collection (ATCC) and cultured in α-MEM without ascorbic acid (Gibco, Thermo Fisher Scientific, Waltham, MA), supplemented with 10% HI-FBS (VWR, Chicago, IL) and 1% penicillin/streptomycin (Corning, Corning, NY) as monolayers at 37 °C in a 5%

CO_2/95% humidified-air atmosphere. 24-well plates were seeded with 0.05 million cells per well, followed by a switch to mineralization media (α-MEM (Gibco, Thermo Fisher Scientific, Waltham, MA) supplemented with 10% HI-FBS, 1% penicillin/streptomycin, and 10 mM β-glycerophosphate) when cells reached confluence, which marked Day 0 of mineralization. Media in each well was switched every 3 days to fresh mineralization media containing the desired concentration of dasatinib (20 mM stock solution dissolved in DMSO). For this purpose, the stock solution was diluted with PBS, sterile-filtered and further diluted in mineralization media to yield media with various concentrations of dasatinib.

2.2.2 Real-Time Quantitative PCR

To determine the mRNA levels of diagnostic markers for osteoblast differentiation and activation, cultured cells (3 wells per dasatinib concentration) were analyzed by real-time quantitative PCR with SYBR Green dye (SensiFAST™ SYBR® No-ROX Kit; Bioline, Taunton, MA). Briefly, total cell RNA from each study group was extracted and purified using a GenCatch Total RNA Extraction Kit (Epoch Life Science, Sugar Land, TX). Approx. 900 ng RNA were reverse transcribed using High-Capacity cDNA Reverse Transcription Kit (Thermo Fisher Scientific, Waltham, MA) on a Bio-Rad T100 Thermal Cycler. cDNA samples were diluted 7.5× before real-time reactions were performed on a Bio-Rad CFX Connect Real Time System using 40 cycles at 95 °C for 5 s, 60 °C for 10 s, and 72 °C for 20 s. Primers for each target gene and the housekeeping gene (Runx2, Osx, Col1A1, ALP, OPN, OPG, RANKL, GAPDH) were purchased from Integrated DNA Technologies (Coralville, IA). Technical triplicates were performed for each of the three biological replicates in each treatment group to ensure reliability of results. The Cq values

obtained were analyzed using the ΔΔCq method and presented as the relative expression level between each target gene and the reference gene (GAPDH). All relative expression levels were normalized against the control (DMSO) value.

2.2.3 Quantitation of Alkaline Phosphatase Activity

Alkaline phosphatase (ALP) activity was quantified with SensoLyte ALP Kit (AnaSpec, Fremont, CA) following the instructions provided by the manufacturer. Briefly, cells in a 24-well plate were washed twice with ice-cold lysis buffer and then lysed in the same buffer supplemented with 0.5% Triton-X 100. Whole cell lysates were collected, centrifuged at 2500g for 10 minutes, then mixed with *p*-nitrophenol phosphate. The absorbance at 405 nM was measured every 5 minutes for 1 hour at 37 °C. The ALP activity was calculated from the rate of absorbance change, using only data with a linear correlation coefficient of $R^2 > 0.99$. Protein content in each whole cell lysate was also determined using QuickStart Bradford Assay Kit (Bio-Rad, Hercules, CA) according to manufacturer's procedures.

2.3 Results

2.3.1 Expression of Osteogenesis-Related Genes in Response to Dasatinib Treatment

Analysis of osteoblast-related gene expression on days 7 and 14 revealed that transcripts of RUNX2 and OSX were significantly upregulated in MC3T3-E1 cells during exposure to 100 nM dasatinib (Fig. 2.1A-B), indicating a strong stimulation of osteoblastic differentiation.

Fig. 2.1 Dasatinib Stimulates Expression of Multiple Osteogenic Genes. (**A**)-(**G**) Mouse pre-osteoblastic cell line MC3T3-E1 was incubated in mineralization media containing 100 nM dasatinib or DMSO (n = 3 for all groups) and expression levels of selected bone remodeling genes were analyzed and normalized to GAPDH. Specifically, (**I**) shows the ratio of OPG and RANKL expression. (**H**) MC3T3-E1 cells were cultured in mineralization media containing 10 nM, 50 nM, or 100 nM dasatinib or DMSO only, and the enzymatic activity of intracellular alkaline phosphatase (ALP) was measured. Levels of statistical significance are denoted with asterisks according to the following definition: *$p < 0.05$; **$p < 0.01$; ***$p < 0.001$; ****$p < 0.0001$.

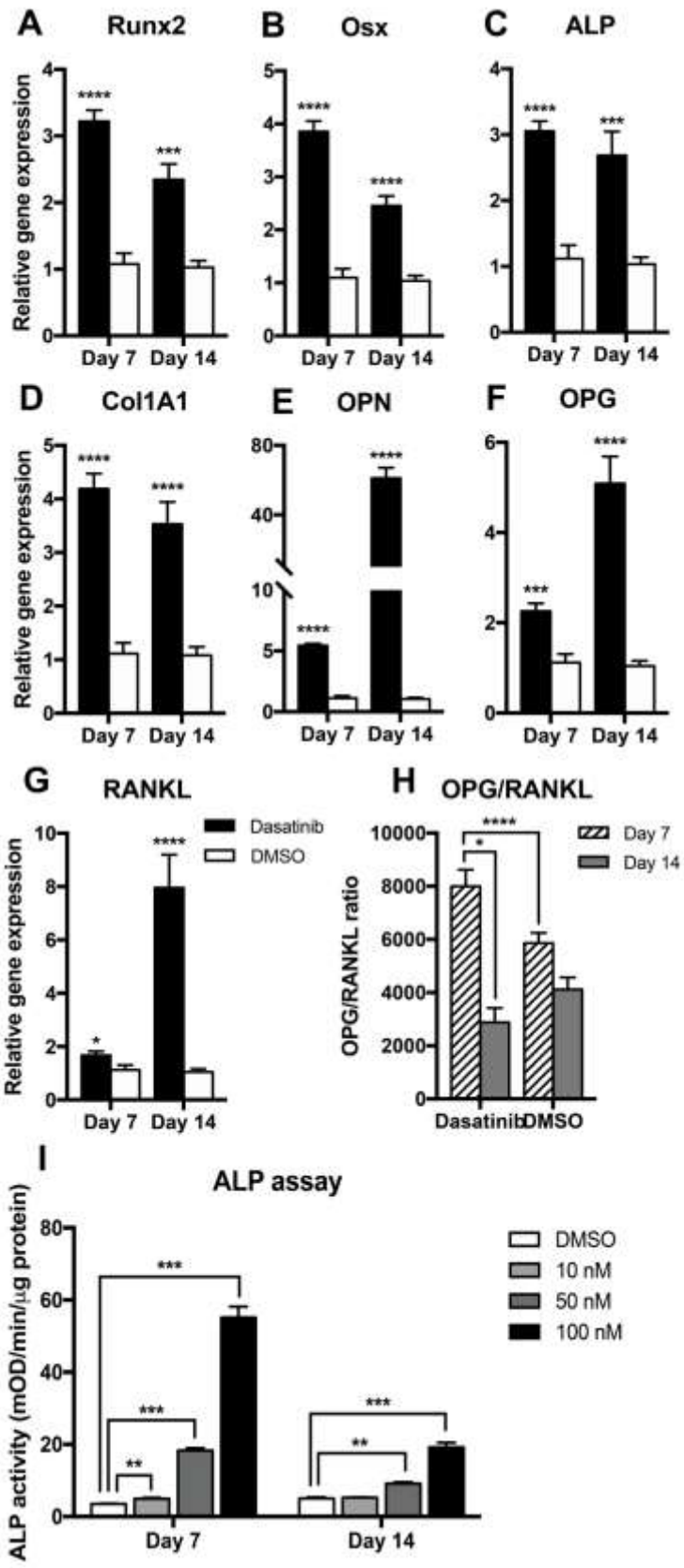
A
Runx2
B
Osx
C
ALP
Relative gene expression
Day 7
Day 14
D
Col1A1
E
OPN
F
OPG
G
RANKL
Dasatinib
DMSO
H
OPG/RANKL
Day 7
Day 14
OPG/RANKL ratio
Dasatinib
DMSO
I
ALP assay
ALP activity (mOD/min/μg protein)
DMSO
10 nM
50 nM
100 nM

Furthermore, Dasatinib has also upregulated the expression of ALP, COL1A1 and OPN (Fig. 2.1C-E), which confirmed its potent ability to facilitate osteoblastic functions by the production of alkaline phosphatase, collagen matrix and osteopontin. Dasatinib treatment also boosted the expression of OPG and RANKL (Fig. 2.1F-G). Moreover, the ratio of OPG to RANKL, a measure of the balance between osteoblastogenesis and osteoclastogenesis, was observed to strongly shift towards the former after 7 days of dasatinib treatment, but this inclination for osteoblastogenesis over osteoclastogenesis was reduced significantly during the following week of dasatinib administration (Fig. 2.1H).

Following dasatinib treatment, ALP activity also demonstrated a strong concentration dependent increase (Fig. 2.1I), suggesting that differentiation of MC3T3-E1 cells into mature osteoblasts was induced by dasatinib.

2.4 Discussion

The seven selected genes the regulates osteoblast differentiation and function have all been upregulated 2- to 60-fold in response to dasatinib treatment. Overall, these data suggest that dasatinib could prove useful in not only promoting the differentiation of osteoblastic progenitor cells into mature bone forming osteoblasts, but enhancing the capability of osteoblasts to produce enzymes, matrix proteins and cellular factors that boost bone growth. The data collectively indicate that treatment of an osteoblast precursor with a Src kinase inhibitor (dasatinib) can reprogram a pre-osteoblastic cell to express genes involved in bone regenerating processes, in accordance with findings from other studies.[6,7,21,22]

Importantly, as Fig. 2.1G and Fig. 2.1H suggest, MC3T3-E1 cells upregulated the expression of RANKL after dasatinib treatment, especially in the late stage of

differentiation, indicating an attempt to elevate osteoclastogenesis. The decline in OGP/RANKL ratio at the last stage of differentiation has also strengthened this point. These data suggest that Src inhibition by dasatinib on osteoblasts would indeed suppress osteoclastogenesis by favoring OPG secretion over RANKL, but this effect considerably declines as osteoblasts further mature, during which OPG production is reduced while RANKL production is elevated. This observation, together with previous reports stating that osteoblasts derived from *Src*-KO mice demonstrated unchanged morphological features compared to those harvested from WT mice and was able to fully regulate normal osteoclast differentiation via the RANKL/RANK/OPG pathway[23], argue that Src inhibition might not function as a pure anti-resorptive agent *in vivo*. Instead, Src inhibition would stimulate osteoblast differentiation and function while suppressing osteoclastogenesis to maximize bone deposition at the early stage of fracture repair but shift towards the induction of osteoclastogenesis at later stages of the repair process, encouraging bone resorption. Since bone resorption is essential for the remodeling phase of fracture repair, this finding enhanced our confidence in dasatinib to be a potentially effective and safe drug to accelerate the natural fracture repair process.

In conclusion, in this chapter, we have demonstrated that the Src kinase inhibitor dasatinib is a potentially valuable bone-anabolic agent that potently stimulates osteoblast differentiation and function. A fracture-targeted version of dasatinib would later be generated to be tested *in vivo*.

2.5 References

(1) Miyazaki, T.; Sanjay, A.; Neff, L.; Tanaka, S.; Horne, W. C.; Baron, R. Src Kinase Activity Is Essential for Osteoclast Function. *J. Biol. Chem.* **2004**, *279* (17), 17660–17666.

(2) Burr, D. B.; Akkus, O. Bone Morphology and Organization. In *Basic and Applied Bone Biology*; Elsevier, 2014; pp 3–25.

(3) Vandyke, K.; Dewar, A. L.; Diamond, P.; Fitter, S.; Schultz, C. G.; Sims, N. A.; Zannettino, A. C. The Tyrosine Kinase Inhibitor Dasatinib Dysregulates Bone Remodeling through Inhibition of Osteoclasts in Vivo. *J. Bone Miner. Res.* **2010**, *25* (8), 1759–1770.

(4) Boyce, B. F.; Yoneda, T.; Lowe, C.; Soriano, P.; Mundy, G. R. Requirement of Pp60c-Src Expression for Osteoclasts to Form Ruffled Borders and Resorb Bone in Mice. *J. Clin. Invest.* **1992**, *90* (4), 1622–1627.

(5) Marzia, M.; Sims, N. A.; Voit, S.; Migliaccio, S.; Taranta, A.; Bernardini, S.; Faraggiana, T.; Yoneda, T.; Mundy, G. R.; Boyce, B. F.; et al. Decreased C-Src Expression Enhances Osteoblast Differentiation and Bone Formation. *J. Cell Biol.* **2000**, *151* (2), 311–320.

(6) Garcia-Gomez, A.; Ocio, E. M.; Crusoe, E.; Santamaria, C.; Hernández-Campo, P.; Blanco, J. F.; Sanchez-Guijo, F. M.; Hernández-Iglesias, T.; Briñón, J. G.; Fisac-Herrero, R. M.; et al. Dasatinib as a Bone-Modifying Agent: Anabolic and Anti-Resorptive Effects. *PLoS ONE* **2012**, *7* (4), e34914.

(7) Id Boufker, H.; Lagneaux, L.; Najar, M.; Piccart, M.; Ghanem, G.; Body, J.-J.; Journé, F. The Src Inhibitor Dasatinib Accelerates the Differentiation of Human Bone Marrow-Derived Mesenchymal Stromal Cells into Osteoblasts. *BMC Cancer* **2010**, *10* (1).

(8) Jönsson, S.; Hjorth-Hansen, H.; Olsson, B.; Wadenvik, H.; Sundan, A.; Standal, T. Second-Generation TKI Dasatinib Inhibits Proliferation of Mesenchymal Stem Cells and Osteoblast Differentiation in Vitro. *Leukemia* **2010**, *24* (7), 1357–1359.

(9) Komori, T.; Yagi, H.; Nomura, S.; Yamaguchi, A.; Sasaki, K.; Deguchi, K.; Shimizu, Y.; Bronson, R. T.; Gao, Y. H.; Inada, M.; et al. Targeted Disruption of Cbfa1 Results in a Complete Lack of Bone Formation Owing to Maturational Arrest of Osteoblasts. *Cell* **1997**, *89* (5), 755–764.

(10) Nakashima, K.; Zhou, X.; Kunkel, G.; Zhang, Z.; Deng, J. M.; Behringer, R. R.; de Crombrugghe, B. The Novel Zinc Finger-Containing Transcription Factor Osterix Is Required for Osteoblast Differentiation and Bone Formation. *Cell* **2002**, *108* (1), 17–29.

(11) Beck, G. R.; Sullivan, E. C.; Moran, E.; Zerler, B. Relationship between Alkaline Phosphatase Levels, Osteopontin Expression, and Mineralization in Differentiating MC3T3-E1 Osteoblasts. *J. Cell. Biochem.* **1998**, *68* (2), 269–280.

(12) Shi, S.; Kirk, M.; Kahn, A. J. The Role of Type I Collagen in the Regulation of the Osteoblast Phenotype. *J. Bone Miner. Res. Off. J. Am. Soc. Bone Miner. Res.* **1996**, *11* (8), 1139–1145.

(13) Boyce, B. F.; Xing, L. The RANKL/RANK/OPG Pathway. *Curr. Osteoporos. Rep.* **2007**, *5* (3), 98–104.

(14) Boyce, B. F.; Xing, L. Functions of RANKL/RANK/OPG in Bone Modeling and Remodeling. *Arch. Biochem. Biophys.* **2008**, *473* (2), 139–146.

(15) Bellido, T.; Plotkin, L. I.; Bruzzaniti, A. Bone Cells. In *Basic and Applied Bone Biology*; Elsevier, 2014; pp 27–45.

(16) Lu, X.; Beck, G. R.; Gilbert, L. C.; Camalier, C. E.; Bateman, N. W.; Hood, B. L.; Conrads, T. P.; Kern, M. J.; You, S.; Chen, H.; et al. Identification of the Homeobox Protein Prx1 (MHox, Prrx-1) as a Regulator of Osterix Expression and Mediator of Tumor Necrosis Factor α Action in Osteoblast Differentiation. *J. Bone Miner. Res.* **2011**, *26* (1), 209–219.

(17) Orimo, H. The Mechanism of Mineralization and the Role of Alkaline Phosphatase in Health and Disease. *J. Nippon Med. Sch. Nippon Ika Daigaku Zasshi* **2010**, *77* (1), 4–12.

(18) Viguet-Carrin, S.; Garnero, P.; Delmas, P. D. The Role of Collagen in Bone Strength. *Osteoporos. Int.* **2006**, *17* (3), 319–336.

(19) Denhardt, D. T.; Noda, M. Osteopontin Expression and Function: Role in Bone Remodeling. *J. Cell. Biochem. Suppl.* **1998**, *30–31*, 92–102.

(20) Rutkovskiy, A.; Stensløkken, K.-O.; Vaage, I. J. Osteoblast Differentiation at a Glance. *Med. Sci. Monit. Basic Res.* **2016**, *22*, 95–106.

(21) Cappariello, A.; Loftus, A.; Muraca, M.; Maurizi, A.; Rucci, N.; Teti, A. Osteoblast-Derived Extracellular Vesicles Are Biological Tools for the Delivery of Active Molecules to Bone. *J. Bone Miner. Res. Off. J. Am. Soc. Bone Miner. Res.* **2018**, *33* (3), 517–533.

(22) Lee, Y.-C.; Huang, C.-F.; Murshed, M.; Chu, K.; Araujo, J. C.; Ye, X.; deCrombrugghe, B.; Yu-Lee, L.-Y.; Gallick, G. E.; Lin, S.-H. Src Family Kinase/Abl Inhibitor Dasatinib Suppresses Proliferation and Enhances Differentiation of Osteoblasts. *Oncogene* **2010**, *29* (22), 3196–3207.

(23) Lowe, C.; Yoneda, T.; Boyce, B. F.; Chen, H.; Mundy, G. R.; Soriano, P. Osteopetrosis in Src-Deficient Mice Is Due to an Autonomous Defect of Osteoclasts. *Proc. Natl. Acad. Sci. U. S. A.* **1993**, *90* (10), 4485–4489.

CHAPTER 3. SYNTHESIS AND CHARACTERIZATION OF THE DASATINIB-ASPARTIC$_{10}$ CONJUGATE (DAC) AND ASPARTIC$_{10}$-S0456 DYE CONJUGATE

3.1 Introduction

As introduced in Chapter 1, a novel, systemically-administered drug for the acceleration of bone fracture repair would benefit from targeted drug delivery, which could be realized by utilizing a fracture-specific deca-aspartic acid (D_{10}) targeting ligand. Thus, we have designed a dasatinib-aspartic$_{10}$ conjugate (DAC) that combines the bone-anabolic efficacy of dasatinib and the fracture-targeting capability of D_{10}. This conjugate is synthesized chemically via a simple and convergent synthetic route, where the D_{10} targeting ligand is synthesized with solid-phase peptide synthesis (SPPS) for its efficiency and high yield,[1] and is later joined to dasatinib with a "click" style reaction. The modularity of this route has enabled us to easily modify it to produce D_{10}-conjugates of other potential bone-anabolic molecules.

In this Chapter, we report the successful synthesis of DAC (Fig. 3.1). As a demonstration of the adaptivity of our synthetic strategy, we also report a slightly modified version of this route for the successful synthesis of a D_{10}-targeted near-IR dye, S0456 (Fig. 3.2). This conjugate is valuable in studying the *in vivo* distribution of the D_{10} targeting ligand, which is a useful addition to previous reports of the biodistribution of other oligo-aspartic acid ligands.[2–4]

3.2 Materials and Methods

3.2.1 Materials

All materials, solvents and reagents were purchased from commercial sources and used without further purification unless specifically noted. DMF, DMSO, TFA, piperidine, TEA, DIPEA, IPA, MeOH, DCM, Et_2O, and β-glycerophosphate were purchased from Sigma-Aldrich (St. Louis, MO). Fmoc-L-Asp(OtBu)-OH, Fmoc-S-trityl-L-cysteine, TIPS, and EDT were purchased from Chem-Impex International (Wood Dale, IL). PyBOP and dasatinib were obtained from AK Scientific (Union City, CA), while 2-chlorotrityl chloride resin was purchased from ChemPep, Inc. (Wellington, FL). 3-maleimidopropionic acid was purchased from Combi-Blocks (San Diego, CA). Mass spectra were obtained on Agilent Technologies 1220 series LC-coupled 6130 quadrupole MS. HPLC purifications were performed on an Agilent Technologies 1200 series semi-preparatory HPLC. Regular phase flash column chromatography was performed on Teledyne CombiFlash Rf+ Lumen system. NMR spectra were obtained on a Bruker Avance III 500 HD Spectrometer.

3.2.2 Synthesis of D_{10}-Cys

For the initial loading of the SPPS resin, 2-chlorotrityl chloride resin (0.4 g, 1.4 mmol/g) was swollen in DCM (10 mL/g resin) followed by addition of Fmoc-L-Asp(OtBu)-OH (1.15 g, 2.8 mmol) and DIPEA (1.66 mL, 9.5 mmol) dissolved in DCM (14 mL). The mixture was agitated by bubbling argon for 1 hour, after which the solution was drained before 20 mL of capping cocktail (DCM:MeOH:DIPEA = 17:2:1) was added and the solution was again bubbled for 20 minutes. The resin was then subjected to standard washing procedures which consisted of washes with DMF (3 times), DCM (3 times) and IPA (3 times) following each coupling reaction, and washes with DMF (3 times) following

each deprotection. After the initial loading, all subsequent coupling reactions were performed with solutions of Fmoc-L-Asp(OtBu)-OH (1.15 g, 2.8 mmol) or Fmoc-S-trityl-L-cysteine (1.64 g, 2.8 mmol), PyBOP (1.42 g, 2.75 mmol), and DIPEA (1.66 mL, 9.5 mmol) in DMF (14 mL). One-hour standard coupling time was used for all aspartic acid and cysteine residues. Fmoc-deprotection was done with 20% piperidine solution in DMF for two sessions of 5 minutes and 10 minutes each. The 11-mer peptidic product was cleaved off the resin using a cleavage cocktail consisting of 90% TFA, 3.3% TIPS, 3.3% water and 3.3% EDT. Following cleavage, the crude product was concentrated under reduced pressure to remove most TFA, water, TIPS, and EDT, and then washed 3x with Et_2O, dried under reduced pressure for 24 hours to give **1** as a white powder (680 mg, 81.3% overall yield, 98.1% average coupling efficiency).

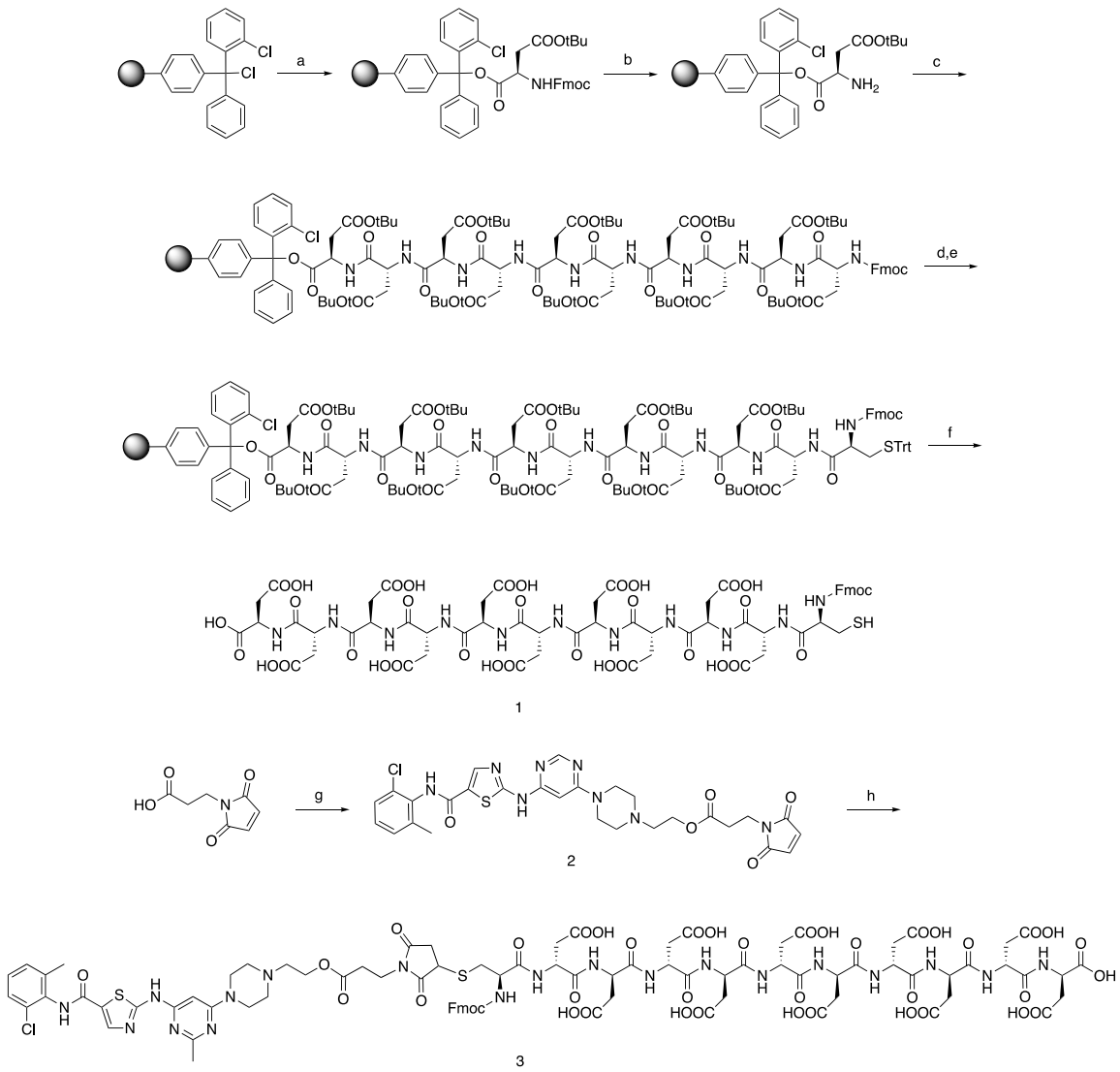

Fig. 3.1 Synthesis for DAC.
Reagents and conditions: a) Fmoc-L-Asp(OtBu)-OH, DIPEA, DCM, 1 h; b) 20% piperidine in DMF, 5 min and 10 min; c) Fmoc-L-Asp(OtBu)-OH, PyBOP, DIPEA, DMF, 1 h; d) 20% piperidine in DMF, 5 min and 10 min; e0 Fmoc-*S*-trityl-L-cysteine, PyBOP, DIPEA, DMF, 1 h; (f) cleavage cocktail (90% TFA, 3.3% TIPS, 3.3% water and 3.3% EDT), 20 min, 81% overall; (g) dasatinib, PyBOP, DIPEA, DMF, 4h, 68%; (h) **1**, DMSO, 5h, 32%.

3.2.3 Synthesis of 2-(4-(6-((5-((2-chloro-6-methylphenyl)carbamoyl)thiazol-2-yl)amino)-2-methylpyrimidin-4-yl)piperazin-1-yl)ethyl 3-(2,5-dioxo-2,5-dihydro-1H-pyrrol-1-yl)propanoate (Dasatinib-Maleimide)

3-maleimidopropionic acid (200 mg, 1.18 mmol) and PyBOP (572 mg, 1.10 mmol) were dissolved in 5 mL anhydrous DMF in a 50-mL round-bottom flask degassed with

argon. The flask was cooled on ice and diisopropylethylamine (1.03 mL, 5.9 mmol) was added and stirred for 5 minutes. Dasatinib (360 mg, 0.738 mmol) dissolved in 2 mL anhydrous DMF was then added dropwise to the mixture and the reaction mixture was warmed slowly to room temperature with stirring over the ensuing 4 hours. Ethyl acetate (~50 ml) was added to the reaction flask and the diluted mixture was washed 2x with DI water followed by 4 washes with saturated aqueous NaCl. The organic phase was then collected, dried over sodium sulfate and concentrated *in vacuo* to yield the crude product. The crude product was purified by flash column chromatography on Teledyne CombiFlash Rf+ Lumen (0-25% MeOH in DCM) to give **2** as a pale-yellow powder (320 mg, 68%).

3.2.4 Synthesis of Dasatinib-Aspartic$_{10}$ Conjugate (DAC)

2 (300 mg, 0.47 mmol) was dissolved in 5.5 mL anhydrous DMSO in a 25-mL round-bottom flask degassed with argon. 640 mg Asp$_{10}$-Cys (**1**) (0.43 mmol) was added quickly to the aforementioned solution and stirred until all solid dissolved. The reaction mixture was stirred for 1 hour under argon atmosphere before purification using preparatory reverse phase HPLC. Pure fractions were collected, concentrated *in vacuo* to remove acetonitrile, frozen and lyophilized to yield the final product DAC (**3)** as a fluffy white solid (228 mg, 32%).

3.2.5 Synthesis of S0456-Maleimide

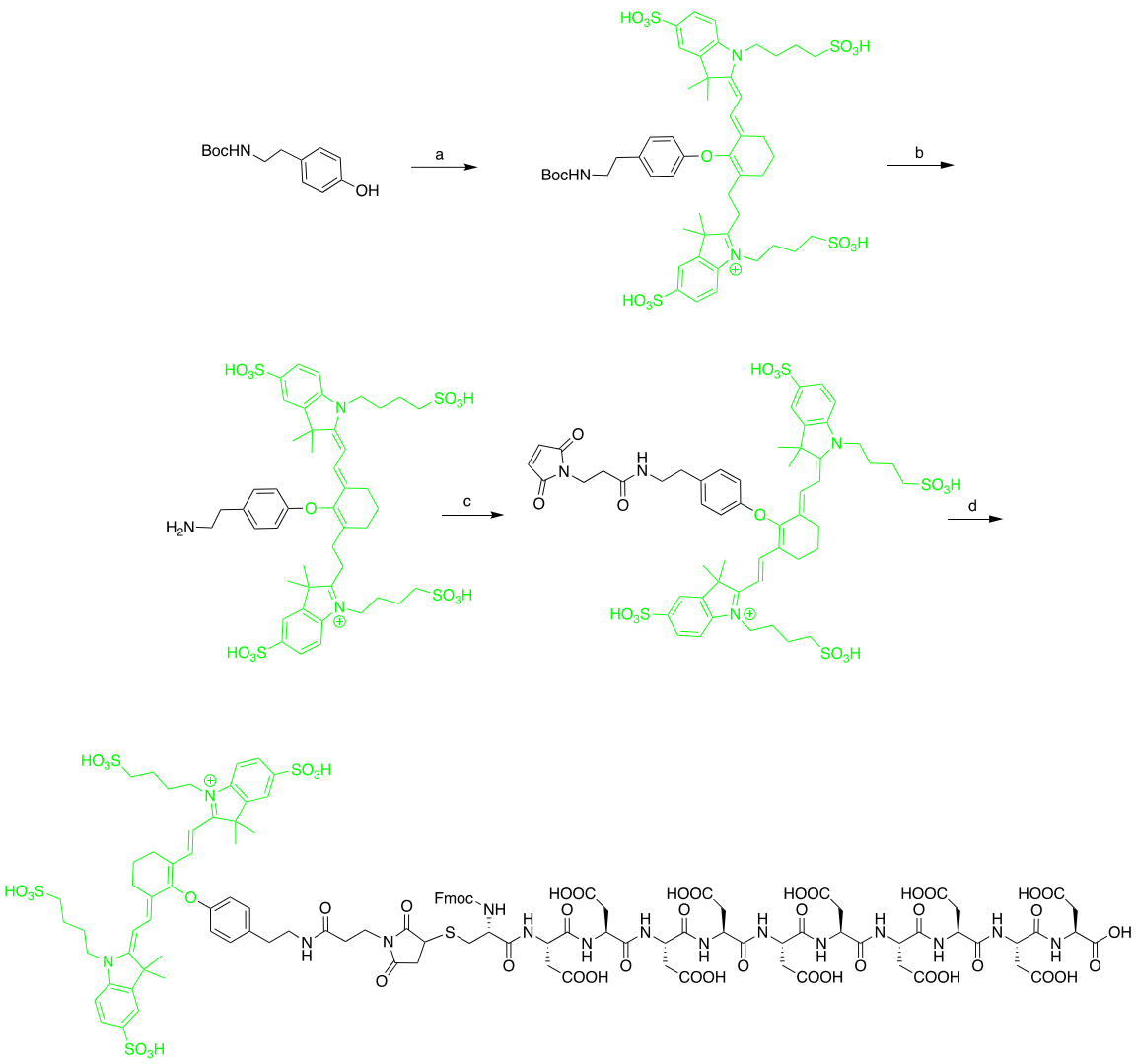

Fig. 3.2 Synthesis of D_{10}-S0456 Conjugate.
Reagents and conditions: a) S0456-Cl, DIPEA, DMSO, 60 °C, quant.; b) 40% TFA/DCM, rt, 47%.; c) N-succinimidyl 3-maleimidopropionate, DIPEA, DMSO, rt, 91%; d) D_{10}-cys, DMSO, rt, 25%.

S0456, boc-tyramine and KOH were charged into a degassed 50-mL RB flask. 5 mL DMSO was added to dissolve all solid, then the mixture was stirred at 60 °C under argon atmosphere for 1.2 hours. The resulting mixture was cooled to room temperature and added to cold ethyl acetate (50 mL) dropwise. The resulting mixture was vigorously agitated, then

centrifuged at 3000 rpm for 3 minutes. After centrifugation, dark green solid can be seen on the bottom of the conical tube. The supernatant (very slightly greenish clear solution) was discarded before a new batch of cold ethyl acetate was added to the solid. The mixture was vigorously agitated and subjected to the same centrifugation process as before. The resulting dark green solid was dried in a vacuum desiccator overnight before 5 mL 40 % TFA/DCM solution was added, together with 5% TIPS as a cation scavenger. The mixture was stirred at rt for 30 mins before being concentrated *in vacuo* to remove all TFA and DCM. The concentrated crude was dissolved in 3 mL water and subject to prep-HPLC purification. Pure fractions of S0456-tyramine were collected, concentrated in vacuo, frozen, and lyophilized to yield the pure product as a dark green fluffy solid. This solid (120 mg) was dissolved in 3 mL DMSO together with N-succinimidyl 3-maleimidopropionate (30 mg) and DIPEA (40 μL) and stirred under argon atmosphere for one hour before purification with prep-HPLC. Pure fractions of S0456-maleimide were collected, concentrated in vacuo, frozen, and lyophilized to yield the pure product as a dark green fluffy solid (125 mg).

3.2.6 Synthesis of D_{10}-S0456 Conjugate

S0456-maleimide (100 mg) was dissolved in 2 mL DMSO in a flask degassed with argon, followed by the addition of D_{10}-cys to the solution with stirring. The mixture was stirred at room temperature for 2.5 hours before purification with prep-HPLC. The purified and lyophilized product appeared as a green fluffy solid (57 mg).

3.3 Characterization of Intermediates and Products

In this section, mass spectra of D_{10}-cys, dasatinib-maleimide, DAC, and D_{10}-S0456, together with HPLC chromatograms of DAC and D_{10}-S0456 are reported. Mass spectra verify the correct composition of the aforementioned compounds. HPLC chromatograms of the two final conjugates serve as proof of purity for animal use.

3.3.1 Mass Spectrometry

D_{10}-cys: LRMS− LC/MS (m/z): $[M - H]^-$ calculated for $C_{58}H_{67}N_{11}O_{34}S$, 1492.4; found, 1492.4 ($[M - H]^-$), 745.7 ($[M-2]^{2-}/2$).

Dasatinib-maleimide: LRMS− LC/MS (m/z): $[M + H]^+$ calculated for $C_{29}H_{31}ClN_8O_5S$, 639.2; found, 639.1.

DAC: LRMS− LC/MS (m/z): $[M - H]^-$ calculated for $C_{87}H_{98}ClN_{19}O_{39}S_2$, 2131.5; found, 1064.8 ($[M-2]^{2-}/2$), 709.5 ($[M-3]^{3-}/3$).

D_{10}-S0456: LRMS− LC/MS (m/z): $[M - H]^-$ calculated for $C_{111}H_{130}N_{15}O_{50}S_5$, 2632.7; found, 1315.3 ($[M-2]^{2-}/2$), 876.6 ($[M-3]^{3-}/3$).

3.3.2 HPLC Chromatograms

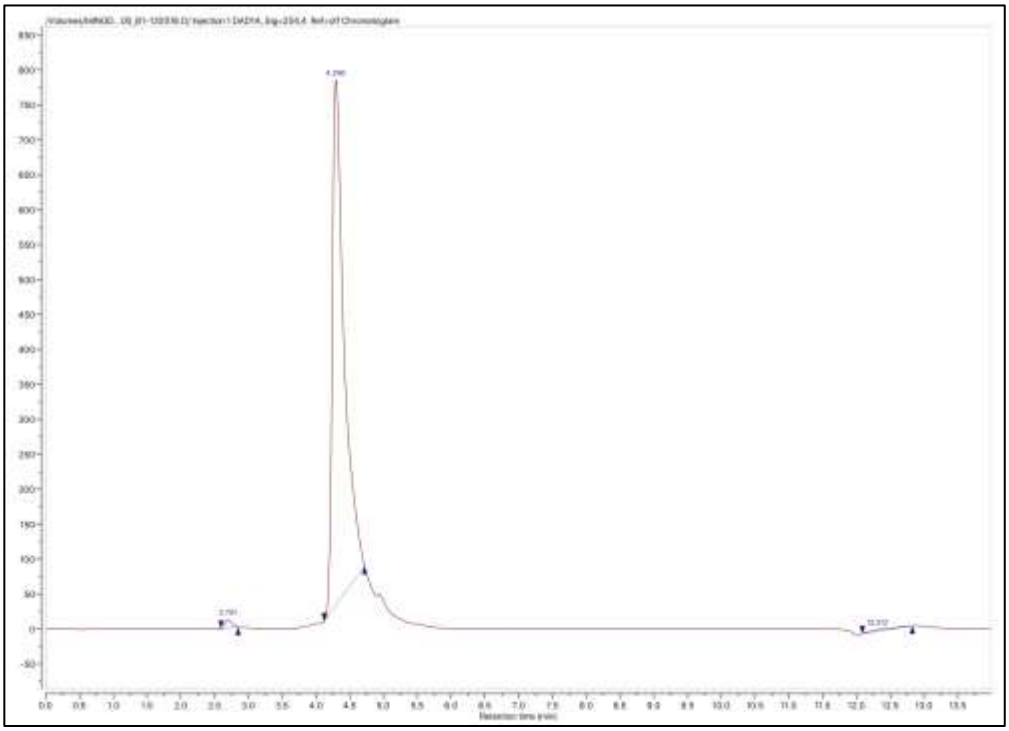

Fig. 3.3 HPLC Chromatogram for DAC.

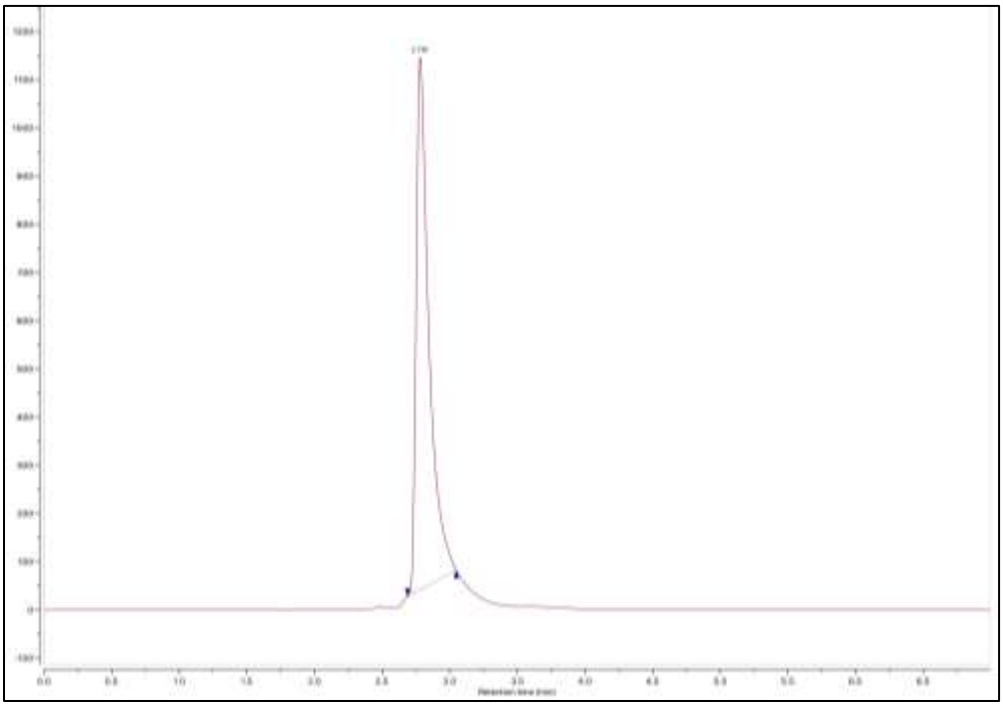

Fig. 3.4 HPLC Chromatogram for D_{10}-S0456 Conjugate.

3.4 Discussion

3.4.1 Synthesis of DAC

As shown in Fig. 3.1, the synthesis of DAC is divided into two halves: synthesis of D_{10}-cys, and synthesis of dasatinib-maleimide. The two halves are finally joined by a nucleophilic addition between a thiol group on the peptide and a maleimide group on the dasatinib-maleimide half. The thiol-maleimide "click" reaction is highly specific and efficient,[5,6] lending this synthetic route the flexibility to be applied to other drug payloads with ease. The peptidic half is synthesized by standard fluorenylmethoxycarbonyl (Fmoc) solid phase peptide synthesis (SPPS), which has given high yield while only taking 3-4 days to complete. Overall, this synthetic route is simple, efficient, and convergent, with the ability to be expanded to other potential bone-anabolic molecules with free hydroxyl/thiol/oxime functional groups.

3.4.2 Synthesis of D_{10}-S0456 Dye Conjugate

Synthesis of the D_{10}-S0456 conjugate is an extrapolation of the convergent synthesis of DAC discussed in the previous section. Synthesis of the targeting peptide has been kept unchanged, and in order to react with N-succinimidyl 3-maleimidopropionate, an amine group is added to S0456 in the form of tyramine via nucleophilic substitution. The resulting S0456-maleimide reacts with the thiol group on D_{10}-cys via the same thiol-maleimide "click" reaction. In Chapter 6, more molecules will be conjugated with D_{10}-cys using this convergent synthetic system.

In conclusion, D_{10}-S0456 and DAC have both been successfully synthesized and purified. Next, a mouse model of femoral fracture will be implemented to test the fracture-

targeting ability of D_{10}-S0456, and most importantly, DAC's efficacy to promote bone fracture healing.

3.5 References

(1) Palomo, J. M. Solid-Phase Peptide Synthesis: An Overview Focused on the Preparation of Biologically Relevant Peptides. *RSC Adv* **2014**, *4* (62), 32658–32672.

(2) Low, S. A.; Galliford, C. V.; Yang, J.; Low, P. S.; Kopeček, J. Biodistribution of Fracture-Targeted GSK3β Inhibitor-Loaded Micelles for Improved Fracture Healing. *Biomacromolecules* **2015**, *16* (10), 3145–3153.

(3) Ishizaki, J.; Waki, Y.; Takahashi-Nishioka, T.; Yokogawa, K.; Miyamoto, K.-I. Selective Drug Delivery to Bone Using Acidic Oligopeptides. *J. Bone Miner. Metab.* **2009**, *27* (1), 1–8.

(4) Sekido, T.; Sakura, N.; Higashi, Y.; Miya, K.; Nitta, Y.; Nomura, M.; Sawanishi, H.; Morito, K.; Masamune, Y.; Kasugai, S.; et al. Novel Drug Delivery System to Bone Using Acidic Oligopeptide: Pharmacokinetic Characteristics and Pharmacological Potential. *J. Drug Target.* **2001**, *9* (2), 111–121.

(5) Nair, D. P.; Podgórski, M.; Chatani, S.; Gong, T.; Xi, W.; Fenoli, C. R.; Bowman, C. N. The Thiol-Michael Addition Click Reaction: A Powerful and Widely Used Tool in Materials Chemistry. *Chem. Mater.* **2014**, *26* (1), 724–744.

(6) Northrop, B. H.; Frayne, S. H.; Choudhary, U. Thiol–Maleimide "Click" Chemistry: Evaluating the Influence of Solvent, Initiator, and Thiol on the Reaction Mechanism, Kinetics, and Selectivity. *Polym Chem* **2015**, *6* (18), 3415–3430.

CHAPTER 4. IN VIVO EVALUATION OF THE BONE-FRACTURE TARGETING CAPABILITY OF ASPARTIC$_{10}$ AND DAC'S EFFICACY FOR THE ACCELERATION OF BONE-FRACTURE REPAIR

4.1 Introduction

To test our hypothesis that targeted delivery of dasatinib to bone fracture site may accelerate the rate of fracture repair, we need to first verify the fracture-targeting capability of D_{10}, then test the D_{10}-targeted version of dasatinib, DAC, on fracture-bearing mice for its efficacy to enhance fracture repair. Despite multiple reports on the *in vitro* influence of dasatinib on bone cells,[1–5] to the best of our knowledge, this is the first report of dasatinib (or any of its derivatives) being examined *in vivo* for a bone-fracture-related purpose.

Beside the investigation of the potential clinical implications of a fracture-targeted dasatinib conjugate, another important objective of the *in vivo* studies is elucidating whether dasatinib acts as a mere antiresorptive agent, and whether its reported inhibitory effect to osteoclastogenesis obstructs the bone remodeling stage of fracture repair. Should the answer to either question be negative, DAC might not be suited as a therapy for bone fracture repair, because bone remodeling is essential and the lack of such would result in an unresolved fracture callus with poor mechanical properties.[6] In this chapter, we report that DAC is a potent bone-anabolic agent that promotes bone fracture repair *in vivo*, without either overt systemic toxicity or apparent inhibition to the bone remodeling process.

4.2 Materials and Methods

4.2.1 Animal Husbandry and Femoral Fracture Induction

All animal protocols were reviewed and approved by Purdue's Animal Care and Use Committee (PACUC). Female ND4 Swiss Webster mice (12-week) were purchased from Envigo (Indianapolis, IN) and maintained on a standard 12 h light-dark cycle (5 animals per cage). All mice were acclimated in the housing facility for one week before initiation of any studies.

Preparation of a stabilized femoral fracture with intramedullary pin fixation was performed following a modified method described previously[7]. ND4 Swiss Webster mice were anesthetized by isoflurane inhalation, after which the right hind knee was shaved and sanitized first with 10% (w/v) povidone-iodine solution (Fisher Scientific, Pittsburg, PA) and then with 70% aqueous ethanol. A small incision through the skin was made with surgical scissors followed by the removal of the knee cap to reveal the distal femur. The femur was then stabilized by insertion of a 22-gauge stainless steel pin down the intramedullary cavity of the bone followed by creation of a controlled fracture near the middle of the femur using surgical scissors. Excess pin was removed with a wire cutter, and the wound was closed with sutures. Fracture induction and implant position were confirmed using an X-ray Multispectral Imaging System (IS4000; Kodak, Rochester, NY) after surgery. For pain relief, all mice were injected subcutaneously with 0.1 mg/kg buprenorphine solution at the time of the surgery, followed by two doses per day for three days post-surgery.

4.2.2 Drug Formulation and Injection Schedule

Vehicle solution (85% Millipore water, 10% ethanol, and 5% Kolliphor EL) for delivery of dasatinib or dasatinib-Asp_{10} conjugate (**3**, DAC) was prepared according to a modified procedure[8]. Dasatinib or DAC was dissolved in DMSO and then diluted with the vehicle solution to yield a final drug and DMSO concentration of 2.5 mM and 0.1%, respectively. Buprenorphine solution (0.03 mg/mL final) was prepared by dissolving buprenorphine HCl (Sigma-Aldrich, St. Louis, MO) in DMSO (0.1% final) and then diluting to 0.03 mg/mL with phosphate-buffered saline (PBS). In studies involving only saline or DAC groups, DAC was dissolved in PBS to reach a final concentration of 2.5 mM. All injections were performed subcutaneously. In biodistribution studies, D_{10}-S0456 was dissolved in PBS to reach a final concentration of 2.5 mM, 12.5 mM, or 25 mM. All solutions were sterile-filtered before injection, and each mouse was administered 0.1 mL of solution for each injection.

All drug solutions were administered to mice subcutaneously above the neck. Initial injections of test articles were always administered immediately after surgery. Subsequent injections were given at frequencies of everyday (QD), every other day (QAD), every four days, every seven days, or every ten days, depending on the requirement of the study. The injection schedules are specified in each figure legend. In biodistribution studies, D_{10}-S0456 was administered 10 days post-fracture followed by the retrieval of fractured femurs after 24 hours.

4.2.3 Microcomputed Tomography

Following the desired treatments with DAC, vehicle or PBS, mice were euthanized with CO_2 followed by cervical dislocation to assure the mice were dead. Both fractured and

contralateral femurs were removed, cleaned, wrapped in Kimwipes wetted with PBS, and stored at -20 °C. The diaphysis of broken femurs that contained the fracture calluses or the entire length of healthy femurs were scanned using high-resolution microcomputed tomography (μCT 40; Scanco Medical AG, Brüttisellen, Switzerland) after removal of the stabilization pins from the femurs. Images were acquired at a tube potential of 70 kVp, an X-ray intensity of 113 μA, and 300-ms integration time, with voxel sizes of $8 \times 8 \times 8$ μm^3. Slide images (2048×2048) were analyzed with ImageJ (version 1.51) containing BoneJ plugin (version 1.4.2)[9]. 100 continuous slices with the largest diameter were selected from each image to represent the center portion of the fracture callus. Manual contouring of the fracture callus region was performed on the first, last and middle slices, followed by automated interpolation for all remaining slices. 3-dimentional (3D) image reconstruction of those slices were used to calculate bone density (bone volume/total volume, or BV/TV), trabecular thickness (Tb.Th), and trabecular separation (Tb.Sp) according to Bouxsein, Dempster, and their colleagues[10,11].

4.2.4 Four-Point Bending Test

Stabilization pins were removed from the femurs prior to mechanical analysis. Quantitation of the mechanical properties associated with bending and refracturing the repaired femurs was also performed using a four-point bending apparatus (ElectroForce TestBench; TA Instruments). The lower supports were set 10 mm apart on the anterior face of the femur in contact with the proximal and distal diaphysis. The upper supports were 4 mm apart and were placed such that they spanned the entire fracture callus on the diaphysis. Force was applied from the posterior face of the femur with a displacement rate of 0.3 mm/sec. Maximum load, stiffness, displacement to yield, and work to fracture data were

then generated. Stiffness is defined as the slope of the linear region of the load-displacement curve. Displacement to yield is defined as the displacement to the fracture point after reaching the yield point. Work to fracture is defined as the total area under the load-displacement curve[12].

4.2.5 Quantification of Aspartic$_{10}$-S0456 Conjugate in Bone

12% neutral buffered EDTA solution was prepared by dissolving 27 g anhydrous EDTA in 200 mL Milli-Q water with vigorous stirring. 7.5 g sodium hydroxide pellets were dissolved in the solution, and the pH of the solution was adjusted to 7.2 with small amounts of additional sodium hydroxide.

Broken femurs were collected at the indicated time for each group, rinsed with PBS for three times, thoroughly dried overnight in a vacuum desiccator, broken into small pieces, and weighed. 0.5 mL of 12% neutral buffered EDTA solution were added to each bone sample and mixed on a shaker for 8 hours to decalcify the bone mineral and extract the dye conjugate. Following the decalcification, samples were centrifuged for 5 min @8000 rpm. OD780 of 200 μL supernatant was obtained with a microplate reader. Dye was quantified by comparing OD780 to the standard curve. Standard curve was generated by measuring OD780 of serially diluted samples of D_{10}-S0456, using EDTA bone-extract solution of femurs unexposed to D_{10}-S0456 as diluent.

4.2.6 Statistical Analyses

All statistical analyses were performed with GraphPad Prism (version 7.0; GraphPad Software, CA). Unpaired two-tailed *t*-tests were carried out with a 95% confidence interval to assess statistical significance. Data are displayed as mean ± standard error of mean

(SEM). In the figures, levels of statistical significance are denoted with asterisks according to the following definition: *p < 0.05; **p < 0.01; ***p < 0.001; ****p < 0.0001.

4.3 Results

4.3.1 Fracture-Specificity of Aspartic$_{10}$-S0456 Dye Conjugate

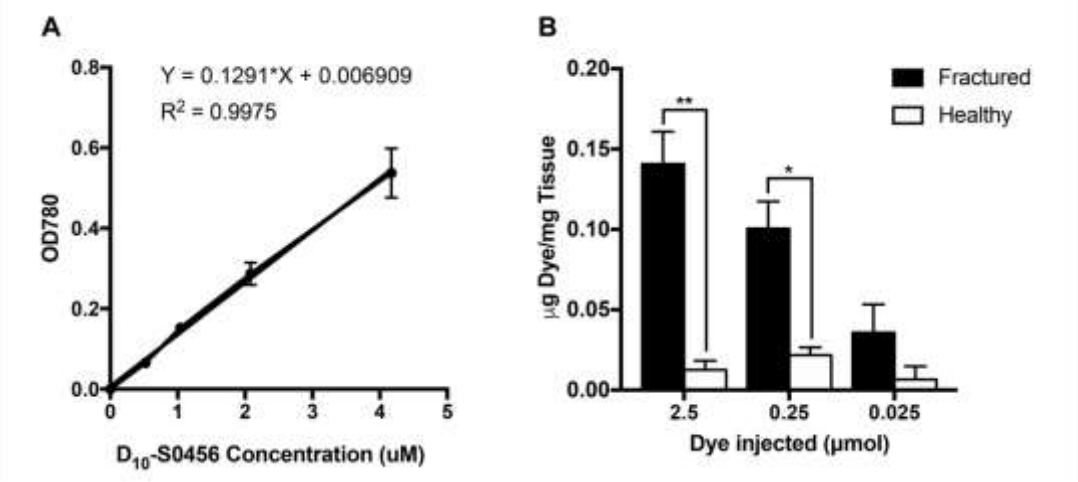

Fig. 4.1 Quantification of D_{10}-S0456 in Fracture-Bearing Mice.
Femurs were broken in ND4 Swiss Webster mice and stabilized with an internal rod prior to receiving a single injection of D_{10}-S0456 conjugate 10 days post fracture. (**A**) Standard curve that correlates D_{10}-S0456 concentrations to OD780 readings. (**B**) Quantification of the dye conjugate in broken and healthy femurs.

The D_{10}-targeted version of S0456 was injected subcutaneously to ND4 Swiss Webster mice containing broken but stabilized femurs (see Method). First, a standard curve with good linearity (Fig. 4.1A) was generated with D_{10}-S0456 of various concentrations, enabling the quantification of dye in decalcified bone samples just by measurements of OD780. As shown in Fig. 4.1B, D_{10}-S0456 accumulated in fractured femurs 5 to 12 times more than healthy femurs, verifying the fracture-specific targeting ability of D_{10}. Importantly, the dye concentration in fractured femurs was dose-dependent while that in healthy femurs remained relatively constant, indicating that the dye deposition in healthy

bone was non-specific. Meanwhile, there was no sign of saturation of the targeting capacity even with a dosage of 2.5 μmol D_{10}-S0456 (10-times the amount dosed with DAC), promising a wide dosing range of D_{10}-targeted drugs with respectable targeting efficacy.

4.3.2 Fracture-Healing Efficacy of DAC With Daily Dosage

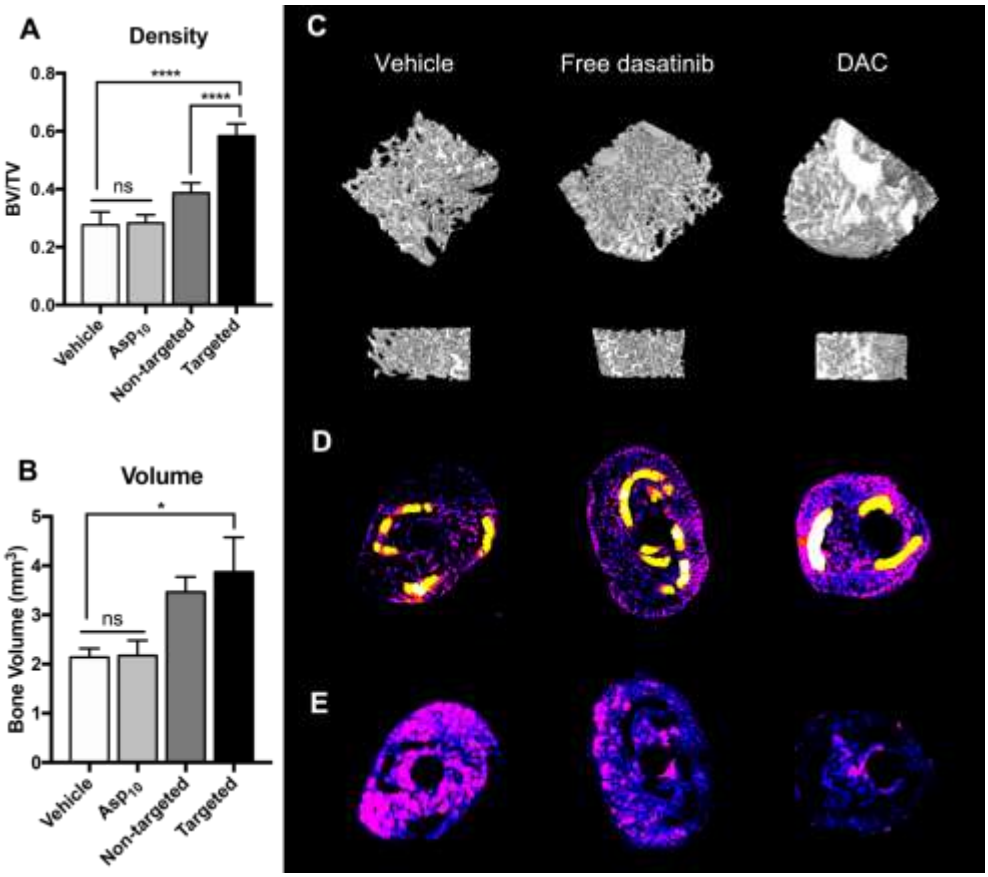

Fig. 4.2 DAC Increases Bone Density and Volume While Reducing Trabecular Spacing at the Fracture Site.

Femurs were broken in ND4 Swiss Webster mice and stabilized with an internal rod prior to daily therapy with either vehicle, free targeting ligand Asp_{10} (10 μmol/kg), free dasatinib (10 μmol/kg), or DAC (10 μmol/kg) (n = 8 in each group, except for n = 13 in DAC group). After 3 weeks mice were euthanized and analyzed for (**A**) bone density (bone volume/total volume) and (**B**) bone volume (mineral volume) at the fracture callus site. μCT images at the fracture callus site were also obtained, and representative images of (**C**) trabecular structure, (**D**) trabecular thickness (with colors from blue to magenta representing thinner to thicker, and bright yellow indicating cortical bone), and (**E**) trabecular spacing (with colors from magenta to blue representing the open spacing between trabeculae from larger to smaller, respectively). Complete dark denotes spaces fully filled with trabecular or cortical bone.

As described in Chapter 3, dasatinib was linked to an aspartic acid decapeptide to yield DAC, a fracture-targeted dasatinib conjugate. This conjugate was administered daily to ND4 Swiss Webster mice containing broken but stabilized femurs (see Method). As shown in Fig. 4.2A, daily injection of 10 μmol/kg dasatinib-Asp_{10} conjugate (DAC) essentially doubled the bone density at the fracture site relative to vehicle-treated controls. While non-targeted dasatinib also enhanced mineralization by the end of the three-week evaluation period, its impact was less than half that of its targeted counterpart. In terms of total bone volume (Fig. 4.2B), treatment with DAC also exceeded vehicle-treated controls by 82%. Importantly, daily dosage of the free targeting oligopeptide, Asp_{10}, had no impact on either bone density or total bone volume, confirming that the enhanced therapeutic effect of DAC is entirely due to the targeted delivery of dasatinib.

More detailed analysis of μCT data demonstrated that DAC-treated mice have denser trabecular bone microstructures than either vehicle- or free dasatinib-treated controls (Fig. 4.2C). Fracture calluses from DAC-targeted mice were also characterized by increases in trabecular thickness (Fig. 4.2D) and decreases in trabecular separation (Fig. 4.2E); i.e. further establishing that the repair process was leading to stronger bone. Because each of these changes occurs much sooner in the DAC-treated than control mice, we conclude that fracture healing process is accelerated in DAC-treated mice.

4.3.3 Fracture-Healing Efficacy of DAC With Dosage at Lower Dosing Frequencies

To determine whether DAC dosing frequency might be reduced without compromising therapeutic efficacy, similar studies to that described in Section 4.3.2 were performed with increasingly longer intervals between DAC administration.

4.3.3.1 Bone Properties at the Fracture Site

As seen in Fig. 4.3A, treatment with DAC every other day for 3 weeks was equally effective as daily injection of DAC, more than doubling the bone density relative to PBS-treated controls. Reducing dosing frequency to every four days, however, resulted in a measurable decline in potency (~62% increase over saline controls), and this potency was further diminished when DAC was dosed only weekly (i.e. ~39% increase over saline controls). As expected, analysis of μCT scans of fracture calluses (Fig. 4.4) confirmed this trend towards reduced mineralization with decreasing dosing frequency. However, even the weekly dosing schedule resulted in a callus density that was comparable to that seen in mice treated daily with nontargeted dasatinib, suggesting that dasatinib's potency is dramatically increased by concentrating the drug on the fracture surface.

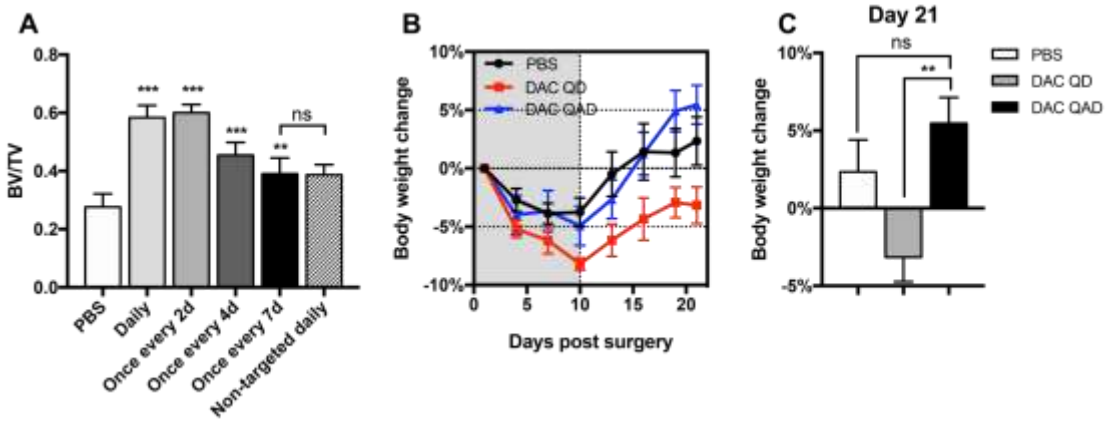

Fig. 4.3 DAC Stimulates Bone Growth at Lower Dosing Frequencies.
Mouse femurs were broken and stabilized as described in Methods, and affected mice were treated with PBS, dasatinib (10 μmol/kg), or DAC (10 μmol/kg) at the indicated dosing frequencies prior to analysis at 3weeks post-fracture. (**A**) Bone density (bone volume/total volume) at the fracture callus site. (**B**) Percent body weight change during therapy. (**C**) Percent body weight on the last day of the study. (n = 7 in each group).

4.3.3.2 Mouse Body Weight Change

Fig. 4.4 Efficacy of DAC Declines as Dosing Frequency Lowers.
μCT images of trabecular microstructure at the fracture callus site after mice were treated with DAC (10 μmol/kg) at the indicated dosing frequencies prior to analysis at 3 weeks post-fracture.

Although the dose of DAC used in these studies (equivalent to 4.9 mg/kg dasatinib) was more than 8-fold lower than free dasatinib's MTD (40 mg/kg[13]), it was still important to obtain a crude measure of the systemic toxicity of the different DAC treatment regimens. Because weight loss constitutes a widely employed metric for whole animal toxicity, we monitored the weight of all animals in each of the studies. As seen in Fig. 4.3B, all animals lost weight over the first 10 days following femur fracturing, presumably due to loss of appetite or discomfort associated with moving to a feeding station. However, persistence of weight loss differed among the treatment groups, with the daily dosed cohort displaying the slowest recovery to normal weight and the alternate day dosed cohort experiencing weight recovery at least as rapid as PBS-treated controls (Fig. 4.3C). Because the alternate day dosing schedule maintained the accelerated rate of fracture repair without inducing overt toxicity, all subsequent studies were performed using every-other-day dosing.

4.3.4 The Time Course of DAC-Stimulated Bone Fracture Healing

Although it was difficult to quantitate the minimum time for affected mice to return to normal mobility, it was nevertheless possible to accurately compare both the rates of

fracture callus remineralization and restoration of mechanical strength among treatment groups. For this purpose, fracture-bearing mice were dosed with DAC every other day for as long as 8 weeks, accompanied by analyses of radiological and mechanical properties of fractured femurs at various time-points.

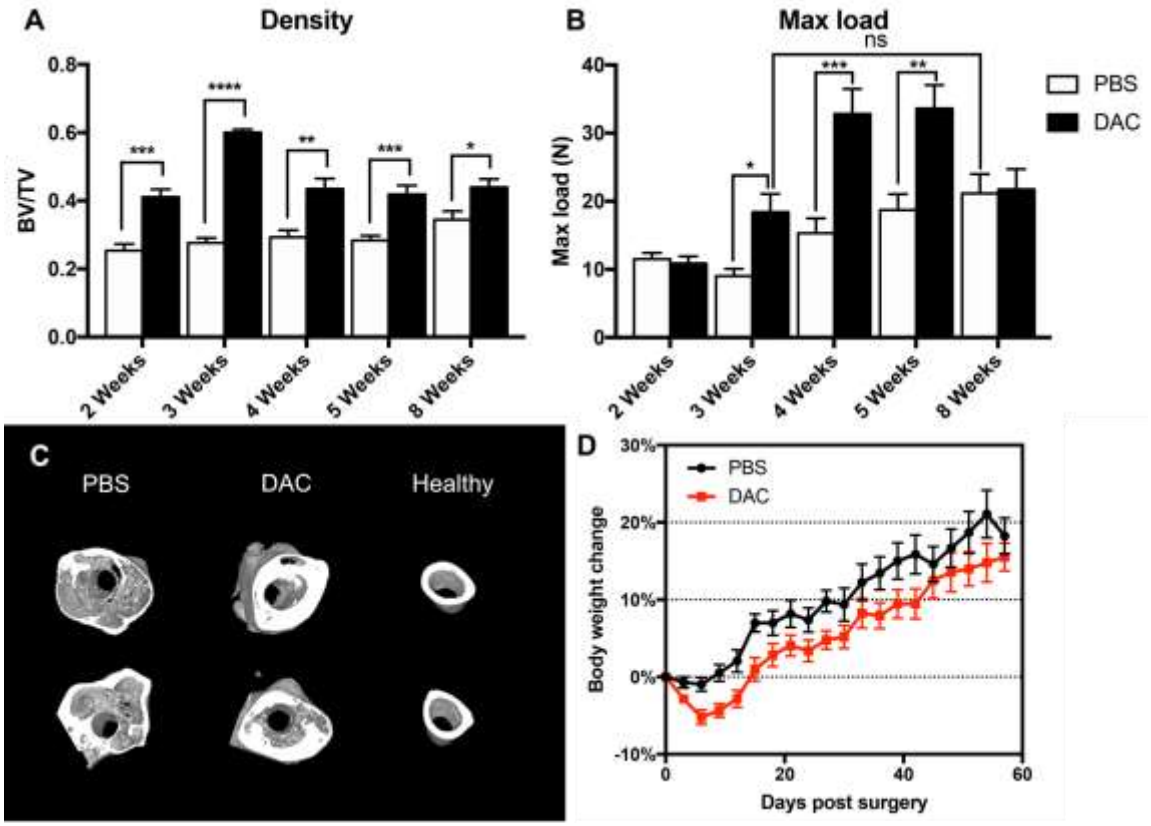

Fig. 4.5 DAC Accelerates Fracture Repair and Return to Normal Mechanical Strength. Mouse femurs were broken and stabilized as described in Methods, and affected mice were treated every other day with either PBS or DAC (10 μmol/kg) for the indicated duration prior to euthania and analysis. (**A**) Bone density (bone volume/total volume) at the fracture callus site. (**B**) Maximum load quantitated using a four-point bending apparatus as described in Methods. (**C)** μCT images of bone microstructure at the fracture callus site after 8 weeks of therapy. (**D**) Percent change in body weight of mice undergoing the aforementioned treatments. (n = 9 in each group, except n = 8 for DAC and PBS groups in 2-week dosing group)

4.3.4.1 Bone Density at the Fracture Callus and Mechanical Strength of the Healed Femurs

As shown in Fig. 4.5A, DAC-dosed mice showed significantly greater bone density than PBS-treated mice at every time point during the 8-week dosing period, i.e. confirming the accelerated healing process enabled by DAC.

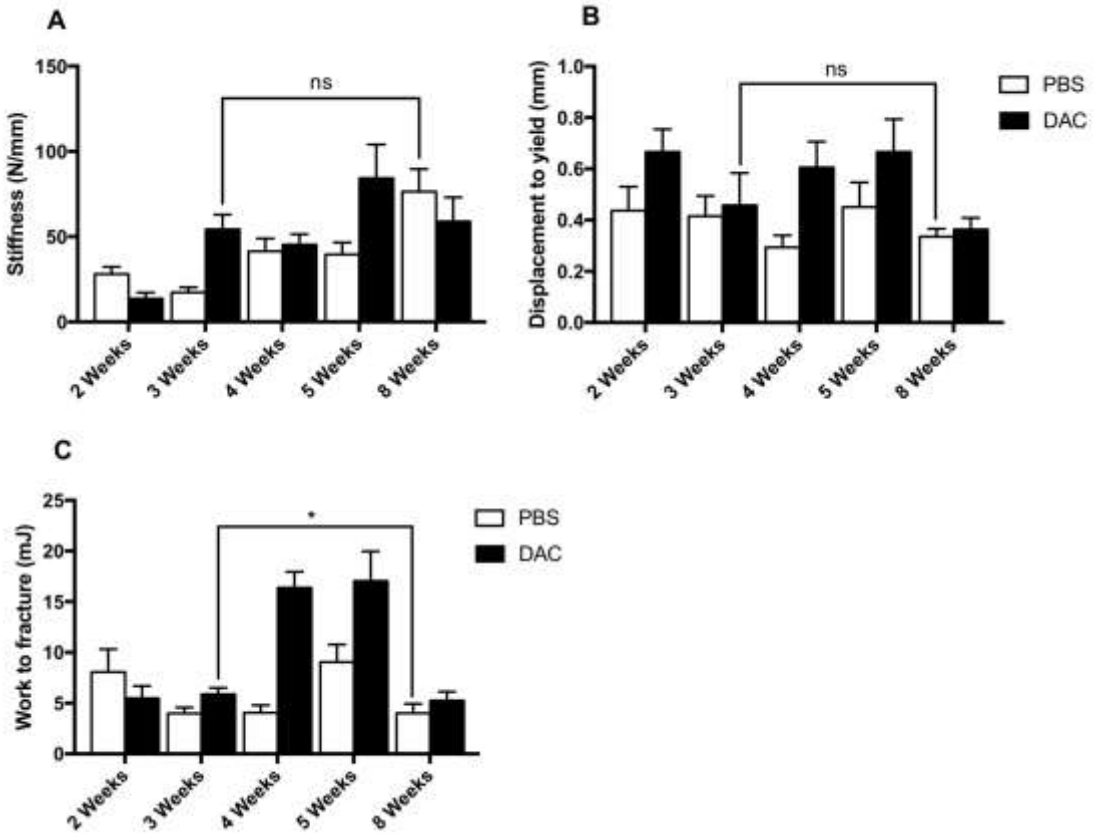

Fig. 4.6 DAC Accelerates Return to Normal Mechanical Strength.
Comparison of repaired fracture stiffness (**A**), post-yield displacement (**B**), and work to fracture (**C**) with PBS-treated controls. All conditions are as outlined in the legend to Fig. 4.5. Stiffness is defined as the slope of the linear region of the load-displacement curve. Post-yield displacement is defined as the displacement to the fracture point after reaching the yield point. Work to fracture is defined as the total area under the load-displacement curve.

Moreover, comparison of the forces required to refracture the healing femurs (maximum sustainable loads) at each time point (Fig. 4.5B) revealed that DAC-treated

animals recovered weight-bearing mechanical strength more than twice as fast as their PBS-treated counterparts. Thus, DAC-treated femurs required only 3 weeks to develop the same mechanical strength achieved by PBS-treated controls only after 8 weeks. In addition to this dramatically improved resistance to refracture, DAC-treated femurs were also mechanically stiffer (Fig. 4.6A) and ductile (Fig. 4.6B) than their PBS-treated counterparts, requiring more work to refracture the repaired bones (Fig. 4.6C) at every time point during the healing process than PBS-treated controls. In fact, PBS-treated femurs achieved the same desirable mechanical properties realized by DAC-treated femurs only after 8 weeks of healing (Fig. 4.6A-C).

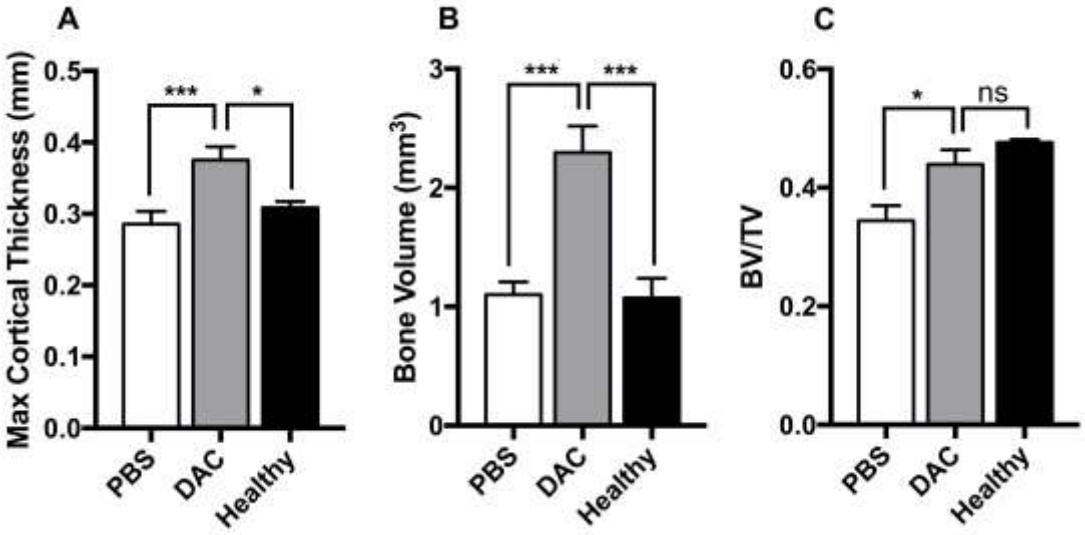

Fig. 4.7 DAC Accelerates Fracture Repair and Return to Normal Morphology. Comparison of maximum cortical bone thickness (**A**), bone volume (**B**), and bone density (**C**) at fracture sites in PBS- and DAC-treated mice after 8 weeks. All conditions are as outlined in the legend to Fig. 4.5. Measurements of healthy femurs were obtained at the femoral midshaft of contralateral femurs in mice receiving PBS.

As expected, differences in bone properties at the fracture site between treated and untreated mice gradually decreased as both cohorts remodeled to form normal bone; i.e.,

demonstrating that the final repaired bone eventually became similar between treated and untreated groups. Thus, as noted in Fig. 4.5C, trabecular bone eventually remodeled into cortical bone in both groups, however, the cortical bone remained slightly thicker and more voluminous in the DAC- than PBS-treated group (Fig. 4.7A-B); i.e. enabling the DAC-remodeled bone to more closely resemble healthy femur than the PBS-treated controls (Fig. 4.7C).

4.3.4.2 Mouse Body Weight Change

Analysis of body weight changes during the course of these studies revealed no obvious toxicities that were not attributed to the short-term trauma associated with the broken femurs (Fig. 4.5D). Together with the lack of overt toxicity observed with the 3-week dosing course, the finding here reiterates the safety of DAC to be dosed long-term.

4.3.4.3 Analysis of Healthy Contralateral Femurs

While an absence of body weight loss suggested no obvious systemic toxicity deriving from DAC therapy, a concern nevertheless remained that systemic administration of a bone anabolic agent might promote unwanted growth of healthy bones. To assess whether DAC might have altered the properties of healthy bones, unbroken femurs from the contralateral legs of both DAC- and PBS-treated mice were analyzed by μCT. Comparison of bone density, trabecular thickness, and trabecular separation at the distal femurs showed no significant differences between PBS- and DAC-treated mice following continuous QAD dosing for 8 weeks. Moreover, comparison of the properties of the healthy femurs following both 2 and 8 weeks of continuous DAC dosing revealed no changes in bone characteristics (Fig. 4.8A); i.e. BV/TV, trabecular thickness, and trabecular separation did not change in healthy femurs during 8 weeks of treatment with DAC.

Because nontargeted dasatinib has been shown to increase trabecular bone growth in healthy distal femurs[8], the absence of impact of the fracture-targeted DAC on healthy femur properties (Fig. 4.8B) reinforces that fracture-specific targeting of dasatinib can avoid unwanted systemic effects that arise when dasatinib is not targeted.

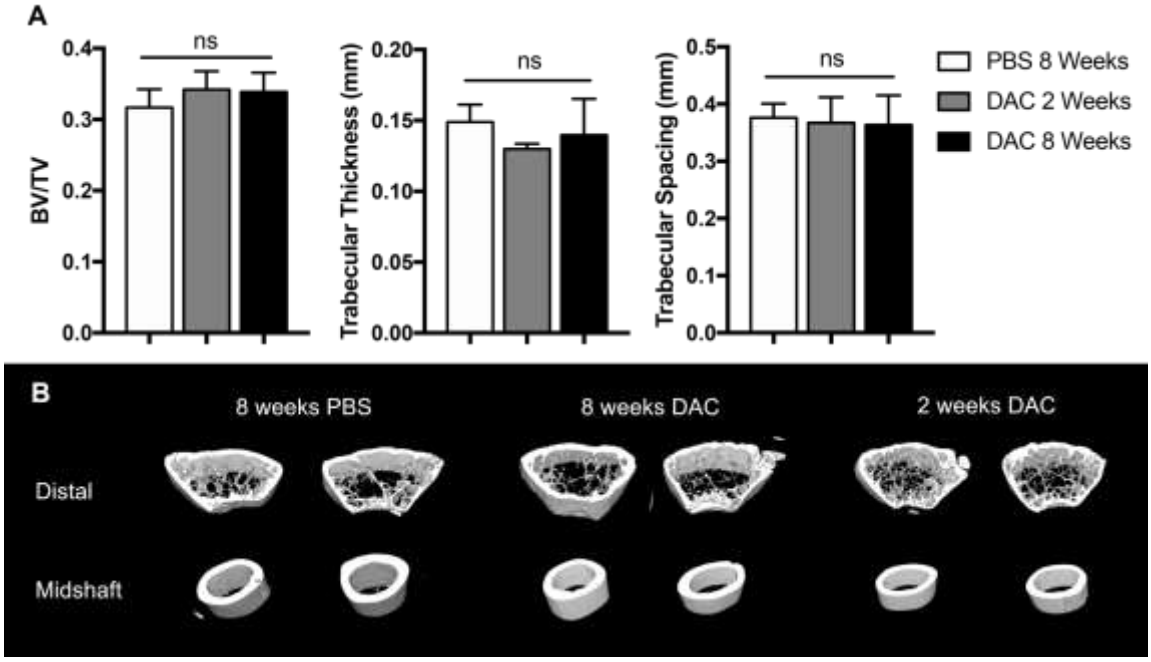

Fig. 4.8 DAC Causes No Detectable Changes in Healthy Contralateral Femurs. (**A**) Bone volume fraction (bone volume/total volume), trabecular thickness, and trabecular spacing at the distal femur of healthy contralateral femurs in mice after receiving either PBS for 8 weeks, or DAC (10 μmol/kg) therapy q.a.d. for 2 weeks/8 weeks. (**B**) μCT images of femoral midshaft or distal femur cross-sections from healthy contralateral femurs of mice after various durations of therapy with either PBS or DAC (10 μmol/kg) q.a.d. (n = 9 in each group, except n = 8 for DAC and PBS groups in 2-week dosing group)

4.4 Discussion

Although a variety of cytokines, hormones, peptides, and low molecular weight drugs have been found to exhibit bone anabolic activity[8,14–18], we elected to target dasatinib to fracture surfaces because it was previously reported to potently promote bone

formation[1,2,19]. Thus, while the mechanism underpinning dasatinib's acceleration of fracture repair remains uncertain, we speculate that it derives from inhibition of Src kinase, since systemic knockdown of Src in mice has been shown to increase osteoblast number and activity as well as induce excessive bone formation[20,21]. Indeed, analysis of osteoblast mRNA levels that changed in response to dasatinib administration (Fig. 2.1) revealed that transcription of genes involved in i) differentiation of mesenchymal precursors into osteoblasts, ii) biosynthesis of enzymes and extracellular matrix proteins critical for osteoblast function, and iii) bone turnover and remodeling were all amplified considerably. This dramatic reprograming of bone metabolic processes, however, also raised a concern that the plethora of induced osteogenic activities might not be properly balanced, resulting in an abnormal healing process at the fracture site and stimulation of bone growth at healthy/undamaged sites. Fortunately, as shown in Figs. 4.3-4.8, neither major concern was realized, as the fracture healing chronology seemed to track the normal process, only at an accelerated rate, and since healthy bone elsewhere in the body remained essentially unperturbed.

Although the duration of any bone fracture therapy should ideally last only a few weeks, the fact that nontargeted dasatinib has been administered daily at higher doses for many years to CML patients without significant toxicity suggests that the likelihood of encountering disqualifying toxicities with DAC should be minimal. Thus, as shown in Fig. 4.3, the optimal dosing regimen for DAC was 10 μmol/kg DAC every other day for 3 weeks (i.e. the equivalent of 4.9 mg/kg free dasatinib QAD). Considering that the recommended human dose for advanced CML therapy (180 mg/day; equivalent to 5.2 mg/kg/day in a mouse with the oral bioavailability taken into account[3,22]) is higher, one

might anticipate that a lower dasatinib dose that was targeted specifically to a fracture surface on alternate days should cause significantly fewer adverse effects.

As noted above, we were initially concerned that the diverse effects of dasatinib on calcium fixation[19], bone matrix protein biosynthesis[23], release of bone remodeling hormones[24], and differentiation of osteoblast and osteoclast precursors[8], etc. (see also Fig. 1) might not be physiologically balanced and thereby result in an altered or functionally inadequate bone structure. For example, reports of reduced osteoclast viability and function following exposure to dasatinib[15,22,23] raised concern that DAC might yield a "healed" fracture comprised of excessive trabecular bone characterized by weaker mechanical properties; i.e. similar to the trabecular bone commonly seen after antiresorptive therapy [24]. However, this concern was soon dismissed when DAC-treated femurs were observed to gradually remodel to a density and morphology approaching that of healthy femurs. Thus, fracture calluses at the 8-week time point consisted almost exclusively of desired cortical bone, implying that a normal remodeling process had been stimulated. More importantly, by the 8-week juncture, DAC-treated femurs displayed similar mechanical properties to PBS-treated controls, confirming that DAC does not alter the final repaired fracture, but simply accelerates its development. These results, combined with the decline in OPG/RANKL ratio during later stages of mineralization (Fig. 2.1H), confirm that DAC therapy differs significantly from antiresorptive therapy in that it more accurately recapitulates normal fracture repair.

Although accelerated fracture repair may seem unimportant when the fracture minimally impedes normal activity, more complicated fractures that significantly limit mobility can lead to serious morbidities and even mortality, especially in the elderly. Thus,

when fracture immobilization that prevents ambulation is required, quality of life can decrease, muscle mass and bone density can decline[25], blood perfusion of internal organs can be compromised, and earned income can be lost[26]. In the case of hip fractures in older individuals, associated complications will lead to death in ~25% of patients[27,28]. Clearly, a safe and effective therapy that accelerates return to normal activity should find application in some patient populations. Although the ~60% reduction in healing time (i.e. time to restoration of normal bone mechanical strength) suggests that DAC might fulfill this need (Fig. 4.5B), several challenges must still be addressed before DAC or a similar molecule can be moved towards a clinical trial. Thus, while every-other-day dosing constitutes an improvement over the initial daily dosing regimen, every-other-day dosing might still be too frequent for widespread compliance. Moreover, although DAC can apparently be administered without injection site reactions, an orally bioavailable formulation would still be preferred by most patients. Finally, while initial data look encouraging for use of DAC in treating long bone fractures, additional studies will be required before DAC should be considered as a potential treatment for nonunion fractures, hip fractures, stress fractures, or spinal fusions, especially when comorbidities such as diabetes, infections, or smoking exist.

In conclusion, we have shown that a fracture-targeted version of dasatinib works as a powerful bone-anabolic agent that significantly accelerates bone fracture healing without overt systemic toxicities or unwanted negative influences on the bone remodeling process. With possible improvements in dosing schedule and confirmation of efficacy in other species, a DAC–like molecule could soon be ready for human clinical trials.

4.5 References

(1) Garcia-Gomez, A.; Ocio, E. M.; Crusoe, E.; Santamaria, C.; Hernández-Campo, P.; Blanco, J. F.; Sanchez-Guijo, F. M.; Hernández-Iglesias, T.; Briñón, J. G.; Fisac-Herrero, R. M.; et al. Dasatinib as a Bone-Modifying Agent: Anabolic and Anti-Resorptive Effects. *PLoS ONE* **2012**, *7* (4), e34914.

(2) Vandyke, K.; Dewar, A. L.; Diamond, P.; Fitter, S.; Schultz, C. G.; Sims, N. A.; Zannettino, A. C. The Tyrosine Kinase Inhibitor Dasatinib Dysregulates Bone Remodeling through Inhibition of Osteoclasts in Vivo. *J. Bone Miner. Res.* **2010**, *25* (8), 1759–1770.

(3) Kamath, A. V.; Wang, J.; Lee, F. Y.; Marathe, P. H. Preclinical Pharmacokinetics and in Vitro Metabolism of Dasatinib (BMS-354825): A Potent Oral Multi-Targeted Kinase Inhibitor against SRC and BCR-ABL. *Cancer Chemother. Pharmacol.* **2008**, *61* (3), 365–376.

(4) Brownlow, N.; Mol, C.; Hayford, C.; Ghaem-Maghami, S.; Dibb, N. J. Dasatinib Is a Potent Inhibitor of Tumour-Associated Macrophages, Osteoclasts and the FMS Receptor. *Leukemia* **2009**, *23* (3), 590–594.

(5) Jönsson, S.; Hjorth-Hansen, H.; Olsson, B.; Wadenvik, H.; Sundan, A.; Standal, T. Second-Generation TKI Dasatinib Inhibits Proliferation of Mesenchymal Stem Cells and Osteoblast Differentiation in Vitro. *Leukemia* **2010**, *24* (7), 1357–1359.

(6) Li, J.; Stocum, D. L. Fracture Healing. In *Basic and Applied Bone Biology*; Elsevier, 2014; pp 205–223.

(7) Low, S. A.; Galliford, C. V.; Yang, J.; Low, P. S.; Kopeček, J. Biodistribution of Fracture-Targeted GSK3β Inhibitor-Loaded Micelles for Improved Fracture Healing. *Biomacromolecules* **2015**, *16* (10), 3145–3153.

(8) Zhang, Y.; Desai, A.; Yang, S. Y.; Bae, K. B.; Antczak, M. I.; Fink, S. P.; Tiwari, S.; Willis, J. E.; Williams, N. S.; Dawson, D. M.; et al. Inhibition of the Prostaglandin-Degrading Enzyme 15-PGDH Potentiates Tissue Regeneration. *Science* **2015**, *348* (6240), aaa2340–aaa2340.

(9) Doube, M.; Kłosowski, M. M.; Arganda-Carreras, I.; Cordelières, F. P.; Dougherty, R. P.; Jackson, J. S.; Schmid, B.; Hutchinson, J. R.; Shefelbine, S. J. BoneJ: Free and Extensible Bone Image Analysis in ImageJ. *Bone* **2010**, *47* (6), 1076–1079.

(10) Bouxsein, M. L.; Boyd, S. K.; Christiansen, B. A.; Guldberg, R. E.; Jepsen, K. J.; Müller, R. Guidelines for Assessment of Bone Microstructure in Rodents Using Micro-Computed Tomography. *J. Bone Miner. Res.* **2010**, *25* (7), 1468–1486.

(11) Dempster, D. W.; Compston, J. E.; Drezner, M. K.; Glorieux, F. H.; Kanis, J. A.; Malluche, H.; Meunier, P. J.; Ott, S. M.; Recker, R. R.; Parfitt, A. M. Standardized Nomenclature, Symbols, and Units for Bone Histomorphometry: A 2012 Update of the Report of the ASBMR Histomorphometry Nomenclature Committee. *J. Bone Miner. Res.* **2013**, *28* (1), 2–17.

(12) Jepsen, K. J.; Silva, M. J.; Vashishth, D.; Guo, X. E.; van der Meulen, M. C. H. Establishing Biomechanical Mechanisms in Mouse Models: Practical Guidelines for Systematically Evaluating Phenotypic Changes in the Diaphyses of Long Bones. *J. Bone Miner. Res. Off. J. Am. Soc. Bone Miner. Res.* **2015**, *30* (6), 951–966.

(13) Dubrovsky, L.; Pankov, D.; Brea, E. J.; Dao, T.; Scott, A.; Yan, S.; O'Reilly, R. J.; Liu, C.; Scheinberg, D. A. A TCR-Mimic Antibody to WT1 Bypasses Tyrosine Kinase Inhibitor Resistance in Human BCR-ABL+ Leukemias. *Blood* **2014**, *123* (21), 3296–3304.

(14) Chew, C. K.; Clarke, B. L. Abaloparatide: Recombinant Human PTHrP (1-34) Anabolic Therapy for Osteoporosis. *Maturitas* **2017**, *97*, 53–60.

(15) Amso, Z.; Cornish, J.; Brimble, M. A. Short Anabolic Peptides for Bone Growth: SHORT ANABOLIC PEPTIDES FOR BONE GROWTH. *Med. Res. Rev.* **2016**, *36* (4), 579–640.

(16) Kim, H.-Y.; Choi, S.; Yoon, J.-H.; Lim, H. J.; Lee, H.; Choi, J.; Ro, E. J.; Heo, J.-N.; Lee, W.; No, K. T.; et al. Small Molecule Inhibitors of the Dishevelled-CXXC5 Interaction Are New Drug Candidates for Bone Anabolic Osteoporosis Therapy. *EMBO Mol. Med.* **2016**, *8* (4), 375–387.

(17) Kulkarni, N. H.; Onyia, J. E.; Zeng, Q.; Tian, X.; Liu, M.; Halladay, D. L.; Frolik, C. A.; Engler, T.; Wei, T.; Kriauciunas, A.; et al. Orally Bioavailable GSK-3α/β Dual Inhibitor Increases Markers of Cellular Differentiation In Vitro and Bone Mass In Vivo. *J. Bone Miner. Res.* **2006**, *21* (6), 910–920.

(18) Mediero, A.; Wilder, T.; Perez-Aso, M.; Cronstein, B. N. Direct or Indirect Stimulation of Adenosine A2A Receptors Enhances Bone Regeneration as Well as Bone Morphogenetic Protein-2. *FASEB J.* **2015**, *29* (4), 1577–1590.

(19) Id Boufker, H.; Lagneaux, L.; Najar, M.; Piccart, M.; Ghanem, G.; Body, J.-J.; Journé, F. The Src Inhibitor Dasatinib Accelerates the Differentiation of Human Bone Marrow-Derived Mesenchymal Stromal Cells into Osteoblasts. *BMC Cancer* **2010**, *10* (1).

(20) Soriano, P.; Montgomery, C.; Geske, R.; Bradley, A. Targeted Disruption of the C-Src Proto-Oncogene Leads to Osteopetrosis in Mice. *Cell* **1991**, *64* (4), 693–702.

(21) Marzia, M.; Sims, N. A.; Voit, S.; Migliaccio, S.; Taranta, A.; Bernardini, S.; Faraggiana, T.; Yoneda, T.; Mundy, G. R.; Boyce, B. F.; et al. Decreased C-Src Expression Enhances Osteoblast Differentiation and Bone Formation. *J. Cell Biol.* **2000**, *151* (2), 311–320.

(22) Nair, A.; Jacob, S. A Simple Practice Guide for Dose Conversion between Animals and Human. *J. Basic Clin. Pharm.* **2016**, *7* (2), 27.

(23) Borriello, A.; Caldarelli, I.; Bencivenga, D.; Stampone, E.; Perrotta, S.; Oliva, A.; Della Ragione, F. Tyrosine Kinase Inhibitors and Mesenchymal Stromal Cells: Effects on Self-Renewal, Commitment and Functions. *Oncotarget* **2017**, *8* (3), 5540–5565.

(24) Aleman, J. O.; Farooki, A.; Girotra, M. Effects of Tyrosine Kinase Inhibition on Bone Metabolism: Untargeted Consequences of Targeted Therapies. *Endocr. Relat. Cancer* **2014**, *21* (3), R247–R259.

(25) Dittmer, D. K.; Teasell, R. Complications of Immobilization and Bed Rest. Part 1: Musculoskeletal and Cardiovascular Complications. *Can. Fam. Physician Med. Fam. Can.* **1993**, *39*, 1428–1432, 1435–1437.

(26) Arangio, G. A.; Lehr, S.; Reed, J. F. Reemployment of Patients with Surgical Salvage of Open, High-Energy Tibial Fractures: An Outcome Study. *J. Trauma* **1997**, *42* (5), 942–945.

(27) Bentler, S. E.; Liu, L.; Obrizan, M.; Cook, E. A.; Wright, K. B.; Geweke, J. F.; Chrischilles, E. A.; Pavlik, C. E.; Wallace, R. B.; Ohsfeldt, R. L.; et al. The Aftermath of Hip Fracture: Discharge Placement, Functional Status Change, and Mortality. *Am. J. Epidemiol.* **2009**, *170* (10), 1290–1299.

(28) Braithwaite, R. S.; Col, N. F.; Wong, J. B. Estimating Hip Fracture Morbidity, Mortality and Costs. *J. Am. Geriatr. Soc.* **2003**, *51* (3), 364–370.

CHAPTER 5. FURTHER OPTIMIZATION OF THE DOSING SCHEDULE OF DAC

5.1 Introduction

In Chapter 4, we have demonstrated that an every-other-day-dosed DAC serves as a promising therapy to accelerate fracture healing, and that a mere 3-week dosing course was able to reduce the fracture healing time by 60%. However, one major aspect that remains to be improved is the dosing schedule. An every-other-day injection schedule of DAC, despite its short dosing course (3 weeks), involves 11 total doses and would still account for a considerable burden towards patients bearing broken bones. In order to minimize the inconvenience of frequent injections for patients, DAC needs to be dosed less often.

One might simply trade the low dosage of DAC for less frequent dosing, but raising dosage could also significantly increase toxicity, which should be avoided at all costs. Thus, understanding the physiological processes during different stages of fracture repair is the key to the optimization of dosing schedule. Meanwhile, the rate of release of dasatinib from the conjugate bound to the fracture site may also be tweaked to maximize the exposure of dasatinib to cells in the fracture microenvironment. In this chapter, we report our hypotheses and attempts to reduce the dosing frequency of fracture-targeted dasatinib.

5.1.1 DAC's Proposed Function at Different Stages of Fracture Repair

Dasatinib does not facilitate all stages of the fracture repair process. As mentioned in Chapter 1 (Section 1.2.2), repair of a fracture involves four stages: inflammatory response, soft callus formation, hard callus formation, and bone remodeling.[1] As a stimulant for osteoblast differentiation and function, dasatinib is supposed to have the biggest impact on fracture healing during the stage of hard callus formation, during which

osteoblasts play a central role in the mineralization of the soft callus. This stage takes place during week 2 and 3 of the healing process, and peaks around day 14 post fracture in rodent models.[2] Despite the observation that DAC enhances fracture healing even with long-term dosing, the dosages outside of the stage of hard callus formation might have been meaningless or even detrimental to the efficacy. Avoiding unnecessary dosing should not only reduce the total doses required for the patients, but potentially improve the efficacy while circumventing additional toxicities.

The first stage of fracture repair involves an influx of inflammatory cytokines and inflammation responder cells, which play important roles in fibrogenesis and formation of soft callus.[3,4] However, dasatinib has been reported to be anti-inflammatory[5,6] and anti-fibrotic[7,8], making it a potential inhibitor of the initiation of fracture repair and soft callus formation. Furthermore, revascularization does not complete until day 5-10 post fracture,[9,10] deferring the delivery of DAC to the fracture surface. Thus, we hypothesize that doses of DAC during the first week of fracture repair are unnecessary for the acceleration of the process.

Similar speculation holds true for doses past week 3 of fracture repair. Even though inhibition of bone resorption was not seen with DAC therapy during week 4-8 of fracture repair (Section 4.3.4), a molecule to stimulate osteoblast function might not contribute meaningfully to bone remodeling. This concern, together with the observation that DAC restores the mechanical strength of a fractured femur to normal with a 3-week dosing schedule, precludes the need for doses beyond the end of the third week of fracture repair. Thus, the main evolution of DAC is based on finding an optimal combination of dosing

frequency and dosing window to achieve a similar efficacy to an every-other-day dosage but with considerably fewer total doses.

5.1.2 Tweaking the Drug Release Rate and Retention Kinetics of DAC at Fracture Site

Aside of the strategy elaborated in the previous section, methods that prolong the availability of dasatinib at the fracture site for each dose might also result in a reduction of required total doses. This might be realized by either slowing down the release of dasatinib after DAC's accumulation or lengthening the time DAC stays at the fracture site, both of which require adjustments of the chemical composition of the targeted conjugate.

To slow down the release of dasatinib from a targeted conjugate, a linker less labile than the ester found on DAC might be used. One example is α-substituted esters, which have increased steric hindrance compared to normal esters and are consequently less prone to hydrolysis. Another chemical linker that could allow for slower release rate than an ester linker is carbamate linker.[11–13] When a version of DAC with a slower-release linker is bound to the fracture surface, the linker is expected to sustainably release dasatinib over a longer period of time, resulting in reduced demand for DAC administration.

Meanwhile, due to the peptidic nature of the D_{10} targeting ligand, DAC might be degraded prematurely by peptidases at the fracture site before dasatinib could be released.[14] Reducing the propensity of degradation by using unnatural, D-amino acids could be a potential method to improve DAC's retention at the fracture site, which might enable a less frequent dosing frequency while retaining the efficacy towards fracture repair.

It remains unclear which factors may contribute the most to the desired reduction in dosing frequency of DAC. Thus, multiple tweaked versions of DAC were synthesized and tested *in vivo*, while the release kinetics of different linkers were examined *in vitro*.

5.2 Materials and Methods

5.2.1 Materials

All materials, solvents and reagents were purchased from commercial sources and used without further purification unless specifically noted, and materials and instruments described in previous chapters are omitted here. 3-(2,5-dioxo-2,5-dihydro-1H-pyrrol-1-yl)-2,2-dimethylpropanoic acid was purchased from Combi-Blocks (San Diego, CA).

5.2.2 Synthesis of Dasatinib Protected Ester Slow-Release Conjugate (MW0346)

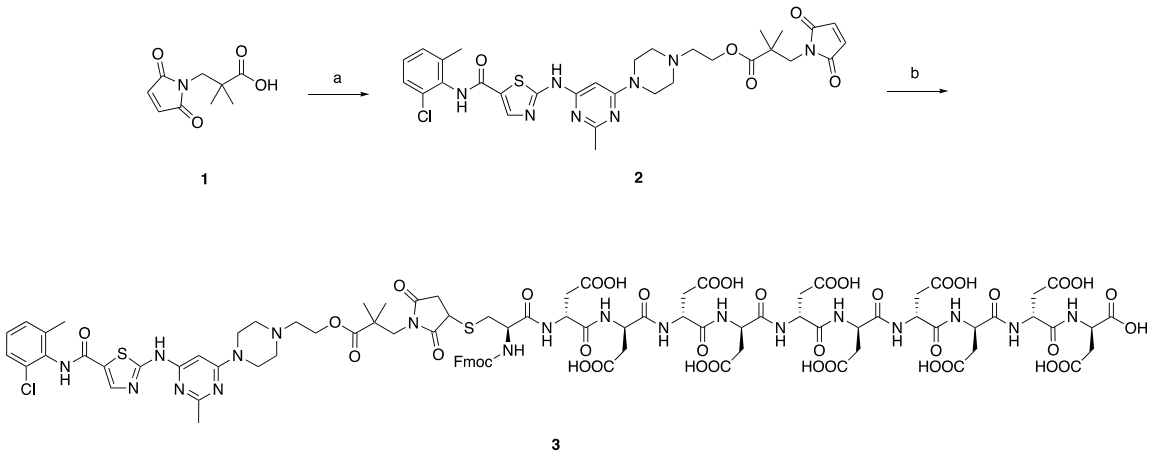

Fig. 5.1 Synthesis of Dasatinib Protected Ester Slow-Release Conjugate (MW0346). Reagents and conditions: a) dasatinib, PyBOP, DIPEA, DMF, 4h, 91%; b) **1**, DMSO, 1h, 24%

The synthesis for D_{10}-cys followed the procedure described in Chapter 3, and the dasatinib-protected-ester-maleimide was synthesized similarly to dasatinib-maleimide (Fig. 5.1). **1** (50 mg, 0.25 mmol) and PyBOP (122 mg, 0.235 mmol) were dissolved in 2 mL anhydrous DMF in a 10-mL round-bottom flask degassed with argon. The flask was cooled on ice and diisopropylethylamine (221 μL, 1.25 mmol) was added and stirred for 5 minutes. Dasatinib (100 mg, 0.738 mmol) dissolved in 2 mL anhydrous DMF was then added dropwise to the mixture and the reaction mixture was warmed slowly to room temperature

with stirring over the ensuing 4 hours. EtOAc (~20 ml) was added to the reaction flask and the diluted mixture was washed 2x with DI water followed by 4 washes with saturated aqueous NaCl. The organic phase was then collected, dried over sodium sulfate and concentrated *in vacuo* to yield the crude product. The crude product was purified by flash column chromatography on Teledyne CombiFlash Rf+ Lumen (0-25% MeOH in DCM) to give **2** as a yellow powder (123 mg, 91%).

2 (100 mg, 0.15 mmol) was dissolved in 1.8 mL anhydrous DMSO in a 10-mL round-bottom flask degassed with argon. 170 mg D_{10}-Cys (0.11 mmol) was added quickly to the aforementioned solution and stirred until all solid dissolved. The reaction mixture was stirred for 1 hour under argon atmosphere before purification using preparatory reverse phase HPLC. Pure fractions were collected, concentrated *in vacuo* to remove acetonitrile, frozen and lyophilized to yield the final product dasatinib protected ester slow-release conjugate MW0346 (**3)** as a fluffy off-white solid (60 mg, 24%).

5.2.3 Synthesis of D-Aspartic$_{10}$-S0456 Conjugate

Fmoc-D-Asp(OtBu)-OH and Fmoc-*S*-trityl-D-cysteine were purchased from Chem-Impex International (Wood Dale, IL). S0456-maleimide was synthesized following the procedures described in Chapter 3.2.6, while the targeting ligand consisting of only D-amino acids (DD_{10}-cys) was synthesized with SPPS (Fig. 5.2). For the initial loading of the resin, 2-chlorotrityl chloride resin (0.4 g, 1.4 mmol/g) was swollen in DCM (10 mL/g resin) followed by addition of Fmoc-D-Asp(OtBu)-OH (1.15 g, 2.8 mmol) and DIPEA (1.66 mL, 9.5 mmol) dissolved in DCM (14 mL). After this step, the same resin capping, coupling, deprotection, wash, and cleavage procedures were followed as described in Chapter 3.2.2, using Fmoc-D-Asp(OtBu)-OH and Fmoc-*S*-trityl-D-cysteine. The cleavage solution was

concentrated in vacuo, washed 3 times with cold Et_2O, dried overnight to give DD_{10}-cys as a white powder (630 mg, 75% overall yield, 97.2% average coupling efficiency).

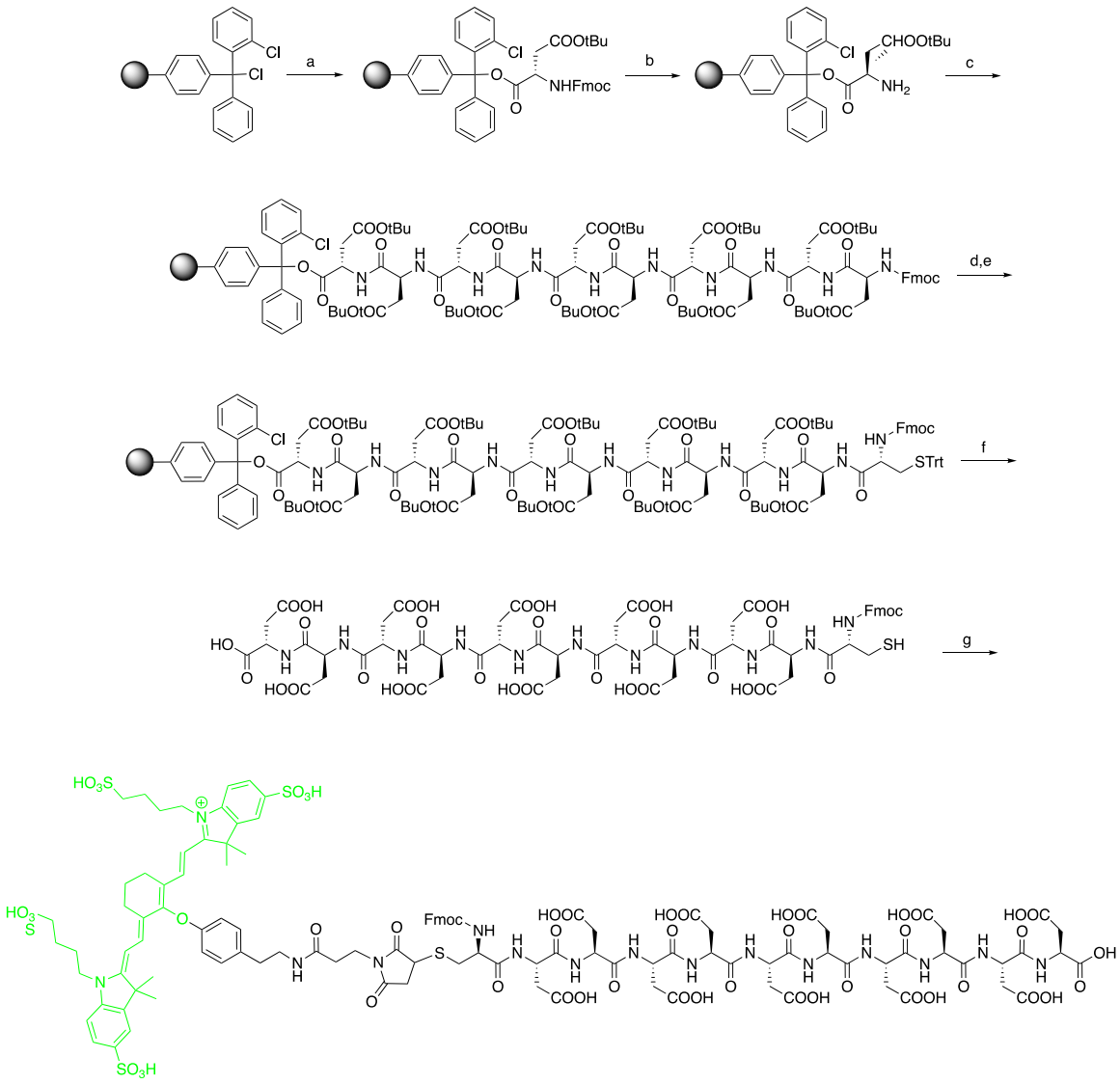

Fig. 5.2 Synthesis of DD_{10}-S0456.
Reagents and conditions: a) Fmoc-L-Asp(OtBu)-OH, DIPEA, DCM, 1 h; b) 20% piperidine in DMF, 5 min and 10 min; c) Fmoc-L-Asp(OtBu)-OH, PyBOP, DIPEA, DMF, 1 h; d) 20% piperidine in DMF, 5 min and 10 min; e) Fmoc-*S*-trityl-L-cysteine, PyBOP, DIPEA, DMF, 1 h; (f) cleavage cocktail (90% TFA, 3.3% TIPS, 3.3% water and 3.3% EDT), 20 min, 75% overall; g) S0456-maleimide, DMSO, rt, 25%.

S0456-maleimide (100 mg) was dissolved in 2 mL DMSO in a flask degassed with argon, followed by the addition of D-D_{10}-cys to the solution with stirring. The mixture was stirred at room temperature for 2.5 hours before purification with prep-HPLC. The purified and lyophilized product DD_{10}-S0456 appeared as a green fluffy solid (57 mg).

5.2.4 Synthesis of D-Aspartic$_{10}$-Dasatinib Conjugate

As shown in Fig. 5.3, the synthesis of D-D_{10}-cys followed the method described in Section 5.2.2, and the synthesis of dasatinib-maleimide and D-D_{10}-dasatinib followed the method described in Section 3.2.3.

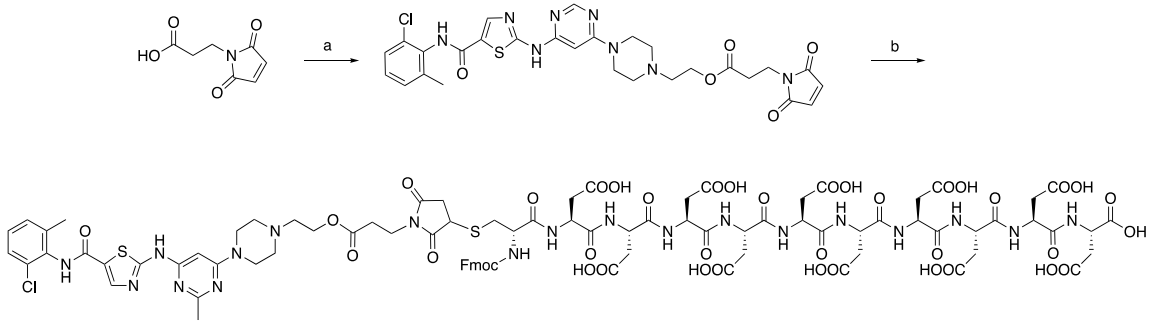

Fig. 5.3 Synthesis of D-D_{10}-Dasatinib.
Reagents and conditions: a) dasatinib, PyBOP, DIPEA, DMF, 4h, 70%; b) D-D_{10}-cys, DMSO, 1h, 25%

5.2.5 Kinetics of Conjugate Hydrolysis and Drug Release

Tris stock buffer (1M, pH 7) was prepared by first dissolving 60.5 g Tris base in 400 mL Milli-Q water. The pH of the buffer was adjusted to pH 7 with HCl, then Milli-Q water was added to reach a final volume of 500 mL. Before use, the stock buffer was diluted 20X to yield the 50 mM Tris buffer. Citrate buffer (50 mM, pH 4) was prepared by dissolving 4.9 g sodium citrate dihydrate and 6.4 g citric acid in 800 mL Milli-Q water. The pH of the

buffer was adjusted to pH 4 with 10% NaOH solution, followed by the dilution of the buffer to 1 L with Milli-Q water.

DAC and MW0346 were dissolved in 50 mM Tris or citrate buffer to reach a final concentration of 0.1 mg/mL, and aliquoted in 1-mL Eppendorfs in triplets. The aliquots were incubated in a shaker at 37 °C before 45 μL of each aliquot were analyzed with LCMS at the indicated time points. In studies with HAp, 5 mg HAp was added to 500 μL aliquot in Eppendorf, followed by constant agitation in a 37 °C shaker. At each time point, samples with HAp were centrifuged for 1 min at 10000 rpm, followed by the retrieval of 45 μL of supernatant from each sample for LCMS analysis. A separate set of aliquots were prepared for each time point of the studies with HAp.

5.2.6 Drug Formulation and Injection Schedule

Buprenorphine solution (0.03 mg/mL final) was prepared by dissolving buprenorphine HCl (Sigma-Aldrich, St. Louis, MO) in DMSO (0.1% final) and then diluting to 0.03 mg/mL with phosphate-buffered saline (PBS). DAC, MW0346, D_{10}-S0456, DD_{10}-S0456, and DD_{10}-dasatinib was dissolved in PBS to reach a final concentration of 2.5 mM (1X), 5 mM (2X), or 7.5 mM (3X). All solutions were sterile-filtered before injection, and each mouse was administered 0.1 mL of solution for each injection.

All drug solutions were administered to mice subcutaneously above the neck following the injection schedule specified in each figure legend. In retention kinetics studies, D_{10}-S0456 and DD_{10}-S0456 was administered 10 days post-fracture followed by the retrieval of fractured femurs after 2, 24, 48, 72, and 96 hours post injection.

5.3 Results

5.3.1 Optimizing the Dosing Schedule for DAC

5.3.1.1 Choosing the Best Dosage Starting Point

As hypothesized in Section 5.1.1, doses of DAC during the first week following a fracture might be unnecessary, if not detrimental to the final healing result. To find out whether DAC therapy could be initiated at a later stage during fracture repair, DAC (10 μmol/kg, 1X) was administered to fracture-bearing mice during the first, or the second, or the third week post-surgery. In each dosing week, 3 doses were injected with two-day intervals. All broken femurs were harvested and analyzed after 3 weeks post-surgery. The results are shown in Fig. 5.4.

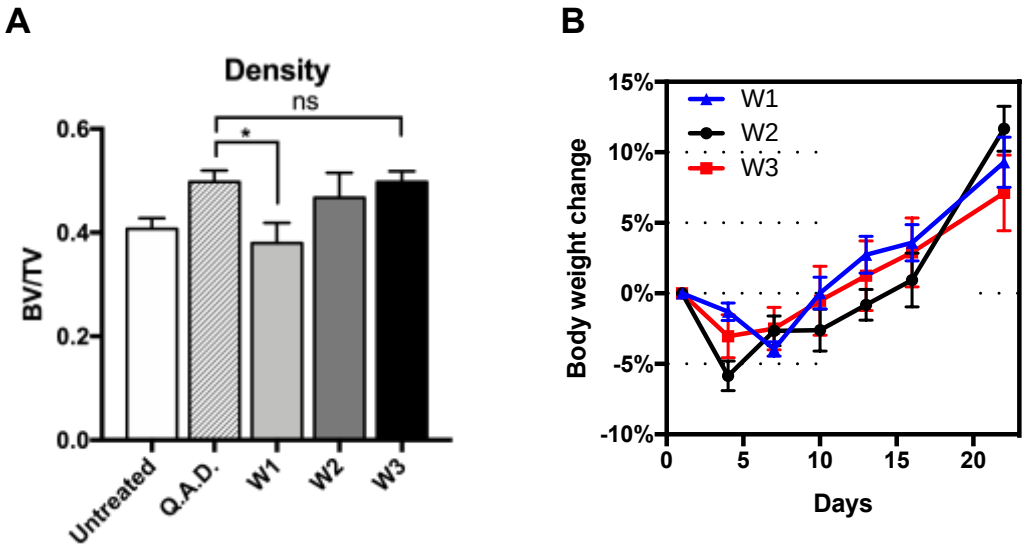

Fig. 5.4 Determining the Optimal Dosing Starting Point for DAC.
Femurs were broken in ND4 Swiss Webster mice and stabilized with an internal rod prior to DAC therapy (10 μmol/kg) dosed every other day, three times in the first, or the second, or the third week post fracture (n = 7 in each group). After 3 weeks mice were euthanized and analyzed for (**A**) bone density (bone volume/total volume) and (**B**) percent body weight change. Q.A.D.: every-other-day dosage; W1: three doses in the first week post fracture; W2: three doses in the second week post fracture; W3: three doses in the third week post fracture.

The results of this study argue that dosing during the first week of fracture repair is unnecessary and might harm the overall healing. After three weeks, femurs dosed only during the first week after surgery had considerably less bone density at the fracture callus compared to the every-other-day treated femurs and was similar to untreated ones (Fig. 5.4A), suggesting that those doses failed to make a difference to the healing. This observation is in accordance with our hypothesis that the anti-inflammatory and anti-fibrotic properties of dasatinib could suppress the inflammatory stage of fracture healing, and that damage to the vasculature due to the wound could delay the delivery of DAC to the fracture site. Importantly, all three new dosing schedules imposed no additional toxicity, which was expected given the remarkably lower dosing frequency in those schedules (Fig. 5.4B).

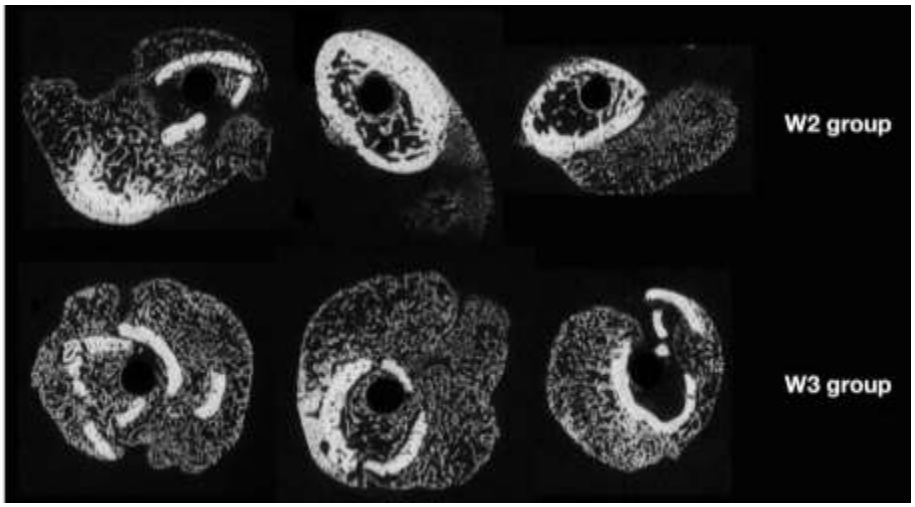

Fig. 5.5 Fracture Callus Comparison Between Doses During Week 2 and Week 3. μCT images of trabecular microstructure at the fracture calluses of mice treated with three doses of DAC in either the second week (W2) or the third week (W3) post fracture.

Doses during both the second and third week of the repair process promoted the fracture repair to some extent (Fig. 5.4A). However, the three doses during the third week

contributed more significantly to the repair, demonstrating a similar efficacy as the tried-and-true every-other-day dosing schedule. Dosing three times during the second week resulted in a less dramatic improvement to the callus density, and as can be seen in Fig. 5.5, the fracture calluses in W2 group had notably less trabecular bone, indicating an inferior healing process. These results suggest that DAC therapy would perform well even if the dosing begins at the third week after fracture, and that doses during the first and second week of a Q.A.D. dosing schedule could be avoided for the same fracture repair efficacy. The stage of hard callus formation peaks by the end of the second week and the beginning of the third week,[1] thus doses during the third week maximizes the osteoblast-stimulating efficacy of dasatinib. Whether or not doses during the second week are meaningful remains to be further tested, but the ability to administer DAC only during the third week has enabled us to potentially escalate dosage without overt increase in toxicity, which is investigated in the next section.

5.3.1.2 Increasing Dosage with Different Dosing Schedules

To examine whether a higher dosage of DAC would bring about improved efficacy, a Q.A.D. DAC therapy was repeated on fracture-bearing mice with different dosages. As shown in Fig. 5.6A, the fracture-healing efficacy of DAC did demonstrate dose-dependency, with 2X yielding the highest callus density and 0.5X yielding the lowest. However, analysis of the body weight change (Fig. 5.6B) has indicated an increased systemic toxicity with slower restoration to normal weight in mice dosed with 2X DAC (20 μmol/kg). This result has ruled out the use of higher dosage with Q.A.D. dosing frequency despite the enhanced efficacy.

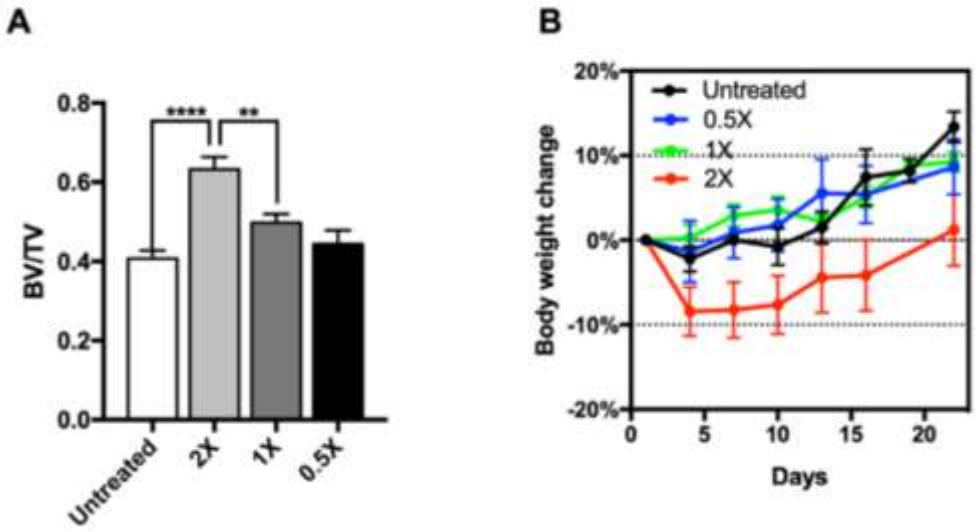

Fig. 5.6 High Dosage with Q.A.D. Dosing Schedule Induces Toxicity.
ND4 Swiss Webster mice bearing stabilized femoral fracture received DAC therapy dosed every other day at 0.5X (5 μmol/kg), 1X (10 μmol/kg), and 2X (20 μmol/kg) (*n* = 7 in each group). After 3 weeks mice were euthanized and analyzed for (**A**) bone density (bone volume/total volume) and (**B**) percent body weight change.

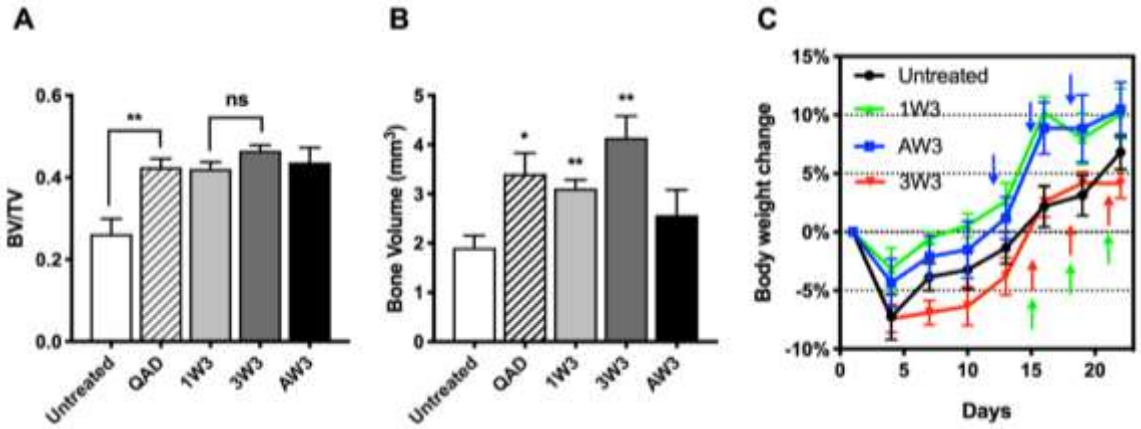

Fig. 5.7 High Dosage with W3 Dosing Schedule Retains Efficacy and Circumvents Toxicity.
ND4 Swiss Webster mice bearing stabilized femoral fracture received DAC therapy dosed every other day at 1X (QAD), three doses in the third week (days 15,18, and 21) at 1X (1W3), three doses in the third week at 3X (3W3), three doses on days 12,15, and 18 at 3X (AW3) (*n* = 6 in each group). After 3 weeks mice were euthanized and analyzed for (**A**) bone density (bone volume/total volume), (**B**) bone volume, and (**C**) percent body weight change. Red and green arrows indicate time points of the three doses for 1W3/3W3 dosing schedule, while blue arrows indicate time points of the three doses for AW3 dosing schedule.

However, systemic toxicity associated with high dosage might be circumvented with reduced dosing frequency. To test this hypothesis, fracture-bearing mice were dosed with the W3 dosing schedule detailed in the previous section (three times during the third week post fracture), but with 3X dosage (30 μmol/kg). As shown in Fig. 5.7A-B, the 3W3 dosing schedule has yielded callus density and bone volume that are comparable to (if not slightly better than) the Q.A.D. schedule. However, it would perform slightly worse than Q.A.D when paired with 1X dosage (1W3). Considering the drastic reduction in the number of total doses and delay in the initiation of the therapy, these were impressive fracture-repair results. These data further suggest that dosing during the early stages of fracture repair is unnecessary. At the meantime, the AW3 dosing schedule, which involves one dose by the end of the second week (the peak of hard callus formation) and two doses flanking the aforementioned one with three-day intervals, failed to yield a comparable level of bone volume despite having a more uniform coverage of the peak of hard callus formation. This observation has called for further insights into the maximizing DAC's interaction with the hard callus formation stage.

Importantly, the trend of body weight change with 3W3 dosing schedule did not show significant signs of systemic toxicity compared to the untreated control with no body weight loss during the week of dosing (Fig. 5.7C),, giving it a substantial advantage to the 2X group in Fig. 5.6 despite having a higher dosage (3X vs. 2X). These data imply that systemic toxicity with high dosage was preventable by lowering the dosing frequency, e.g. dosing only three times during the third week of fracture repair. Collectively, a dosing schedule consisting of only three doses during the third week of fracture healing be one

method to lower the dosing frequency of DAC while retaining its fracture healing efficacy and avoiding excessive systemic toxicity.

5.3.1.3 Selection of the Optimal Dosing Window

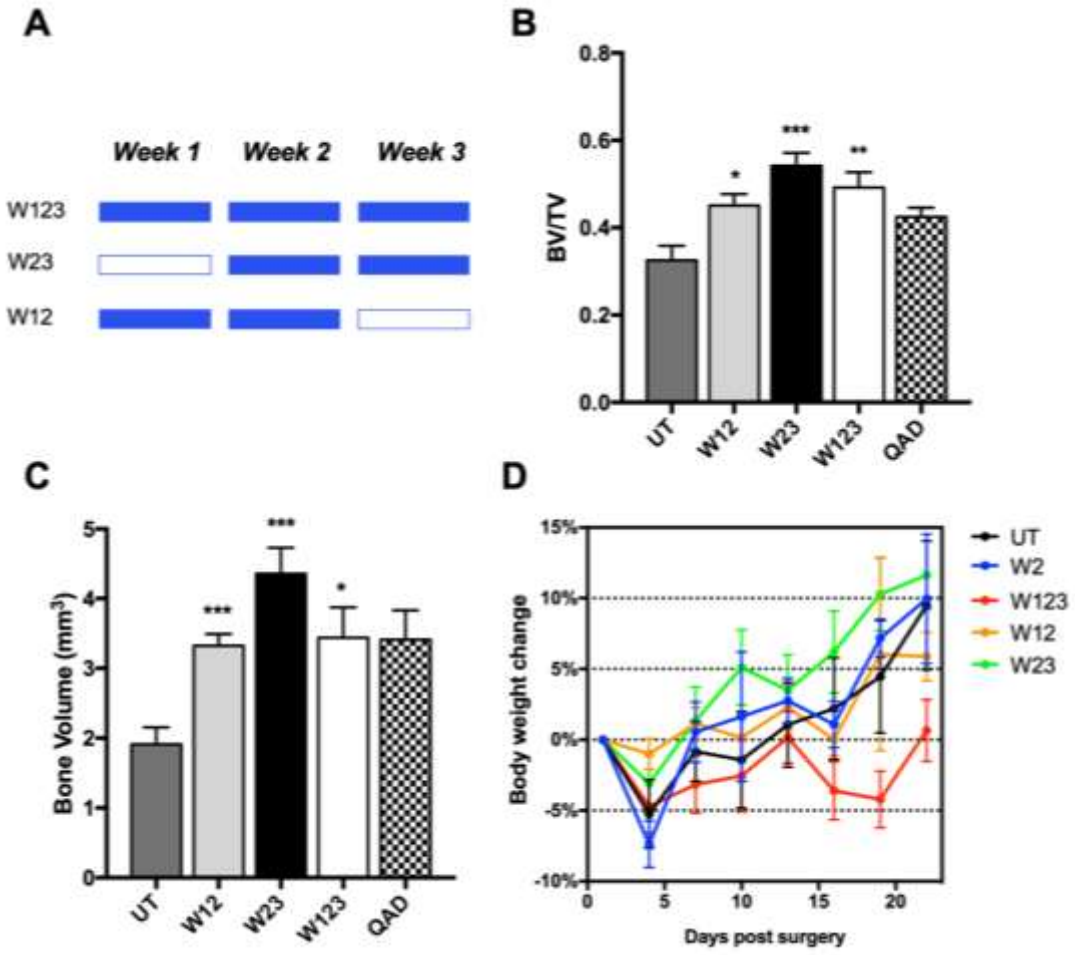

Fig. 5.8 Finding the Optimal Dosing Window of DAC.
ND4 Swiss Webster mice bearing stabilized femoral fracture received DAC therapy at 1X dosage (10 μmol/kg) with the dosing schedule detailed in (**A**), where each filled box indicates three doses in the corresponding week, while an empty box indicates no dosing (n = 7 in each group). After 3 weeks mice were euthanized and analyzed for (**B**) bone density (bone volume/total volume), (**C**) bone volume, and (**D**) percent body weight change.

Although the W3 dosing schedule was proven effective in the previous section, the influence of DAC during each week of fracture repair still remained elusive. It has been shown in the previous sections that W2 dosing schedule did not perform well while both W3 and AW3 dosing schedules performed similarly to Q.A.D., even though those schedules have covered the dosing windows in week 2, week 3, and halfway between week 2 and 3, respectively. We hypothesize that those dosing schedules do not represent the optimal therapeutic window, and that a dosing window overlapping with the hard callus formation stage more thoroughly might bring further improvements to DAC's therapeutic efficacy to promote fracture healing. Thus, mice bearing femoral fracture were treated with DAC at 1X dosage with the dosing schedule specified in Fig. 5.8A. The W123 dosing schedule is a simplified version of Q.A.D. dosing schedule with three doses in all of the three weeks post fracture, while the W12 dosing schedule skips doses in the third week and the W23 dosing schedule skips doses in the first week. As shown in Fig. 5.8B-C, the fracture healing efficacy of the W123 dosing schedule was very similar to that of the Q.A.D. dosing schedule, which was expected considering the similarity between the two schedules. Nonetheless, W123 constitutes an improvement over Q.A.D. since it consists of less doses (9 versus 11) and avoids weekend dosing. The W23 dosing schedule showed the best healing efficacy with both bone density and bone volume being significantly higher than the W123 dosing schedule, which was slightly more effective than the W12 dosing schedule. These results have confirmed that dosing during the first week is not only unnecessary but detrimental to DAC's efficacy, and should be avoided for patients' benefit. Additionally, the W23 dosing schedule demonstrated a better therapeutic efficacy compared to the W3 schedule at the same dosage, suggesting that doses during the second

week should be considered meaningful. Dosing over both the second- and third-week post fracture would allow DAC to interact with the stage of hard callus formation more thoroughly, resulting in a denser fracture callus with more trabecular bone after three weeks.

Furthermore, analysis of the body weight change has shown that a higher systemic toxicity was associated with the W123 dosing schedule compared to W12 and W23 dosing schedules (Fig. 5.8D). Although this observation might be attributed to experimental error since the Q.A.D. dosing schedule did not invoke toxicity before, it was sensible that a higher dosing frequency might lead to less tolerance. Collectively, we have identified the second and third week post fracture as the optimal dosing window for DAC to fully take advantage of its bone-formation-stimulating capacity while allowing for a reduction of the total doses by almost 50% compared to an ever-other-day dosing schedule.

5.3.2 Hydrolysis and Retention Kinetics of DAC and Slow-Release Conjugate

In Section 5.3.1, we have identified the optimal dosing starting point and dosing window for DAC. However, fundamental properties of DAC, such as the release rate of dasatinib from DAC or the time DAC stays on the fracture surface might be fine-tuned to further regulate its therapeutic efficacy and toxicity. Thus, the hydrolysis and retention properties of tweaked versions of DAC are investigated in this section.

5.3.2.1 Hydrolysis Kinetics of DAC at Different pHs

HAP crystalline lattice surface is largely negative, attracting a layer of protons at the very vicinity of its surface. This results in a negative zeta potential, as well as an acidic surface layer good for acid-labile linker cleavage,[15–18] which serves as the basis of our design of DAC with an ester linker. This linker allows dasatinib to be released from DAC on the fracture surface owing to the acidity, but also poses a risk of being prematurely

hydrolyzed in the blood stream at neutral pH. To assess dasatinib's rate of release under both neutral and acidic environments, DAC was incubated at 37 °C in both pH 7 and pH 4 buffers and analyzed with LCMS for the release kinetics.

As pointed out Fig. 5.9, the ester linker on DAC hydrolyzed quickly at pH 7, releasing about 72% of dasatinib after 24 hours. Surprisingly, the hydrolysis slowed down drastically at pH 4, releasing merely ~9% after 24 hours while leaving approximately 70% of dasatinib unreleased after 72 hours. These unexpected results propose that the ester linker on DAC is more labile to hydrolysis under neutral pH in comparison to acidic pH, and that instead of having a fracture-accelerated release mechanism as originally assumed, DAC actually features a fracture-specific sustained-release mechanism.

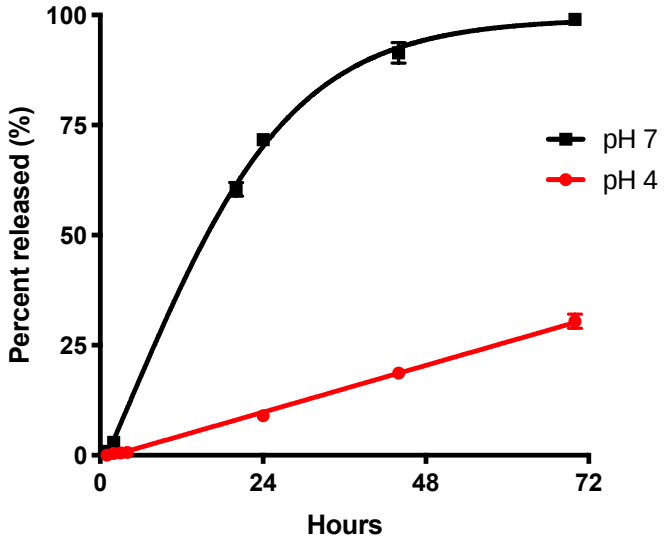

Fig. 5.9 DAC Hydrolysis Curves at pH 7 and pH 4.
DAC was dissolved in either 50 mM Tris-HCl buffer (pH = 7) or 50 mM citrate buffer (pH = 4) to reach a final concentration of 0.1 mg/mL, and incubated in a 37 °C shaker before analysis with LCMS at indicated time points for the percentage of hydrolysis.

The surprising results presented in this section has subverted our initial idea of using a less labile linker to achieve slower release rate on a fracture surface, since the release rate of the ester linker on DAC is already rather slow at acidic pH. Moreover, DAC is far more

labile to hydrolysis at neutral pH, implying a fast degradation rate during circulation in the blood stream. This has raised a concern of premature release, which could lead to unwanted toxicity and reduced therapeutic efficacy. Thus, a linker that is more labile than ester would not be considered suitable for the improvement of DAC, even if it might facilitate the release of dasatinib on the fracture surface. Instead, a more stable linker should be implemented to limit premature release in the plasma.

5.3.2.2 Hydrolysis Kinetics of DAC at pH 7 in the Presence of Hydroxyapatite

In Section 5.3.2.1, the rate of DAC hydrolysis at the fracture site was simulated at pH 4. In this section, the hydrolysis rate of DAC bound on the surface of HAp is examined for a more accurate representation of the hydrolysis taking place on a fracture surface.

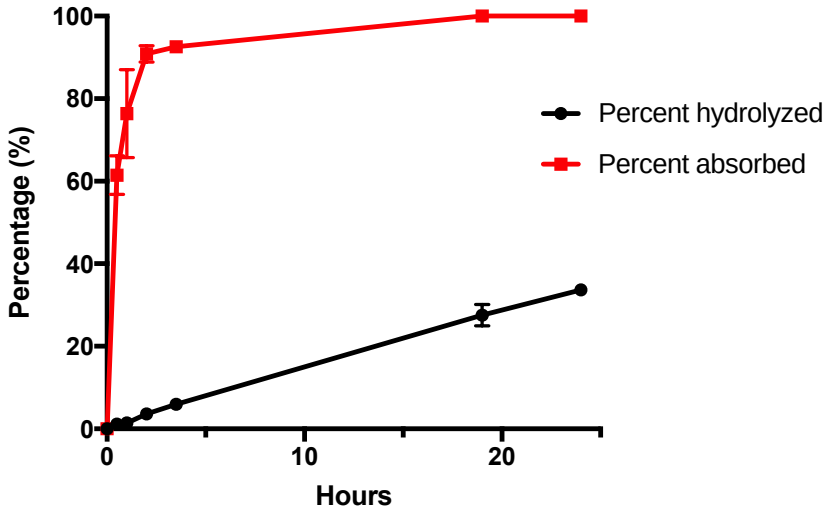

Fig. 5.10 DAC Absorption and Hydrolysis Curves at pH 7 with HAp.
DAC was dissolved in 50 mM Tris-HCl buffer (pH = 7) to reach a final concentration of 0.1 mg/mL, followed by the addition of HAp powder and constant agitation in a 37 °C shaker. Samples were centrifugated and the supernatant was analyzed with LCMS at indicated time points for the percentages of hydrolysis as well as absorption.

As shown in Fig. 5.10, DAC was absorbed to HAp very efficiently, with more than 90% DAC bound within 2 hours, by which time less than 3% of DAC has hydrolyzed in plasma (Fig. 5.9). This is a crucial finding since a fast absorption to HAp ensures good targeting efficacy of DAC prior to its excessive degradation during circulation. Meanwhile, the actual pH level on the surface of HAp could be higher than 4, which might have contributed to a faster hydrolysis rate of DAC as see in Fig. 5.10 though it was still far slower than at pH 7. The results in this section have verified our conclusions from the last section that DAC actually hydrolyzes notably slower at acidic pH or on the surface of HAp. Thus, the justification for a slower-release linker has changed from achieving sustained release to reducing premature degradation during circulation in plasma.

5.3.2.3 Hydrolysis Kinetics of Slow-Release Conjugate MW0346 at pH 7

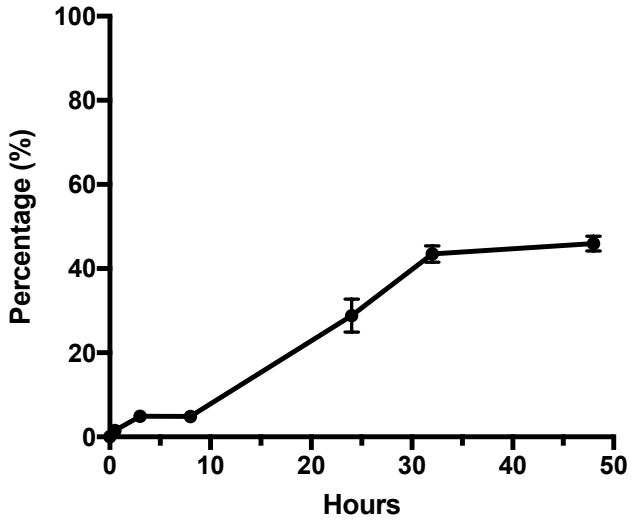

Fig. 5.11 Slow Release Conjugate MW0346 Degrades Slower at pH 7.
MW0346 was dissolved in 50 mM Tris-HCl buffer (pH = 7) to reach a final concentration of 0.1 mg/mL, and incubated in a 37 °C shaker before analysis with LCMS at indicated time points for the percentage of hydrolysis.

MW0346 is a version of DAC that features two methyl groups on the α-carbon of the ester carbonyl, which increases steric hindrance and slows down the nucleophilic addition of water to the carbonyl, hence slowing down the rate of hydrolysis. This presumably slower-release conjugate was put to the same hydrolysis test described in Section 5.3.2.1 at pH 7. Predictably, MW0346 hydrolyzed considerably slower than DAC at pH 7, merely releasing less than half of dasatinib after 48 hours compared to more than 90% released from DAC at the same time point. Thus, MW0346 should alleviate the worry of DAC's potential to pre-release in the blood stream, which could invoke additional toxicity while negatively affecting the therapeutic effect. However, since the ester linker in MW0346 is more stable, the release rate of MW0346 on a fracture surface also decreases, leading to the concern about its fracture healing efficacy. Thus, MW0346 needs to be tested *in vivo* to assess its balance of slower degradation in plasma and slower release of the therapeutic warhead at the fracture site.

5.3.3 Retention Kinetics of L- and D-Aspartic$_{10}$ at the Fracture Site

In Section 5.1.2, we have expressed concerns regarding the potential for D_{10} to be prematurely degraded by proteases before completing the targeting or releasing of dasatinib. To put this concern to the test, S0456 dye conjugates targeted with both regular D_{10} and DD_{10}, which is not digestible by natural enzymes, were injected into fracture-bearing mice to study the retention kinetics.

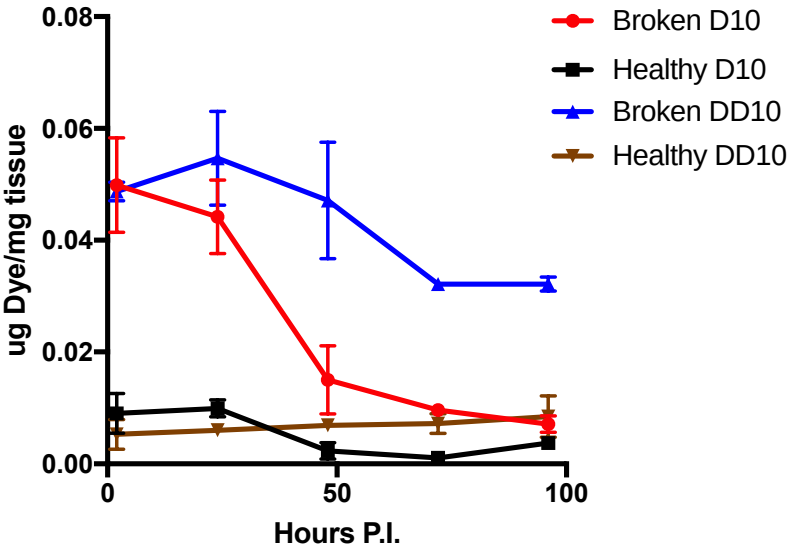

Fig. 5.12 DD_{10} Remains Undamaged at the Fracture Site Longer Than D_{10}.
ND4 Swiss Webster mice bearing stabilized femoral fracture received a single injection of D_{10}-S0456 or DD_{10}-S0456 conjugate 10 days post fracture. The dye conjugate in broken and healthy femurs were quantified at the indicated time points.

As displayed in Fig. 5.12, the accumulated dye conjugate in the broken femurs decreased over time for both conjugates. which could have been caused by either the degradation of the targeting ligand absorbed on the HAp surface or the. Specifically, the decline in quantification of the non-digestible DD_{10}-S0456 conjugate in broken femurs could only be associated with detachment of the conjugate from the fracture surface. Naturally, D_{10}-S0456 was subjected to enzymatic degradation, which contributed to the significantly faster clearance than its D-amino acid counterpart. The retention half-life of D_{10} was estimated to be ~35 hours, whereas that of DD_{10} was projected to be over 100 hours. Given the slow release rate of the ester linker discussed in Section 5.3.2, the relatively short half-life of D_{10} at the fracture site might reduce the available amount of dasatinib during the fracture repair process. Consequently, DD_{10} is valuable in the attempt to truly constitute a “sustained release” conjugate with the ester linker to enable a reduction

of the dosing frequency. Yet, this hypothesis awaits confirmation with *in vivo* therapeutic studies. The half-life of D_{10} at the fracture site in healthy femurs followed the trend of the fractured ones. However, DD_{10}-S0456 did not appear to be cleared from the healthy femurs over time. Despite the low level of accumulation, this raises some worries regarding the safety of this strategy, since prolonged half-life in bone and teeth has been the major safety concern plaguing tetracycline and bisphosphonates.[19,20]

Together, these data have confirmed that D_{10} binds very tightly to HAp with little potential to break loose, and that the main route of clearance for D_{10} at the fracture site is biological degradation. Additional therapeutic studies are required to fully uncover the possible benefits of using a non-degradable targeting ligand.

5.3.4 In Vivo Evaluation of Slow-Release Conjugate MW0346 and DD_{10}-Dasatinib Conjugates

In this section, both the slow-release dasatinib conjugate MW0346 and DD_{10}-dasatinib conjugate were subject to *in vivo* therapeutic studies to assess their abilities to accelerate bone fracture healing.

5.3.4.1 Fracture-Repair Efficacy of MW0346 Conjugate

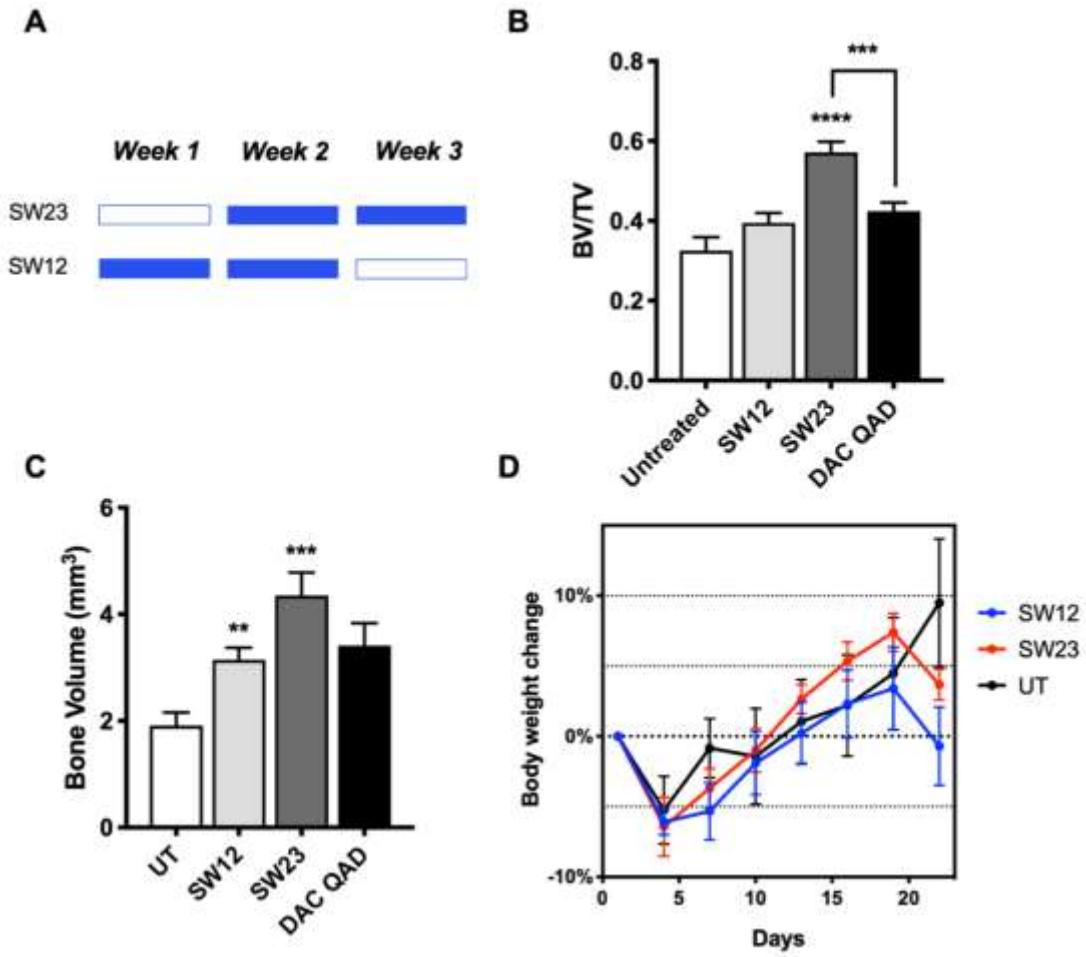

Fig. 5.13 Slow-Release Conjugate MW0346 Increases Bone Density and Volume in Mice.

ND4 Swiss Webster mice bearing stabilized femoral fracture received MW0346 therapy at 1X dosage (10 μmol/kg) with the dosing schedule detailed in (**A**), where each filled box indicates three doses in the corresponding week, while an empty box indicates no dosing (n = 7 in each group, except n = 6 for SW2 group). After 3 weeks mice were euthanized and analyzed for (**B**) bone density (bone volume/total volume), (**C**) bone volume, and (**D**) percent body weight change.

The slow-release conjugate MW0346 were dosed to fracture-bearing mice with the same dosing schedules described in Section 5.3.1.3 except for the W123 schedule, since dosing during the first week should be prevented (Fig. 5.13A). As indicated in Fig. 5.13B-

C, MW0346 worked very well as an enhancer for fracture healing. The SW23 ("S" denotes slow-release) dosing schedule with MW0346 displayed impressive ability to increase bone density and bone volume at the fracture callus. MW0346 demonstrated similar (or slightly better) therapeutic efficacy as DAC with the W23 dosing schedule (Fig. 5.14A-B), both of which were a drastic improvement over the original Q.A.D. or W3 dosing schedule (even at 3X dosage). The reason that MW0346 was able to have similar therapeutic efficacy to DAC despite releasing dasatinib at a far slower rate might owe to the reduced degradation in circulation. Considering the similar efficacy and the enhanced stability in the blood stream, MW0346 makes a superior therapeutic agent for the acceleration of fracture repair compared to DAC.

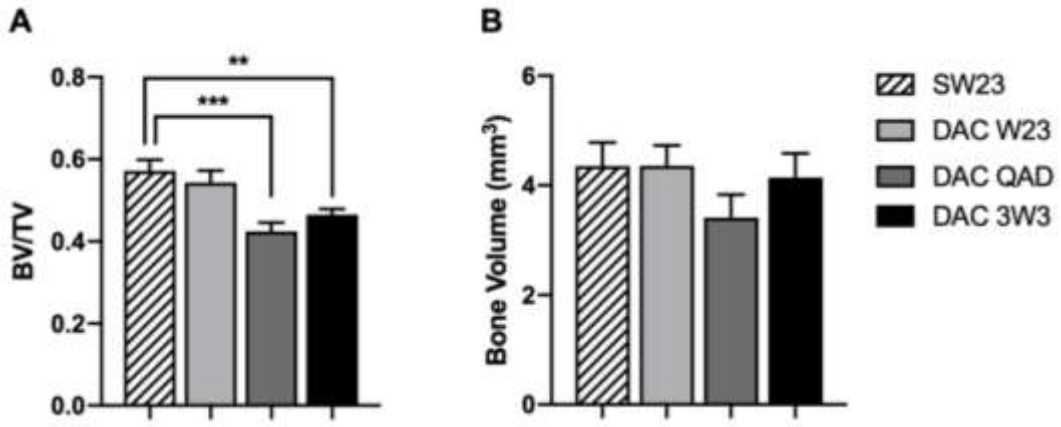

Fig. 5.14 Comparison of Bone Density and Bone Volume Between MW0346 and DAC with Different Dosing Schedules.
All conditions are as described in Fig. 5.7, Fig. 5.8, and Fig. 5.13.

Importantly, neither dosing schedules with MW0346 resulted in systemic toxicity (Fig. 5.13D).

5.3.4.2 Fracture-Repair Efficacy of DD_{10}-Dasatinib Conjugate

As for the DD_{10}-dasatinib conjugate, no apparent acceleration of fracture repair has been observed with Q.A.D., or twice a week, or once a week dosing schedules (Fig. 5.15A-B). Thus, a non-digestible targeting ligand was not only valueless for the reduction in dosing frequency but might harm the therapeutic efficacy of the original DAC. One possible explanation is that the prolonged absorption on the fracture surface could take up HAp binding surface, which could potentially obstruct the binding of newly-delivered conjugate molecules. Plus, due to the slow rate of release on the fracture surface, freshly-deposited bone matrix and mineral could cover up absorbed conjugate before dasatinib is able to be released, rendering a considerable portion of bound conjugate useless.

More importantly, all three dosing schedules for the DD_{10} conjugate demonstrated systemic toxicity to some extent. As mentioned in Section 5.3.3, prolonged half-life in bone is a risk factor for toxicity. Together, the dasatinib conjugate targeted with a non-digestible DD_{10} ligand has not only failed to show efficacy for the promotion of bone fracture healing but induced minor systemic toxicity. Further exploration in the interaction between HAp-targeting ligands and the fracture surface is needed.

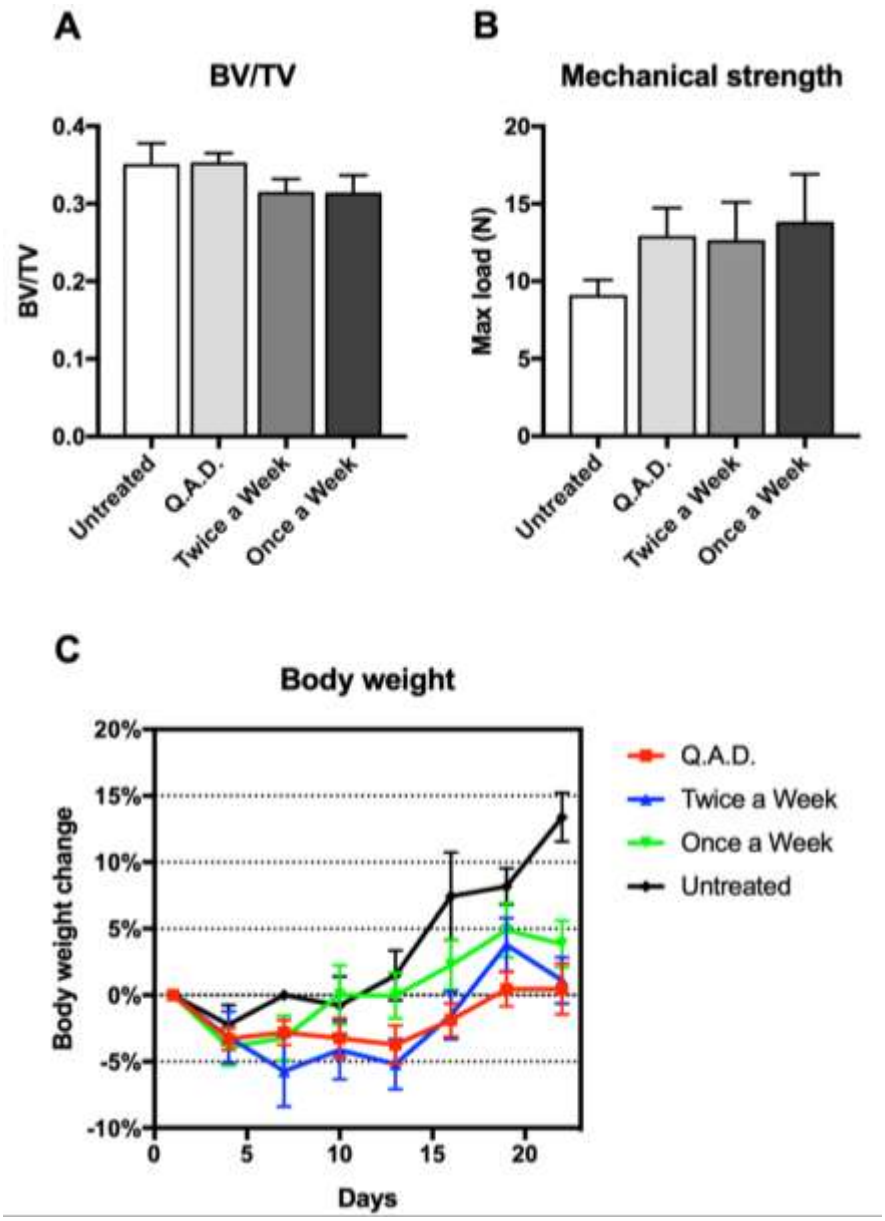

Fig. 5.15 DD_{10}-Dasatinib Conjugate Failed to Accelerate Fracture Healing. ND4 Swiss Webster mice bearing stabilized femoral fracture received DD_{10}-dasatinib therapy at 1X dosage (10 μmol/kg) with Q.A.D., or twice a week, or once a week dosing schedules (n = 6 in each group). After 3 weeks mice were euthanized and analyzed for (**A**) bone density (bone volume/total volume), (**B**) max load, and (**C**) percent body weight change.

5.4 Discussion

In Chapter 4, DAC paired with a Q.A.D. dosing regimen has demonstrated impressive potency as a therapy to accelerate bone fracture repair. However, potency alone

would not make DAC a welcomed medical solution for patients with bone fractures, since the required every-other-day injection would be a major source of inconvenience. Plus, there remained potential for improvement on the efficacy of DAC by dosing in the correct therapeutic window, where it could interact with the physiological processes it has the most significant influence on.[21] Luckily, as shown in this chapter, we have successfully located the optimal dosing window of DAC, which covers the entirety of the stage of hard callus formation. Our speculation that the osteoblast-stimulator dasatinib should have the largest impact on hard callus formation was verified with those results, while the initial inflammatory stage has also been established to be susceptible to inhibition by dasatinib, which could harm the fracture repair result. Thus, skipping dosing during the first week post fracture not only reduces the total doses for the benefit of patients with broken bones, but improves upon the therapeutic efficacy of DAC for a denser and more voluminous fracture callus at three weeks post fracture, at which point a patient is expected to be able to resume a normal, pre-fracture lifestyle.

Although some results suggest that DAC dosing could begin as late as the beginning of the third week and the total doses could be reduced to merely three, the overall fracture repair results with those dosing schedules were very close to that of the Q.A.D. schedule. Those results could have called off the search for a dosing regimen with less doses and comparable therapeutic efficacy, but we continued to look for an optimal dosing window that could allow DAC to contribute to a significantly improved fracture repair. By overlapping the dosing schedule with both the second and third week of fracture healing for a more thorough interaction with the hard callus formation, we identified W23 as the optimal dosing schedule for DAC. W23 features only 6 doses in total, with three in the

second week after fracture occurrence and the other three in the third week. Since the original Q.A.D. dosing schedule features 11 doses in total, W23 has still shortened the dosing course by almost half, which should be welcomed by patients. While the W3 schedule paired with a high dosage (3X) could yield similar callus bone volume to W23 (Fig. 5.14) without overt systemic toxicity, the callus density was notably worse; moreover, the high dose still raises concerns of problems like skin irritation at the injection site. Overall, the reduced number of doses, together with the superior efficacy with regular 1X dosage, has made W23 the ideal new dosing schedule for a DAC therapy.

On top of optimizations of the dosing regimen, the rate that dasatinib is released from DAC has been studied and tweaked in this chapter. Many attempts have been reported on achieving specific drug release at a fracture site, with two of the most popular strategies being linkers hydrolysable by matrix metalloproteinases and cathepsin K (rich in resorptive pit formed by osteoclasts)[22–29] and acid-labile linkers (due to the acidity in fracture hematoma, resorptive pit, and HAp surface).[30–33] We have elected to use an acid-labile ester linker, for its effectiveness, mechanistic simplicity, and its easy translatability to human. Unexpectedly, the ester linker on DAC hydrolyzed slower under acidic pH compared to neutral pH, making the conjugate susceptible to early hydrolysis in the blood stream before the completion of targeting. Thus, a slower release rate has been accomplished by the addition of two α-methyl groups to the ester, which has more than tripled the half-life of the conjugate at pH 7. The slow-release conjugate MW0346, combined with the W23 dosing schedule, has achieved the best therapeutic effect of any targeted dasatinib conjugate tested so far. Conclusively, MW0346 has pointed to us the

direction to address the concern that “every-other-day dosing might still be too frequent for widespread compliance” discussed in Chapter 4.

5.5 References

(1) Li, J.; Stocum, D. L. Fracture Healing. In *Basic and Applied Bone Biology*; Elsevier, 2014; pp 205–223.

(2) Marsell, R.; Einhorn, T. A. The Biology of Fracture Healing. *Injury* **2011**, *42* (6), 551–555.

(3) Kisseleva, T.; Brenner, D. A. Mechanisms of Fibrogenesis. *Exp. Biol. Med. Maywood NJ* **2008**, *233* (2), 109–122.

(4) Glowacki, J. Angiogenesis in Fracture Repair. *Clin. Orthop.* **1998**, No. 355 Suppl, S82-89.

(5) Ozanne, J.; Prescott, A. R.; Clark, K. The Clinically Approved Drugs Dasatinib and Bosutinib Induce Anti-Inflammatory Macrophages by Inhibiting the Salt-Inducible Kinases. *Biochem. J.* **2015**, *465* (2), 271–279.

(6) Knobloch, J.; Jungck, D.; Charron, C.; Stoelben, E.; Ito, K.; Koch, A. Superior Anti-Inflammatory Effects of Narrow-Spectrum Kinase Inhibitors in Airway Smooth Muscle Cells from Subjects with Chronic Obstructive Pulmonary Disease. *J. Allergy Clin. Immunol.* **2018**, *141* (3), 1122-1124.e11.

(7) Yilmaz, O.; Oztay, F.; Kayalar, O. Dasatinib Attenuated Bleomycin-Induced Pulmonary Fibrosis in Mice. *Growth Factors Chur Switz.* **2015**, *33* (5–6), 366–375.

(8) Mohammadalipour, A.; Karimi, J.; Khodadadi, I.; Solgi, G.; Hashemnia, M.; Sheikh, N.; Bahabadi, M. Dasatinib Prevent Hepatic Fibrosis Induced by Carbon Tetrachloride (CCl4) via Anti-Inflammatory and Antioxidant Mechanism. *Immunopharmacol. Immunotoxicol.* **2017**, *39* (1), 19–27.

(9) Lu, C.; Hansen, E.; Sapozhnikova, A.; Hu, D.; Miclau, T.; Marcucio, R. S. Effect of Age on Vascularization during Fracture Repair. *J. Orthop. Res. Off. Publ. Orthop. Res. Soc.* **2008**, *26* (10), 1384–1389.

(10) Saran, U.; Gemini Piperni, S.; Chatterjee, S. Role of Angiogenesis in Bone Repair. *Arch. Biochem. Biophys.* **2014**, *561*, 109–117.

(11) Morioka, M.; Kamizono, A.; Takikawa, H.; Mori, A.; Ueno, H.; Kadowaki, S.; Nakao, Y.; Kato, K.; Umezawa, K. Design, Synthesis, and Biological Evaluation of Novel Estradiol-Bisphosphonate Conjugates as Bone-Specific Estrogens. *Bioorg. Med. Chem.* **2010**, *18* (3), 1143–1148.

(12) Rieger, J. M.; Brown, M. L.; Sullivan, G. W.; Linden, J.; Macdonald, T. L. Design, Synthesis, and Evaluation of Novel A $_{2A}$ Adenosine Receptor Agonists. *J. Med. Chem.* **2001**, *44* (4), 531–539.

(13) Guo, X.; Shi, C.; Wang, J.; Di, S.; Zhou, S. PH-Triggered Intracellular Release from Actively Targeting Polymer Micelles. *Biomaterials* **2013**, *34* (18), 4544–4554.

(14) Kasugai, S.; Fujisawa, R.; Waki, Y.; Miyamoto, K.; Ohya, K. Selective Drug Delivery System to Bone: Small Peptide (Asp)6 Conjugation. *J. Bone Miner. Res. Off. J. Am. Soc. Bone Miner. Res.* **2000**, *15* (5), 936–943.

(15) Waters, N. E. Electrochemical Properties of Human Dental Enamel. *Nature* **1968**, *219* (5149), 62–63.

(16) Wu, L.; Forsling, W.; Schindler, P. W. Surface Complexation of Calcium Minerals in Aqueous Solution. *J. Colloid Interface Sci.* **1991**, *147* (1), 178–185.

(17) Leach, S. A. Electrophoresis of Synthetic Hydroxyapatite. *Arch. Oral Biol.* **1960**, *3* (1), 48–56.

(18) Klein, H. Physico-Chemical Studies On the Structure of Dental Enamel: Viii. the Determination of the Isoelectric Point of Enamel by Means of Membrane-Potential Measurements. *J. Dent. Res.* **1932**, *12* (1), 95–98.

(19) Lin, J. H. Bisphosphonates: A Review of Their Pharmacokinetic Properties. *Bone* **1996**, *18* (2), 75–85.

(20) Botelho, M. G.; Chan, A. W. K.; Newsome, P. R. H.; McGrath, C. P.; Lam, W. Y. H. A Randomized Controlled Trial of Home Bleaching of Tetracycline-Stained Teeth. *J. Dent.* **2017**, *67*, 29–35.

(21) Blair, H. C.; Larrouture, Q. C.; Li, Y.; Lin, H.; Beer-Stoltz, D.; Liu, L.; Tuan, R. S.; Robinson, L. J.; Schlesinger, P. H.; Nelson, D. J. Osteoblast Differentiation and Bone Matrix Formation *In Vivo* and *In Vitro*. *Tissue Eng. Part B Rev.* **2017**, *23* (3), 268–280.

(22) Paiva, K. B. S.; Granjeiro, J. M. Matrix Metalloproteinases in Bone Resorption, Remodeling, and Repair. *Prog. Mol. Biol. Transl. Sci.* **2017**, *148*, 203–303.

(23) Lynch, C. C.; Hikosaka, A.; Acuff, H. B.; Martin, M. D.; Kawai, N.; Singh, R. K.; Vargo-Gogola, T. C.; Begtrup, J. L.; Peterson, T. E.; Fingleton, B.; et al. MMP-7 Promotes Prostate Cancer-Induced Osteolysis via the Solubilization of RANKL. *Cancer Cell* **2005**, *7* (5), 485–496.

(24) Mosig, R. A.; Dowling, O.; DiFeo, A.; Ramirez, M. C. M.; Parker, I. C.; Abe, E.; Diouri, J.; Aqeel, A. A.; Wylie, J. D.; Oblander, S. A.; et al. Loss of MMP-2 Disrupts Skeletal and Craniofacial Development and Results in Decreased Bone Mineralization, Joint Erosion and Defects in Osteoblast and Osteoclast Growth. *Hum. Mol. Genet.* **2007**, *16* (9), 1113–1123.

(25) Franco, G. C. N.; Kajiya, M.; Nakanishi, T.; Ohta, K.; Rosalen, P. L.; Groppo, F. C.; Ernst, C. W. O.; Boyesen, J. L.; Bartlett, J. D.; Stashenko, P.; et al. Inhibition of Matrix Metalloproteinase-9 Activity by Doxycycline Ameliorates RANK Ligand-Induced Osteoclast Differentiation in Vitro and in Vivo. *Exp. Cell Res.* **2011**, *317* (10), 1454–1464.

(26) Takaishi, H.; Kimura, T.; Dalal, S.; Okada, Y.; D'Armiento, J. Joint Diseases and Matrix Metalloproteinases: A Role for MMP-13. *Curr. Pharm. Biotechnol.* **2008**, *9* (1), 47–54.

(27) Nyman, J. S.; Lynch, C. C.; Perrien, D. S.; Thiolloy, S.; O'Quinn, E. C.; Patil, C. A.; Bi, X.; Pharr, G. M.; Mahadevan-Jansen, A.; Mundy, G. R. Differential Effects between the Loss of MMP-2 and MMP-9 on Structural and Tissue-Level Properties of Bone. *J. Bone Miner. Res. Off. J. Am. Soc. Bone Miner. Res.* **2011**, *26* (6), 1252–1260.

(28) Hu, F.; Wang, C.; Guo, S.; Sun, W.; Mi, D.; Gao, Y.; Zhang, J.; Zhu, T.; Yang, S. ΔEF1 Promotes Osteolytic Metastasis of MDA-MB-231 Breast Cancer Cells by Regulating MMP-1 Expression. *Biochim. Biophys. Acta* **2011**, *1809* (3), 200–210.

(29) Noh, E.-M.; Kim, J.-S.; Hur, H.; Park, B.-H.; Song, E.-K.; Han, M.-K.; Kwon, K.-B.; Yoo, W.-H.; Shim, I.-K.; Lee, S. J.; et al. Cordycepin Inhibits IL-1 -Induced MMP-1 and MMP-3 Expression in Rheumatoid Arthritis Synovial Fibroblasts. *Rheumatology* **2008**, *48* (1), 45–48.

(30) Hrubý, M.; Etrych, T.; Kučka, J.; Forsterová, M.; Ulbrich, K. Hydroxybisphosphonate-Containing Polymeric Drug-Delivery Systems Designed for Targeting into Bone Tissue. *J. Appl. Polym. Sci.* **2006**, *101* (5), 3192–3201.

(31) Katunuma, N. Mechanism and Regulation of Bone Resorption by Osteoclasts. In *Current Topics in Cellular Regulation*; Elsevier, 1997; Vol. 35, pp 179–192.

(32) Schell, H.; Duda, G. N.; Peters, A.; Tsitsilonis, S.; Johnson, K. A.; Schmidt-Bleek, K. The Haematoma and Its Role in Bone Healing. *J. Exp. Orthop.* **2017**, *4* (1).

(33) Walters, G.; Pountos, I.; Giannoudis, P. V. The Cytokines and Micro-Environment of Fracture Haematoma: Current Evidence. *J. Tissue Eng. Regen. Med.* **2018**, *12* (3), e1662–e1677.

CHAPTER 6. IN VITRO AND IN VIVO EVALUATION OF OTHER SMALL MOLECULES TO FACILITATE FRACTURE REPAIR

6.1 Introduction

In the previous chapters, dasatinib, the Src kinase inhibitor, has been studied extensively as a therapeutic agent to speed up bone fracture repair. In this chapter, the role of Src inhibition in osteoblast metabolism is further examined with another Src inhibitor, E738. Theoretically, any mechanism that stimulates osteoblastic activity could be exploited for the acceleration of fracture repair, thus the bone-anabolic efficacy of two other osteoblast-stimulating mechanisms (GSK-3β inhibition and S1PR1 agonism) are explored.

6.1.1 Src Kinase Inhibitor E738

In order to be targeted using D_{10} and released at the fracture site, a Src inhibitor bone-anabolic agent eligible for our purpose must have a free hydroxyl functional group for the formation of an ester. Thus, a class of indirubin derivatives with free hydroxyl groups were chosen to be examined for their potential to facilitate fracture repair. Indirubin derivative E804 is a Src kinase inhibitor with an IC_{50} of 0.43 μM (structure shown in Fig. 6.1A),[1,2] which has been reported to promote osteoblast differentiation *in vitro* with an inferior potency to dasatinib.[3] To ensure the effectiveness of the drug, we have elected to study a more potent indirubin derivative Src inhibitor E738 (IC_{50} = 10.7 nM; structure shown in Fig. 6.1B).[1,4] Given the proven efficacy of dasatinib and E804 to stimulate osteoblast differentiation and function, E738 is a promising new small-molecule bone-anabolic agent that might be targeted to a bone fracture surface to improve fracture repair. In this chapter,

we have studied the bone-anabolic efficacy of E738 *in vitro* and the fracture-repair efficacy of a D_{10}-targeted version of E738 *in vivo*.

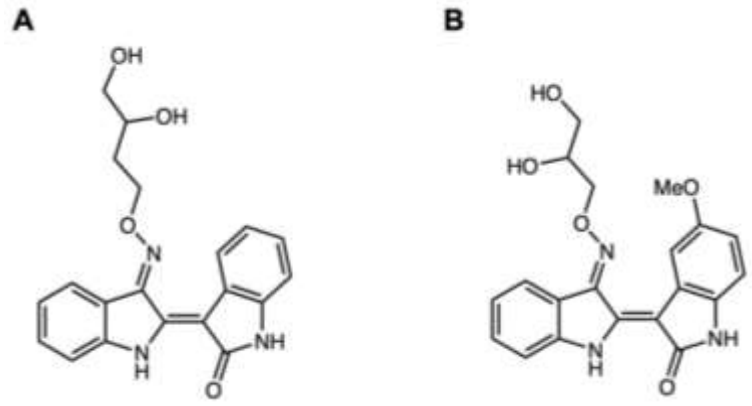

Fig. 6.1 Structures of Indirubin Derivative Src Inhibitors E804 and E738.
(**A**) E804; (**B**) E738.

6.1.2 GSK-3β Inhibitors

As an important player in the Wnt signaling pathway, GSK-3β has been one of the most popular targets for the regulation of bone growth.[5–8] As described in Chapter 1, the activation of Wnt pathway leads to the accumulation of β-catenin in the cytoplasm, which contributes to the proliferation, differentiation, and survival of osteoblasts.[9–11] In this process, GSK3 plays a negative role by phosphorylating β-catenin, which labels β-catenin for subsequent degradation and in turn suppresses Wnt signaling (Fig. 6.2).[5,12,13] In order to offset the physiological suppression of Wnt pathway by GSK-3, many small molecule inhibitors for GSK-3 have been developed with demonstrated ability to enhance Wnt signaling.[14–19] Given the crucial role Wnt signaling plays in tissue and bone regeneration, many of those inhibitors have also been investigated for their efficacy in promoting bone

growth.[16,19–22] Despite the varying degrees of success with those studies, GSK-3β inhibition remains as one of the more promising strategies to promote bone fracture healing.

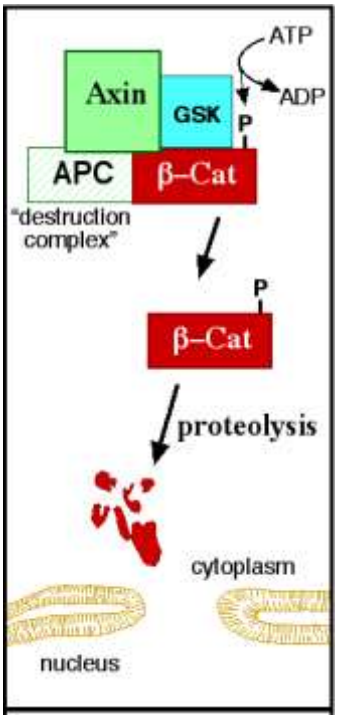

Fig. 6.2 Phosphorylation by GSK3 Marks β-Catenin for Degradation Via Proteolysis. Diagram originally created by JWSchmidt at the English language Wikipedia [CC BY-SA 3.0 (http://creativecommons.org/licenses/by-sa/3.0/)] and modified for use.

Since GSK-3 phosphorylation serves as an ubiquitous signal for the deactivation of the downstream pathway of a protein in a number of cellular pathways in various tissues,[23–25] systemic administration of a GSK-3 inhibitor raises concerns for potential toxicity.[26,27] Thus, the implementation of our targeted delivery strategy is important for a fracture-repair therapy based on GSK-3β inhibition. Low et. al. has used a GSK-3β inhibitor 6BIO incorporated in fracture-targeted micelles to enhance fracture repair while avoiding systemic toxicity.[22] In this chapter, a potent GSK-3β inhibitor CHIR-98014 (IC_{50} = 0.58 nM) is tested for its ability to stimulate the differentiation of mouse osteoblasts, while a

D_{10}-targeted version of a GSK-3β inhibitor, MW0260 (IC_{50} = 0.35 nM[15]), is studied for its ability to promote fracture repair *in vivo*.

6.1.3 Small Molecules that Stimulate Sphingosine-1-Phosphate Receptor 1 (S1PR1)

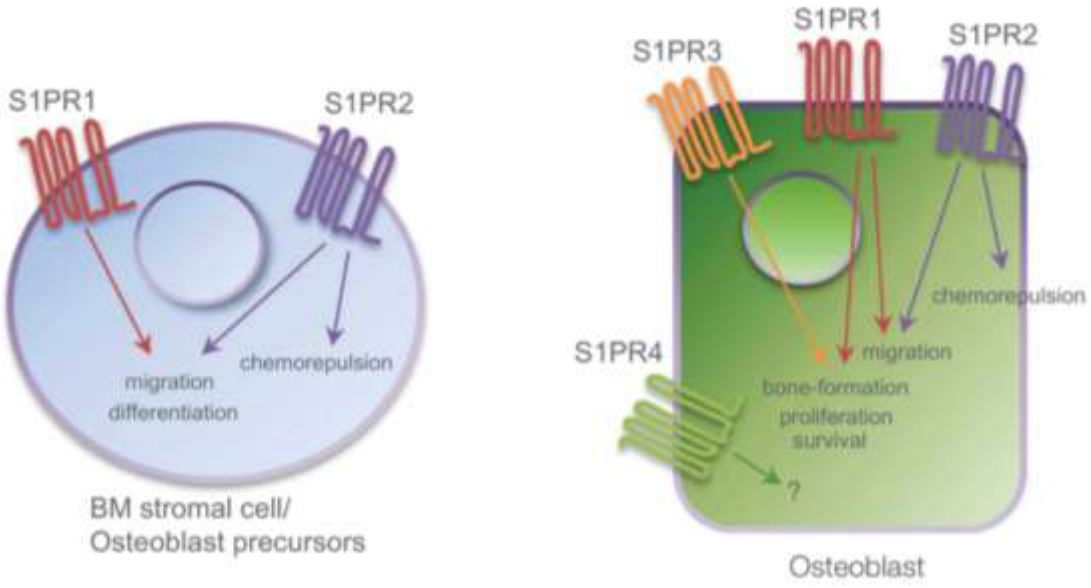

Fig. 6.3 The Role of S1PR1 and S1PR2 in Osteoblast Precursors and Osteoblasts. Signaling of S1PR1 and S1PR2 contributes to osteoblast differentiation from precursor cells, proliferation, survival, migration and bone-formation. Illustration modified from original publication by Meshcheryakova, et. al.[31]

Sphingosine-1-phosphate (S1P) is an important extracellular signaling molecule that mediates a variety of physiological functionalities.[28,29] There are five cell-surface receptors responsible for the downstream signaling pathways related to S1P, namely S1PR1 to S1PR5.[30] In particular, the S1P-S1PR1 and S1P-S1PR2 axes are essential in bone metabolism. It has been reported that S1PR1 knockdown would lead to reduced trabecular thickness and trabecular density *in vivo*, resulting in an osteoporotic phenotype.[31] Meanwhile, S1PR2 signaling boosts OPG production and promotes osteoblast differentiation, which in turn facilitates bone formation.[32] Judging from our experience

with Src inhibition, stimulation of S1P signaling at the fracture site might promote bone growth and facilitate fracture repair.

There are two major methods to stimulate S1P signaling: direct activation of S1P receptor with small molecule agonists or increasing the availability of endogenous S1P by deterring its degradation. Small molecule agonists for S1P receptors with selectivity for a subset of the five S1PRs have been widely reported,[28,33] leaving us with the task of finding a potent one with a free hydroxyl group to derivatize from. On the other hand, the availability of S1P could be increased by the inhibition of S1P lyase, which is the sole enzyme responsible for the irreversible degradation of S1P.[32] Naturally, disruption S1P lyase activity would result in enhanced S1P signaling. Targeted delivery of a S1P inhibitor or a S1PR1 agonist to the fracture surface would boost S1P signaling at the fracture site, which might accelerate fracture repair. By utilizing our targeted delivery strategy, we are able to deliver S1P lyase inhibitors or S1PR1/S1PR2 agonists specifically to the fracture surface for enhanced ability to facilitate fracture healing. We are demonstrating the *in vivo* efficacy for the acceleration of fracture healing from representative S1P lyase inhibitor (DOP) and S1PR1 agonist (ozanimod) in this chapter.

6.2 Materials and Methods

6.2.1 Materials

All materials, solvents and reagents were purchased from commercial sources and used without further purification unless specifically noted, and materials and instruments described in previous chapters are omitted here. Ozanimod was purchased from ChemShuttle (Hayward, CA). DMAP, TBDPSCl, 3-methoxybenzyl alcohol, fluoroindole, ethyl (Triphenylphosphoranylidene)acetate, 5-methoxyisatin, and indoxyl acetate were

purchased from TCI America (Philadelphia, PA). Toluene, THF, Ac_2O, TBAF, MeI, NaH, DOP, chloroacetic chloride, $AlCl_3$, potassium *t*-butoxide, ethyl chlorooxoacetate, TMG, and hydroxylamine hydrochloride Sigma-Aldrich (St. Louis, MO). 3-bromo-1,2-propanediol was purchased from Combi-Blocks (San Diego, CA).

6.2.2 Synthesis of MW0260 and D_{10}-MW0260 Conjugate

The synthesis of MW0260 were performed following a published route.[15] Briefly, 3-methoxybenzyl alcohol (**1**) is protected with acetate group by reacting with acetic anhydride at the presence of DMAP to give **2**. Then **2** undergoes Friedel-Crafts acylation with chloroacetyl chloride to give **3**. **3** cyclizes intracellularly at the presence of base (sodium acetate) to yield the benzofuranone derivative **4**. A Horner–Wadsworth–Emmons reaction follows, giving the ethyl ester **5**, which is then treated with 7 M ammonia in methanol to deprotect the acetate group and transform the ethyl ester into acetamide in one step. In the meantime, fluoroindole **9** is methylated at the N-position with methyl iodide to give **10**, which then undergoes Friedel-Crafts acylation to yield component **11**. The just-freed alcohol is protected with TBDPSCl to give **7**, which is condensed with **11** in the following step then treated with TBAF (TBDPS deprotection) to give the final target molecule **8** (MW0260).

MW0260: LRMS− LC/MS (m/z): $[M + H]^+$ calculated for $C_{22}H_{15}FN_2O_4$, 391.1; found, 391.0. The NMR spectrum for MW0260 was identical to the reported spectrum.

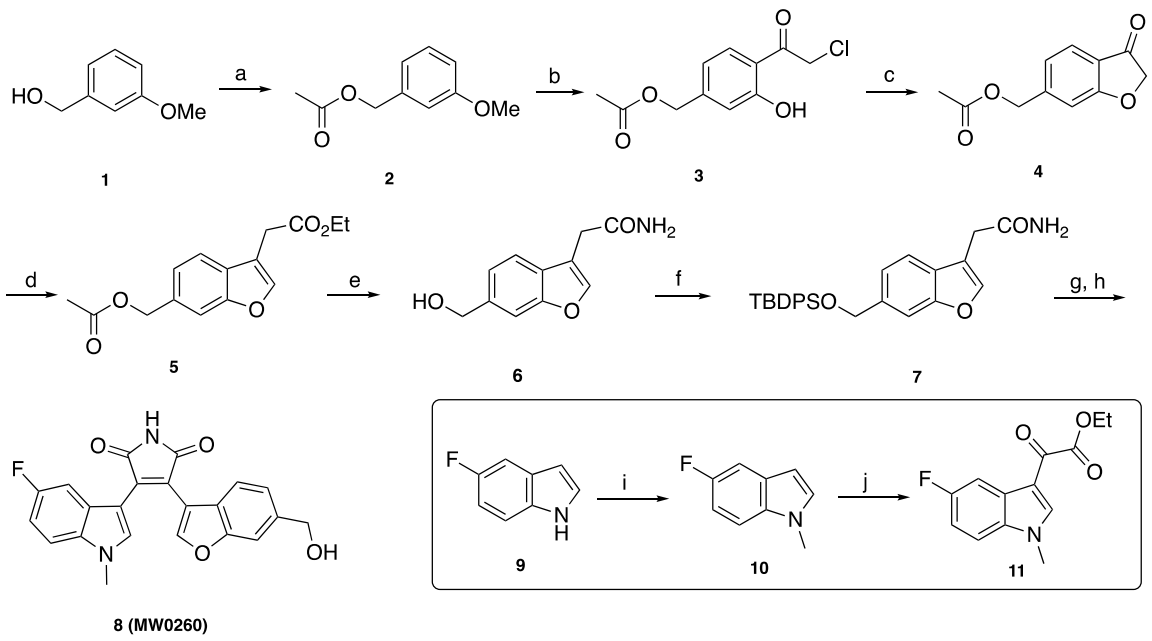

Fig. 6.4 Synthesis of MW0260.
Reagents and conditions: (a) acetic anhydride, TEA, DMAP, DCM, quant.; (b) chloroacetic chloride, aluminum chloride, DCM, 20 %; (c) sodium acetate, MeOH, 70 %; (d) Ethyl (Triphenylphosphoranylidene)acetate, toluene, reflux, 60 %; (e) 7 M ammonia in methanol, 60 °C, 2 days, 90 %; (f) TBDPSCl, imidazole, DMF, DCM, 80 %; (g) potassium *t*-butoxide, THF, 50 %; (h) TBAF, THF, quant.; (i) MeI, NaH, DMF, quant.; (j) ClCOCOOEt, Et_2O, 51 %.

D_{10}-MW0260 conjugate was synthesized using the same modular system described in Chapter 3. The synthesis for D_{10}-cys followed the procedure described in Chapter 3, and MW0260-maleimide was synthesized similarly to dasatinib-maleimide (Fig. 5.1). MW0260 was conjugated to 3-maleimidopropionic acid with coupling reagent PyBOP with the presence of DIPEA in DMF. The reaction mixture was worked up with water and brine, then the organic phase was collected, dried over sodium sulfate and concentrated *in vacuo* to yield the crude product. The crude product was purified by flash column chromatography on Teledyne CombiFlash Rf+ Lumen (0-20% MeOH in DCM) to give MW0260-maleimide as a bright red powder. MW0260-maleimide (90 mg, 0.23 mmol) was dissolved in 2 mL anhydrous DMSO in a 10-mL round-bottom flask degassed with argon.

300 mg D_{10}-Cys (0.2 mmol) was added quickly to the aforementioned solution and stirred until all solid dissolved. The reaction mixture was stirred for 1 hour under argon atmosphere before purification using preparatory reverse phase HPLC. Pure fractions were collected, concentrated *in vacuo* to remove acetonitrile, frozen and lyophilized to yield the final product D_{10}-MW0260 conjugate as a dark orange solid (79 mg, 21%).

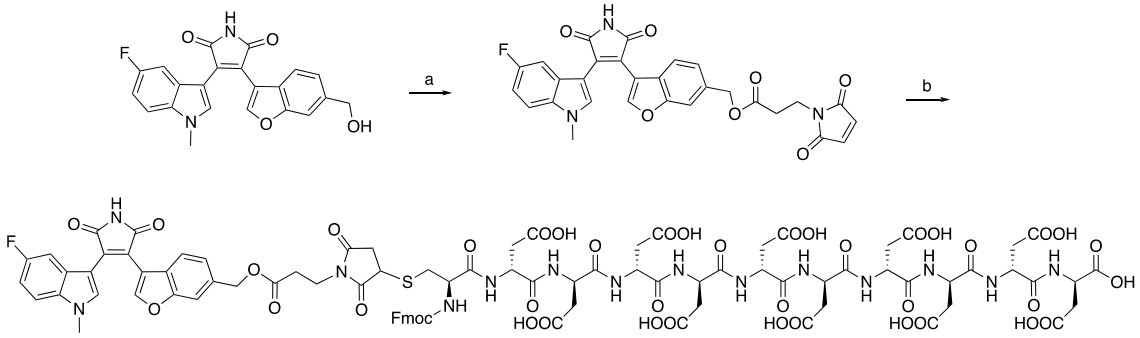

Fig. 6.5 Synthesis of D_{10}-MW0260 Conjugate.
Reagents and conditions: (a) 3-maleimidopropionic acid, PyBOP, DIPEA, DMF, 4h, 75%; (b) D_{10}-cys, DMSO, 1h, 21%

D_{10}-MW0260: LRMS− LC/MS (m/z): $[M + H]^+$ calculated for $C_{87}H_{87}FN_{14}O_{41}S$, 2034.5; found, 1016.2 ($[M-2]^{2-}/2$), 677.1 ($[M-3]^{3-}/3$).

6.2.3 Synthesis of D_{10}-E738 Conjugate

The synthesis of E738 was carried out following a modified published procedure.[4] Indoxyl acetate **1** were dissolved in anhydrous methanol, followed by the addition of 5-methoxyisatin and anhydrous sodium carbonate. The resulting dark purple mixture were stirred at room temperature for 6 hours before the precipitate was isolated with vacuum filtration. The dark red solid **2** was washed 3X with cold methanol before being dissolved in pyridine with hydroxylamine hydrochloride. The mixture was refluxed for 4 hours before neutralization with 0.1 N HCl. The resulting dark red precipitate was isolated with

filtration and washed 3X with Milli-Q water to yield **3**. **3** was charged in a degassed 75 mL pressure tube, followed by the addition of 7.5 mL EtOH. 3-bromo-1,2-propanediol was dissolved in 1.5 mL EtOH and added to the solution, followed by the addition of TMG. The tube was sealed, and the mixture was stirred at 100 °C bath for 3 hours before being cooled to 0 °C and worked up with water and 1N HCl (26 mL). The resulting mixture was extracted with EtOAc for three times, dried over sodium sulfate and concentrated in vacuo to give **4** (E738) as a dark purple/red solid.

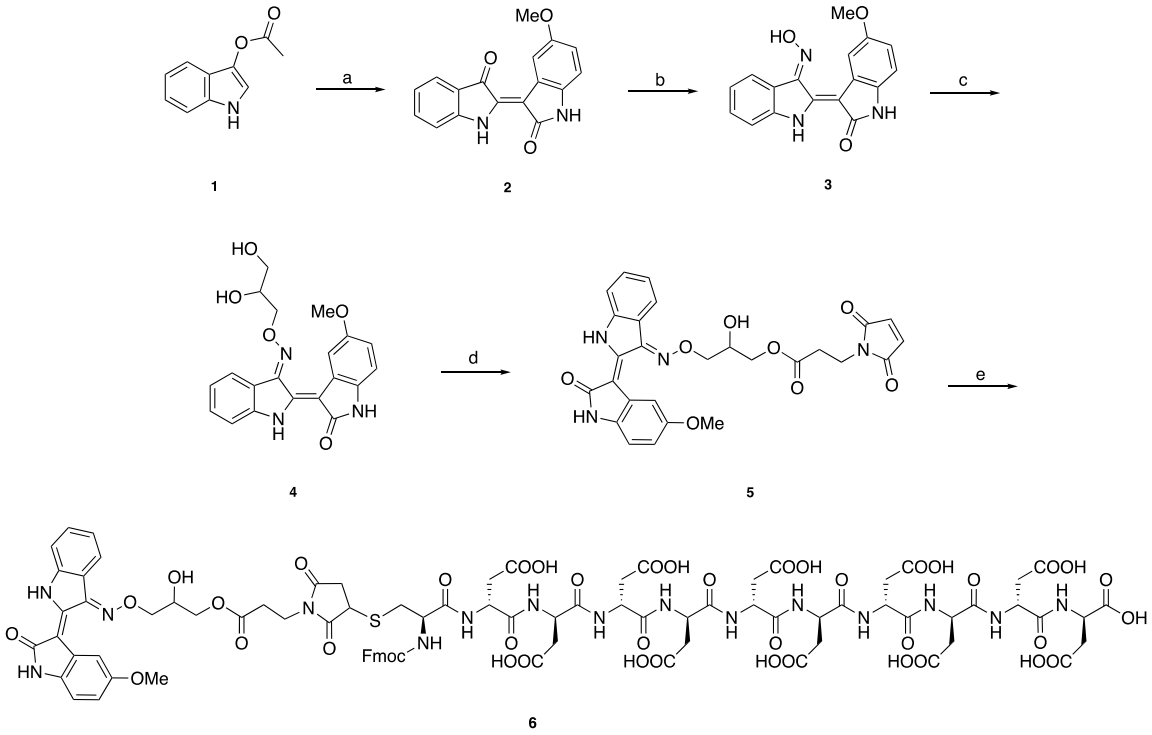

Fig. 6.6 Synthesis of D_{10}-MW0260 Conjugate.
Reagents and conditions: (a) 5-methoxyisatin, MeOH, sodium carbonate, 17%; (b) hydroxylamine hydrochloride, pyridine, *quant.*; (c) 3-bromo-1,2-propanediol, TMG, EtOH, 100 °C, quant.; (d) 3-maleimidopropionic acid, PyBOP, DIPEA, DMF, 4h, 75%; (e) D_{10}-cys, DMSO, 1h, 20%

Both the addition of a maleimide moiety to E738 and the thiol-maleimide conjugation reaction with to yield the final conjugate followed the same procedure

described in the previous section. The final HPLC purification and lyophilization have yielded D_{10}-MW0260 as a bright red/pink solid.

Notably, the product has not been analyzed further to identify which hydroxyl group was esterified, since either hydroxyl would have provided an ester linker that could be hydrolyzed in physiological conditions. The terminal hydroxyl had a higher chance to form the conjugate due to its lack of steric hindrance.

D_{10}-E738: LRMS− LC/MS (m/z): $[M - H]^-$ calculated for $C_{87}H_{87}FN_{14}O_{41}S$, 2033.5; found, 1016.2 ($[M-2]^{2-}/2$), 677.1 ($[M-3]^{3-}/3$).

6.2.4 Synthesis of D_{10}-DOP Conjugate

The synthesis of D_{10}-DOP conjugate followed the same modular system described in previous sections. The free hydroxyl group on DOP was esterified with 3-maleimidopropionic acid with PyBOP and DIPEA in DMF, then the purified DOP-maleimide was conjugated to D_{10}-cys in DMSO. The purified and lyophilized product after HPLC appeared as a white fluffy solid.

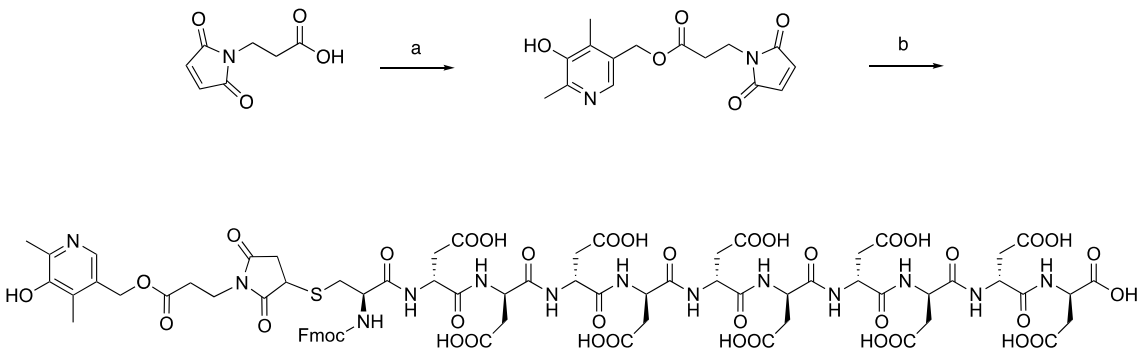

Fig. 6.7 Synthesis of D_{10}-DOP Conjugate.
Reagents and conditions: (a) DOP, PyBOP, DIPEA, DMF, 4h, 73%; (b) D_{10}-cys, DMSO, 1h, 25%.

D_{10}-DOP: LRMS− LC/MS (m/z): $[M - H]^-$ calculated for $C_{73}H_{83}N_{13}O_{39}S$, 1796.6; found, 897.7 ($[M-2]^{2-}/2$), 598.1 ($[M-3]^{3-}/3$).

6.2.5 Synthesis of D_{10}-Ozanimod Conjugate

The synthesis of D_{10}-ozanimod conjugate followed the same modular system described in previous sections.

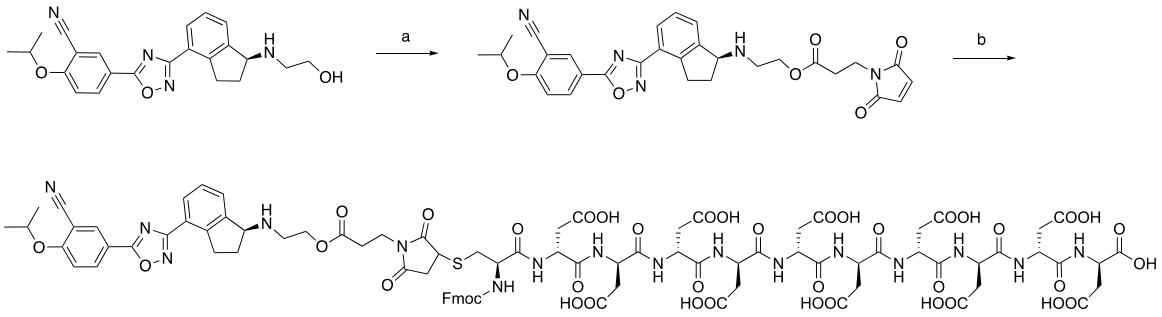

Fig. 6.8 Synthesis of D_{10}-Ozanimod Conjugate.
Reagents and conditions: (a) 3-maleimidopropionic acid, PyBOP, DIPEA, DMF, 4h, 76%; (b) D_{10}-cys, DMSO, 1h, 21%.

D_{10}-ozanimod: LRMS− LC/MS (m/z): $[M - H]^-$ calculated for $C_{88}H_{96}N_{16}O_{40}S$, 2047.6; found, 1022.8 ($[M-2]^{2-}/2$), 681.5 ($[M-3]^{3-}/3$).

6.3 Results

6.3.1 Bone-Fracture-Healing Efficacy of GSK-3β Inhibitors CHIR-98014 and MW0260

6.3.1.1 Effect of CHIR-98014 Treatment on MC3T3-E1 Cells

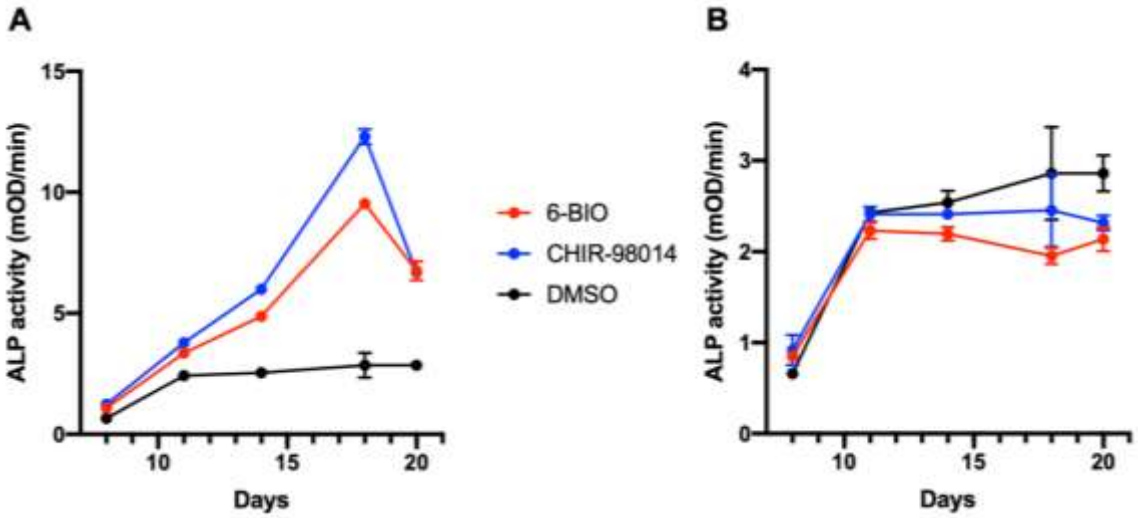

Fig. 6.9 GSK-3β Inhibitor CHIR-98014 Stimulates ALP Activity.
Mouse pre-osteoblastic cell line MC3T3-E1 was incubated in mineralization media containing 100 nM dasatinib or DMSO (n = 3 for all groups) and the enzymatic activity of intracellular alkaline phosphatase (ALP) was measured using the procedures described in Section 2.2.

The ability of the GSK-3β inhibitor CHIR-98014 to promote *in vitro* ALP activity was examined on a murine pre-osteoblast cell line MC3T3-E1. 6BIO, a GSK-3β inhibitor (IC_{50} = 5 nM) reported to facilitate fracture repair *in vivo*,[22] was included as a positive control. As shown in Fig. 6.9A, CHIR-98014 at 7.5 nM concentration was able to potently increase ALP activity in MC3T3-E1 cells, reaching 12 times the activity of the cells treated with DMSO on day 18. 6BIO was also an effective stimulator for ALP activity at the same concentration, but it showed a lower efficacy likely due to its inferior inhibitory potency. It was worth noting that both inhibitors failed to promote ALP activity at a concentration of 500 nM, indicating a bell-shaped curve in their relationship between concentration and

efficacy. Thus, dose-escalation studies are required to locate the optimal dosage for targeted versions of GSK-3 inhibitors.

To sum up, these data suggest that the GSK-3β inhibitor CHIR-98014 potently stimulates osteoblast differentiation, as indicated by the ALP assay. Unfortunately, no point of derivatization existed on CHIR-98014, ruling out the possibility of a D_{10}-targeted version. Thus, another GSK-3β inhibitor MW0260 with similar potency and a free hydroxyl group has been incorporated in a D_{10}-targeted conjugate for *in vivo* investigation.

6.3.1.2 In Vivo Evaluation of D_{10}-MW0260 Conjugate

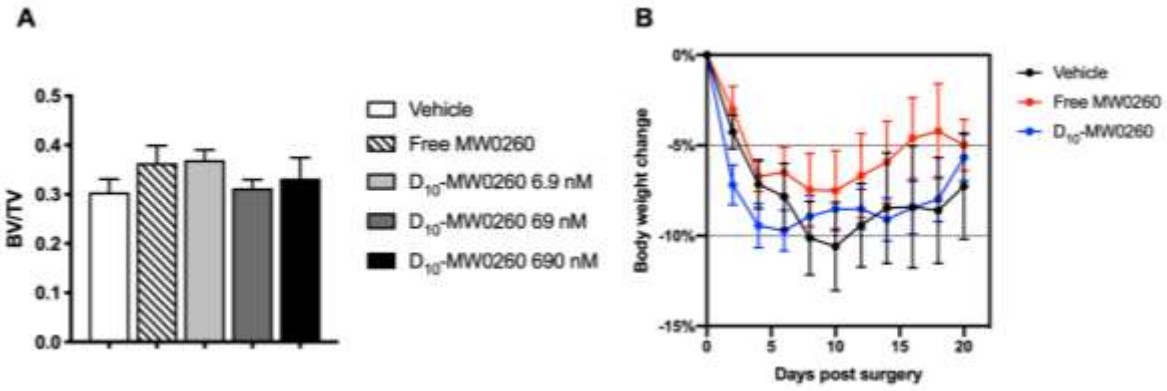

Fig. 6.10 D_{10}-MW0260 Conjugate Did Not Promote Bone Fracture Repair in Vivo. ND4 Swiss Webster mice bearing stabilized femoral fracture received D_{10}-MW0260 therapy dosed daily at 6.9 nmol/kg, 69 nmol/kg, and 690 nmol/kg (n = 5 in each group). After 3 weeks mice were euthanized and analyzed for (**A**) bone density (bone volume/total volume) and (**B**) percent body weight change, in which the D_{10}-MW0260 group was dosed at 6.9 nmol/kg.

As shown in Fig. 6.10, the D_{10}-MW0260 conjugate was not able to increase the bone density at the fracture callus while showing no signs for systemic toxicity (Fig. 6.10B), with dosages ranging from 6.9 to 690 nmol/kg. Notably, the dosage was chosen a published study by Low et. al.,[22] in which a targeted 6BIO were dosed at 6.9 nmol/kg with meaningful bone-anabolic efficacy. The reason that a targeted version of a more potent GSK-3β

inhibitor at a wider range of dosages failed to show bone-anabolic efficacy remains elusive, but given the significantly lower dosage than that of DAC, one might speculate that a higher dosage could improve upon the efficacy. Furthermore, the actual IC_{50} for GSK-3β and the *in vitro* osteoblast-stimulation efficacy of MW0260 need to be verified before a convincing conclusion can be drawn for the potential of using it for the acceleration of fracture repair.

Meanwhile, it is worth noting that during this study, food pellets were not moved to the bedding of the cages in which the study objects were housed. Mice with femoral fracture on their right hind legs had to reach up to the feeding station for food while enduring pain and irritation, which was likely the cause for the increased body weight loss observed in Fig. 6.10B. thus, the D_{10}-MW0260 therapy revealed no obvious toxicities that were not attributed to the short-term trauma associated with the broken femurs.

6.3.2 Bone-Fracture-Healing Efficacy of Src Kinase Inhibitor E738

6.3.2.1 Effect of E738 Treatment on MC3T3-E1 Cells

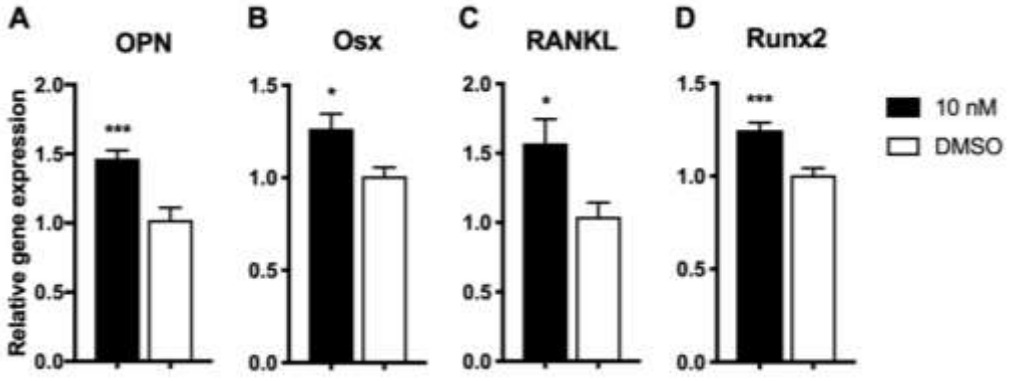

Fig. 6.11 E738 Treatment Upregulates Multiple Osteogenic Genes *in Vitro*.
(**A**)-(**D**) Mouse pre-osteoblastic cell line MC3T3-E1 was incubated in mineralization media containing 10 nM E738 or DMSO (n = 3 for all groups) for 7 days and expression levels of selected bone remodeling genes were analyzed and normalized to GAPDH.

To further testify the bone-anabolic efficacy brought by Src inhibition, E738, a Src inhibitor was incubated with MC3T3-E1, which was later analyzed for the expression of multiple osteogenic genes and ALP activity. As shown in Fig. 6.11A-D, E738 was able to upregulate the expression of OPN, Osx, RANKL and Runx2 at 10 nM on day 7, verified its ability to promote osteoblast differentiation and function. Apparently, E738 was less potent than dasatinib, upregulating less genes than dasatinib on day 7 while not being able to significantly upregulate any genes on day 14. This was not surprising, however, since E738 was 10-15 times less potent than dasatinib in terms of Src inhibition. It was worth noting that despite the inferior potency, E738 were able to stimulate osteoblast differentiation at a lower concentration (10 nM vs. 100 nM). This observation was even more evident with the ALP assay results (Fig. 6.12).

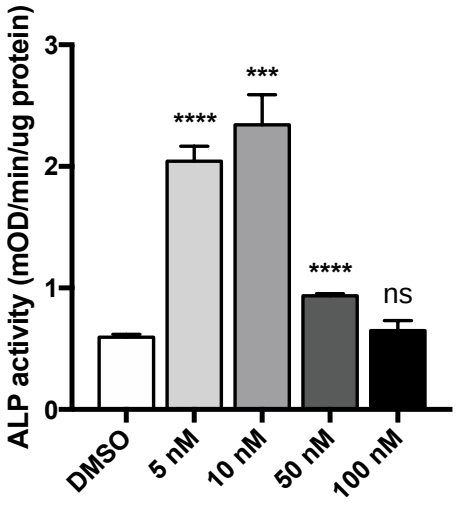

Fig. 6.12 E738 Treatment Promotes ALP Activity in Mouse Osteoblasts.
MC3T3-E1 cells were cultured in mineralization media containing 5 nM, 10 nM, 50 nM, or 100 nM dasatinib or DMSO only, and the enzymatic activity of intracellular alkaline phosphatase (ALP) was measured.

E738 notably upregulated ALP activity on day 7; however, the efficacy was the most prominent at 5 nM and 10 nM, declining steeply at 50 nM and 100 nM. Compared to dasatinib, which had its best efficacy at 100 nM, the optimal working concentration of E738 was clearly lower. This information was important for determining the dosage window for *in vivo* studies with the targeted version.

6.3.2.2 In Vivo Evaluation of D_{10}-E738 Conjugate

As mentioned in the previous section, the optimal working concentration of E738 was lower than that of dasatinib. Thus, lower dosages (0.1X to 1X) were used for the *in vivo* evaluation of the D_{10}-E738 conjugate to maximize the efficacy of the warhead. As indicated in Fig. 6.13A-B, a D_{10}-E738 therapy at 0.1X dosage increased bone density at the fracture callus to a similar level achieved with DAC therapy, though bone volume was markedly lower than the DAC-treated ones. The optimal dosage for D_{10}-E738 should be 0.3X, which achieved comparable bone density and bone volume results as DAC. Considering the different in potency between dasatinib and E738, the therapeutic efficacy of D_{10}-E738 was admirable. Meanwhile, no overt systemic toxicity was observed with D_{10}-E738 at any dosage (Fig. 6.13C).

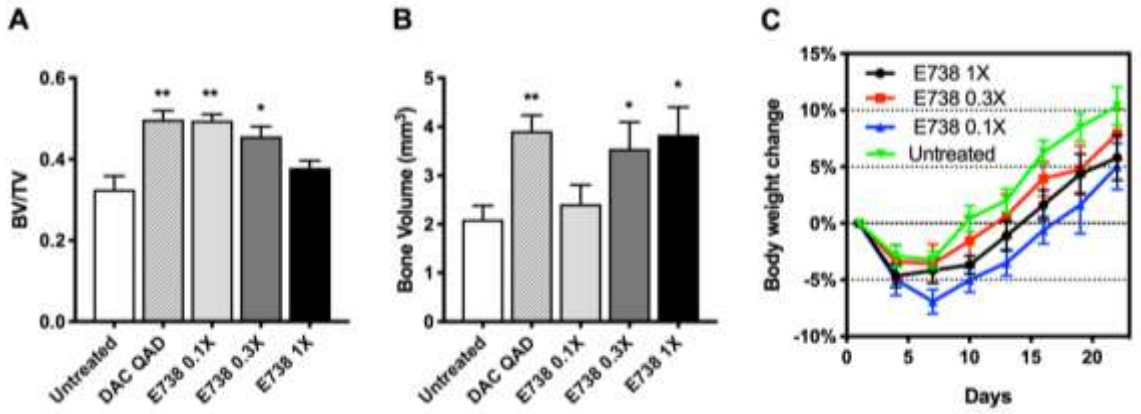

Fig. 6.13 D_{10}-E738 Conjugate Increases Callus Density and Bone Volume. ND4 Swiss Webster mice bearing stabilized femoral fracture received D_{10}-E738 therapy dosed daily at 0.1X (1 μmol/kg), 0.3X (3 μmol/kg), and 1X (10 μmol/kg) (n = 7 in each group). After 3 weeks mice were euthanized and analyzed for (**A**) bone density (bone volume/total volume), (**B**) bone volume, and (**C**) percent body weight change.

Collectively, those data argue that D_{10}-E738 is a promising therapeutic agent for the acceleration of bone fracture repair. A D_{10}-E738 therapy with Q.A.D. dosing schedule could achieve a therapeutic effect only slightly poorer than DAC, at 30% of its dosage. In the future, more detailed studies and optimizations into the targeted delivery of E738 and other targetable Src inhibitors should be planned.

6.3.3 Bone-Fracture-Healing Efficacy of S1PR1-Stimulating Agents

In this section, S1PR1-stimulating agents ozanimod and DOP were tested for their bone-anabolic efficacy. Ozanimod is a potent agonist selective for S1PR1 (0.41 nM) and S1PR5 (11 nM),[34] which is supposed to act directly on S1PR1 receptors on osteoblast surface. Therefore, its osteoblast-stimulating efficacy could be investigated *in vitro* with mouse pre-osteoblast cell line MC3T3-E1. On the other hand, since DOP promotes S1PR1 signaling indirectly by increasing the physiological availability of S1P with the inhibition of S1P lyase,[33] its ability to promote bone growth may only be examined *in vivo*. Thus,

D_{10}-targeted versions of ozanimod and DOP were also administered to fracture-bearing mice for *in vivo* evaluation.

6.3.3.1 Effect of Ozanimod (S1PR1 Agonist) Treatment on MC3T3-E1 Cells

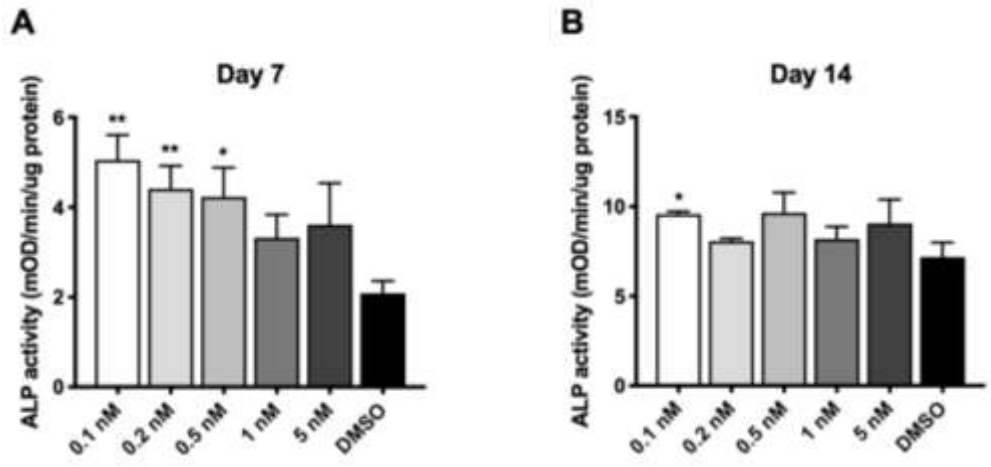

Fig. 6.14 Ozanimod Promotes ALP Activity in Mouse Osteoblasts.
MC3T3-E1 cells were cultured in mineralization media containing 0.1 nM, 0.2 nM, 0.5 nM, 1 nM, 5 nM ozanimod or DMSO only, and the enzymatic activity of intracellular alkaline phosphatase (ALP) was measured on (**A**) day 7 and (**B**) day 14.

As shown in Fig. 6.14A-B, ozanimod showed moderate efficacy toward the differentiation of osteoblasts. On day 7, ozanimod was able to upregulate ALP at concentrations of merely 0.1-0.5 nM, which was significantly lower than the working concentrations of dasatinib or E738. This was expected, however, since ozanimod functions by binding to S1PR1 on the surface osteoblast and was not required to internalize to take effect. Ozanimod was not able to display apparent stimulation of ALP activity on day 14. These data suggest that a low dosage of ozanimod possesses the capacity to promote the early stage of osteoblast differentiation.

6.3.3.2 In Vivo Evaluation of D_{10}-Ozanimod Conjugate

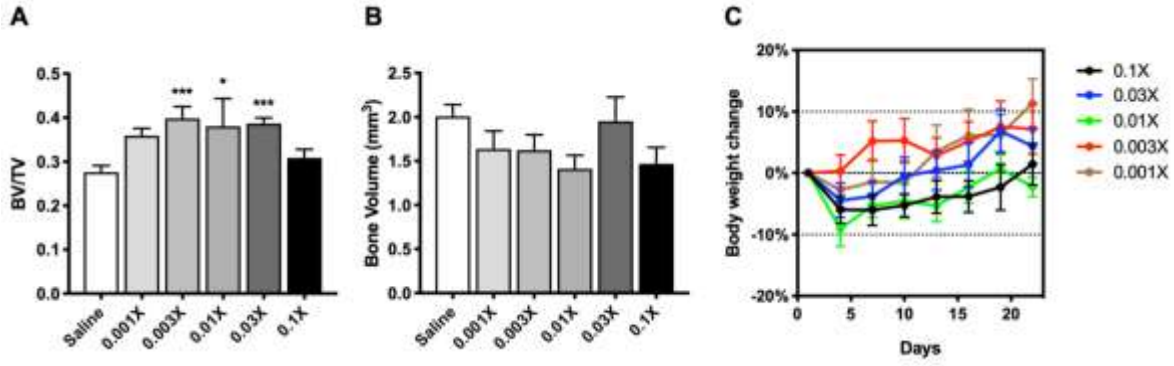

Fig. 6.15 D_{10}-Ozanimod Moderately Accelerate Bone Fracture Repair in Vivo. ND4 Swiss Webster mice bearing stabilized femoral fracture received D_{10}-ozanimod therapy dosed daily at dosages from 0.001X (10 nmol/kg) to 0.1X (1 μmol/kg) (n = 5 in each group). After 3 weeks mice were euthanized and analyzed for (**A**) bone density (bone volume/total volume), (**B**) bone volume, and (**C**) percent body weight change.

To assess whether ozanimod's stimulation of early osteoblast differentiation could translate into enhanced bone fracture repair, D_{10}-ozanimod conjugate was administered to ND4 Swiss mice bearing femoral fractures. As shown in Fig. 6.15A-B, D_{10}-ozanimod was only able to moderately increase bone density at the fracture callus, while failing to bring obvious benefit in terms of bone volume. The trend of body weight change did not show signs of systemic toxicity, which was expected considering the low dosage of D_{10}-ozanimod with an optimal dosing range of 0.003X-0.03X. However, the lack of meaningful therapeutic effect has limited the outlook of D_{10}-ozanimod as a therapy for human patients with bone fractures.

Nonetheless, further investigation into several details regarding a targeted ozanimod therapy is required before drawing a decisive conclusion. First, since the nucleophilic secondary amine on ozanimod could form an amide with 3-maleimidopromionic acid in the presence of PyBOP, D_{10}-ozanimod synthesized using the method described in Section

6.2.5 might have partly yielded a non-releasable conjugate with an amide linker instead of an ester. Although ozanimod is not required to be released to activate S1PR1 signaling on osteoblast surface in theory, the spacer between ozanimod and D_{10} was probably too short to allow for an effective docking of the former to an S1P receptor. In the future, pure conjugates that are releasable and non-releasable need to be synthesized using proper protecting groups on ozanimod, to fully uncover the optimal design for ozanimod or other potential bone-anabolic agents that interact with cell-surface receptors. Further discussion on the future development of ozanimod could be found in Chapter 7.

6.3.3.3 In Vivo Evaluation of D_{10}-DOP Conjugate (S1P Lyase Inhibitor)

As DOP has been reported to alleviate osteoporosis *in vivo*,[32] its ability to improve bone fracture healing is promising. As demonstrated in Fig. 6.16A-B, D_{10}-DOP therapy was able to increase the callus density of ND4 Swiss Webster mice bearing femoral fracture with either QAD or W3 dosing schedules. Specifically, D_{10}-DOP with W3 dosing schedule showed comparable performance to a DAC therapy with QAD dosing schedule. Unfortunately, neither dosing schedules with D_{10}-DOP improved bone volume to the level DAC achieved. Nevertheless, given its safety (Fig. 6.16C) and capacity to increase bone density, D_{10}-DOP remains an encouraging therapy to improve bone fracture healing with further optimizations of its dosing regimen.

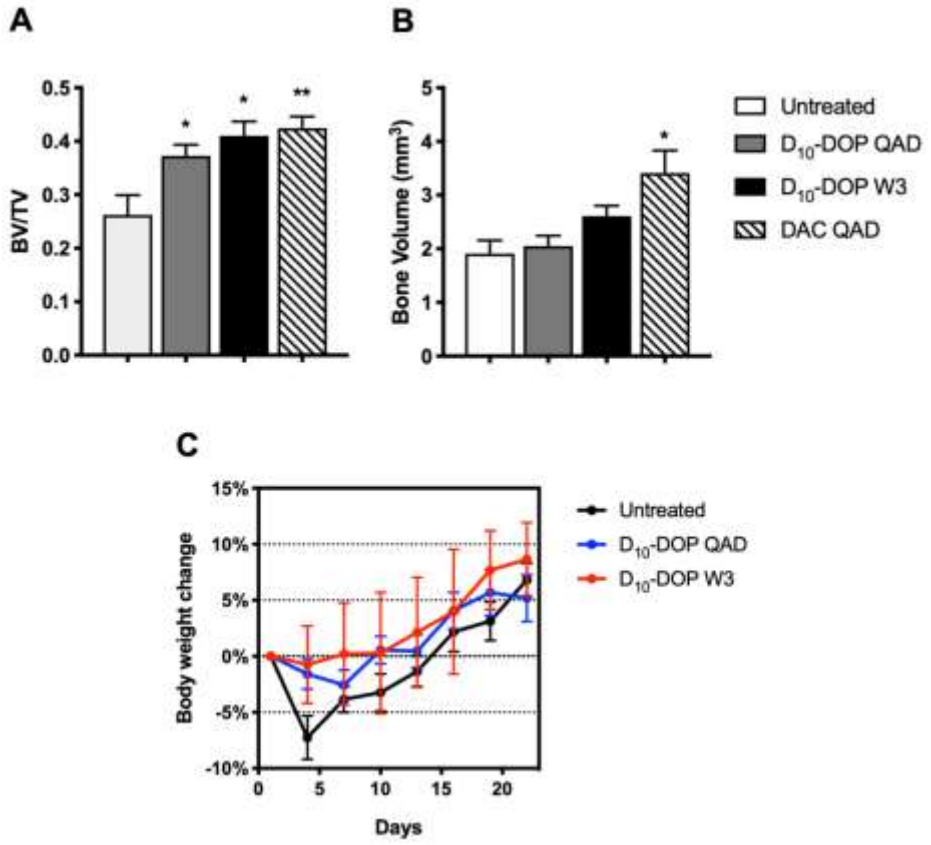

Fig. 6.16 D_{10}-DOP Accelerates Bone Fracture Repair.
ND4 Swiss Webster mice bearing stabilized femoral fracture received D_{10}-DOP therapy dosed at 1X (10 μmol/kg) with Q.A.D. or W3 dosing schedules (n = 7 in each group). After 3 weeks mice were euthanized and analyzed for (**A**) bone density (bone volume/total volume), (**B**) bone volume, and (**C**) percent body weight change.

6.4 Discussion

In this chapter, we have demonstrated our framework for the development of new targeted bone-anabolic agents for the acceleration of bone fracture repair. Essentially, physiological processes that could either activate or suppress bone formation are the basis for the bone-anabolic property, especially those involved in the regulation of osteoblastic activity, are all potentially useful. We would identify small molecules (and peptides) that could drive those processes to the direction we want, i.e. promotion of the activation or inhibition of the suppression of bone growth, as potential drug warheads. A drug warhead

might be subjected to *in vitro* studies with MC3T3-E1 cells to test its ability to activate osteoblast differentiation and function before being delivered specifically to a fracture surface with D_{10} in mice bearing femoral fracture to examine its therapeutic efficacy *in vivo*. Once the efficacy of a conjugate has been verified, further investigation of its optimal dosage and dosing window would be carried out to maximize the therapeutic potential.

The modular, convergent synthetic route for DAC has shown its power in Chapters 5 and 6, which has been used to synthesize seven conjugates with various warheads and targeting ligands, with only minor modifications. Theoretically, any bone-anabolic agent molecule with a free hydroxyl group might be conjugated to D_{10} with this synthetic strategy to yield a targeted conjugate with a self-immolative ester linker. In this chapter, the small molecule Src inhibitor E738, GSK-3β inhibitor MW0260, S1PR1 agonist ozanimod, and S1P lyase inhibitor DOP have all been targeted to bone fracture surfaces in mice to show their different capacities to accelerate bone fracture healing. E738, despite being more than 10 times less potent than dasatinib, has shown respectable bone-anabolic efficacy *in vivo*, proving the legitimacy of exploiting Src inhibition to accelerate fracture repair. Although D_{10}-MW0260 had poor efficacy *in vivo*, the negative result might be attributed to reasons not associated with the underlying mechanism. Given the abundance of success in using GSK-3β inhibitors to promote bone growth, more GSK-3β inhibitors that have been verified for efficacy *in vitro* should be tested in animals in a targeted form.

Moreover, we have recognized S1PR1 as a valuable target for bone regeneration. Activation of S1PR1 signaling through the inhibition of S1P lyase with DOP, which raises the physiological level of S1P, is clever and effective. Still, what exited us the most has been the ability to promote bone growth at the fracture site with a targeted small molecule

agonist for S1PR1. S1PR1 differs from the targets discussed previously in that it is located on the surface of osteoblasts. Thus, a ligand that triggers S1P signaling through S1PR1 is not required to internalize into osteoblasts to function properly, eliminating the need for a release mechanism. Also eliminated are considerations on the rate and condition of release, concerns of premature release, and risk of human translation failure due to a malfunctioning release mechanism in different species. However, challenges facing non-releasable conjugates of S1PR1 agonists are spacer lengths, spacer properties, and linking positions. A spacer with optimal length is crucial to the binding of an agonist to a cell-membrane receptor, and it has been shown that rigid linkers are valuable in improving the binding properties as well.[35,36] More importantly, the position of derivatization from an S1PR1 agonist determines whether or not the resulting conjugate could maintain the affinity to the receptor. Extensive studies into the structure-activity relationship or co-crystal structure of a receptor-agonist complex is required to identify positions for derivatization that are not located in the binding pocket to avoid interference with its agonist efficacy.

Finally, many other mechanisms to promote bone formation fit in our framework and are available to be tested. For instance, Bruton's tyrosine kinase (BTK) has been found to play important roles in osteoclastogenesis, and that mice deficient in BTK displayed severe osteopetrosis.[37,38] Although a mechanism involving osteoclasts does not meet our criteria for the enhancement of bone fracture, inhibitors for BTK might be promising antiresorptives. Another candidate for an antiresorptive therapy is inhibitors for RON kinase, which is essential for osteoclastogenesis.[39] PDGFR, on the other hand, serves as the upstream factor of Src kinase, and plays a negative role in osteoblastogenesis. Thus,

PDGFR inhibitors would made potential osteoblast stimulators for accelerated fracture healing.[40] Many more mechanisms to regulate bone homeostasis have been studied and reported, making the prospect of discovering new warheads for our targeted delivery system bright and enthralling.

6.5 References

(1) Nam, S.; Wen, W.; Schroeder, A.; Herrmann, A.; Yu, H.; Cheng, X.; Merz, K.-H.; Eisenbrand, G.; Li, H.; Yuan, Y.-C.; et al. Dual Inhibition of Janus and Src Family Kinases by Novel Indirubin Derivative Blocks Constitutively-Activated Stat3 Signaling Associated with Apoptosis of Human Pancreatic Cancer Cells. *Mol. Oncol.* **2013**, *7* (3), 369–378.

(2) Nam, S.; Buettner, R.; Turkson, J.; Kim, D.; Cheng, J. Q.; Muehlbeyer, S.; Hippe, F.; Vatter, S.; Merz, K.-H.; Eisenbrand, G.; et al. Indirubin Derivatives Inhibit Stat3 Signaling and Induce Apoptosis in Human Cancer Cells. *Proc. Natl. Acad. Sci. U. S. A.* **2005**, *102* (17), 5998–6003.

(3) Id Boufker, H.; Lagneaux, L.; Najar, M.; Piccart, M.; Ghanem, G.; Body, J.-J.; Journé, F. The Src Inhibitor Dasatinib Accelerates the Differentiation of Human Bone Marrow-Derived Mesenchymal Stromal Cells into Osteoblasts. *BMC Cancer* **2010**, *10* (1).

(4) Cheng, X.; Merz, K.-H.; Vatter, S.; Zeller, J.; Muehlbeyer, S.; Thommet, A.; Christ, J.; Wölfl, S.; Eisenbrand, G. Identification of a Water-Soluble Indirubin Derivative as Potent Inhibitor of Insulin-like Growth Factor 1 Receptor through Structural Modification of the Parent Natural Molecule. *J. Med. Chem.* **2017**, *60* (12), 4949–4962.

(5) Wu, D.; Pan, W. GSK3: A Multifaceted Kinase in Wnt Signaling. *Trends Biochem. Sci.* **2010**, *35* (3), 161–168.

(6) Gillespie, J. R.; Bush, J. R.; Bell, G. I.; Aubrey, L. A.; Dupuis, H.; Ferron, M.; Kream, B.; DiMattia, G.; Patel, S.; Woodgett, J. R.; et al. GSK-3β Function in Bone Regulates Skeletal Development, Whole-Body Metabolism, and Male Life Span. *Endocrinology* **2013**, *154* (10), 3702–3718.

(7) Itoh, S.; Saito, T.; Hirata, M.; Ushita, M.; Ikeda, T.; Woodgett, J. R.; Algül, H.; Schmid, R. M.; Chung, U.; Kawaguchi, H. GSK-3α and GSK-3β Proteins Are Involved in Early Stages of Chondrocyte Differentiation with Functional Redundancy through RelA Protein Phosphorylation. *J. Biol. Chem.* **2012**, *287* (35), 29227–29236.

(8) Kapadia, R. M.; Guntur, A. R.; Reinhold, M. I.; Naski, M. C. Glycogen Synthase Kinase 3 Controls Endochondral Bone Development: Contribution of Fibroblast Growth Factor 18. *Dev. Biol.* **2005**, *285* (2), 496–507.

(9) Logan, C. Y.; Nusse, R. The Wnt Signaling Pathway in Development and Disease. *Annu. Rev. Cell Dev. Biol.* **2004**, *20*, 781–810.

(10) Komiya, Y.; Habas, R. Wnt Signal Transduction Pathways. *Organogenesis* **2008**, *4* (2), 68–75.

(11) Yavropoulou, M. P.; Yovos, J. G. The Role of the Wnt Signaling Pathway in Osteoblast Commitment and Differentiation. *Horm. Athens Greece* **2007**, *6* (4), 279–294.

(12) Metcalfe, C.; Bienz, M. Inhibition of GSK3 by Wnt Signalling - Two Contrasting Models. *J. Cell Sci.* **2011**, *124* (21), 3537–3544.

(13) Mills, C. N.; Nowsheen, S.; Bonner, J. A.; Yang, E. S. Emerging Roles of Glycogen Synthase Kinase 3 in the Treatment of Brain Tumors. *Front. Mol. Neurosci.* **2011**, *4*, 47.

(14) Atilla-Gokcumen, G. E.; Pagano, N.; Streu, C.; Maksimoska, J.; Filippakopoulos, P.; Knapp, S.; Meggers, E. Extremely Tight Binding of a Ruthenium Complex to Glycogen Synthase Kinase 3. *ChemBioChem* **2008**, *9* (18), 2933–2936.

(15) Gaisina, I. N.; Gallier, F.; Ougolkov, A. V.; Kim, K. H.; Kurome, T.; Guo, S.; Holzle, D.; Luchini, D. N.; Blond, S. Y.; Billadeau, D. D.; et al. From a Natural Product Lead to the Identification of Potent and Selective Benzofuran-3-Yl-(Indol-3-Yl)Maleimides as Glycogen Synthase Kinase 3β Inhibitors That Suppress Proliferation and Survival of Pancreatic Cancer Cells. *J. Med. Chem.* **2009**, *52* (7), 1853–1863.

(16) Kulkarni, N. H.; Onyia, J. E.; Zeng, Q.; Tian, X.; Liu, M.; Halladay, D. L.; Frolik, C. A.; Engler, T.; Wei, T.; Kriauciunas, A.; et al. Orally Bioavailable GSK-3α/β Dual Inhibitor Increases Markers of Cellular Differentiation In Vitro and Bone Mass In Vivo. *J. Bone Miner. Res.* **2006**, *21* (6), 910–920.

(17) Kramer, T.; Schmidt, B.; Lo Monte, F. Small-Molecule Inhibitors of GSK-3: Structural Insights and Their Application to Alzheimer's Disease Models. *Int. J. Alzheimers Dis.* **2012**, *2012*, 1–32.

(18) Naujok, O.; Lentes, J.; Diekmann, U.; Davenport, C.; Lenzen, S. Cytotoxicity and Activation of the Wnt/Beta-Catenin Pathway in Mouse Embryonic Stem Cells Treated with Four GSK3 Inhibitors. **2014**, *7*, 273.

(19) Schoeman, M. A. E.; Moester, M. J. C.; Oostlander, A. E.; Kaijzel, E. L.; Valstar, E. R.; Nelissen, R. G. H. H.; Löwik, C. W. G. M.; Rooij, K. E. d. Inhibition of GSK3β Stimulates BMP Signaling and Decreases *SOST* Expression Which Results in Enhanced Osteoblast Differentiation: G SK3B I NHIBITION D ECREASES S OST E XPRESSION. *J. Cell. Biochem.* **2015**, *116* (12), 2938–2946.

(20) Sisask, G.; Marsell, R.; Sundgren-Andersson, A.; Larsson, S.; Nilsson, O.; Ljunggren, Ö.; Jonsson, K. B. Rats Treated with AZD2858, a GSK3 Inhibitor, Heal Fractures Rapidly without Endochondral Bone Formation. *Bone* **2013**, *54* (1), 126–132.

(21) Marsell, R.; Sisask, G.; Nilsson, Y.; Sundgren-Andersson, A. K.; Andersson, U.; Larsson, S.; Nilsson, O.; Ljunggren, Ö.; Jonsson, K. B. GSK-3 Inhibition by an Orally Active Small Molecule Increases Bone Mass in Rats. *Bone* **2012**, *50* (3), 619–627.

(22) Low, S. A.; Galliford, C. V.; Jones-Hall, Y. L.; Roy, J.; Yang, J.; Low, P. S.; Kopeček, J. Healing Efficacy of Fracture-Targeted GSK3β Inhibitor-Loaded Micelles for Improved Fracture Repair. *Nanomed.* **2017**, *12* (3), 185–193.

(23) Ali, A.; Hoeflich, K. P.; Woodgett, J. R. Glycogen Synthase Kinase-3: Properties, Functions, and Regulation. *Chem. Rev.* **2001**, *101* (8), 2527–2540.

(24) Woodgett, J. R. Judging a Protein by More than Its Name: GSK-3. *Sci. STKE Signal Transduct. Knowl. Environ.* **2001**, *2001* (100), re12.

(25) Woodgett, J. R. Regulation and Functions of the Glycogen Synthase Kinase-3 Subfamily. *Semin. Cancer Biol.* **1994**, *5* (4), 269–275.

(26) Hall, A. P.; Escott, K. J.; Sanganee, H.; Hickling, K. C. Preclinical Toxicity of AZD7969: Effects of GSK3β Inhibition in Adult Stem Cells. *Toxicol. Pathol.* **2015**, *43* (3), 384–399.

(27) Walz, A.; Ugolkov, A.; Chandra, S.; Kozikowski, A.; Carneiro, B. A.; O'Halloran, T. V.; Giles, F. J.; Billadeau, D. D.; Mazar, A. P. Molecular Pathways: Revisiting Glycogen Synthase Kinase-3β as a Target for the Treatment of Cancer. *Clin. Cancer Res.* **2017**, *23* (8), 1891–1897.

(28) Maceyka, M.; Harikumar, K. B.; Milstien, S.; Spiegel, S. Sphingosine-1-Phosphate Signaling and Its Role in Disease. *Trends Cell Biol.* **2012**, *22* (1), 50–60.

(29) Wollny, T.; Wątek, M.; Durnaś, B.; Niemirowicz, K.; Piktel, E.; Żendzian-Piotrowska, M.; Góźdź, S.; Bucki, R. Sphingosine-1-Phosphate Metabolism and Its Role in the Development of Inflammatory Bowel Disease. *Int. J. Mol. Sci.* **2017**, *18* (4).

(30) Park, S.-J.; Im, D.-S. Sphingosine 1-Phosphate Receptor Modulators and Drug Discovery. *Biomol. Ther.* **2017**, *25* (1), 80–90.

(31) Meshcheryakova, A.; Mechtcheriakova, D.; Pietschmann, P. Sphingosine 1-Phosphate Signaling in Bone Remodeling: Multifaceted Roles and Therapeutic Potential. *Expert Opin. Ther. Targets* **2017**, *21* (7), 725–737.

(32) Weske, S.; Vaidya, M.; Reese, A.; von Wnuck Lipinski, K.; Keul, P.; Bayer, J. K.; Fischer, J. W.; Flögel, U.; Nelsen, J.; Epple, M.; et al. Targeting Sphingosine-1-Phosphate Lyase as an Anabolic Therapy for Bone Loss. *Nat. Med.* **2018**, *24* (5), 667–678.

(33) Sanllehí, P.; Abad, J.-L.; Casas, J.; Delgado, A. Inhibitors of Sphingosine-1-Phosphate Metabolism (Sphingosine Kinases and Sphingosine-1-Phosphate Lyase). *Chem. Phys. Lipids* **2016**, *197*, 69–81.

(34) Scott, F. L.; Clemons, B.; Brooks, J.; Brahmachary, E.; Powell, R.; Dedman, H.; Desale, H. G.; Timony, G. A.; Martinborough, E.; Rosen, H.; et al. Ozanimod (RPC1063) Is a Potent Sphingosine-1-Phosphate Receptor-1 ($S1P_1$) and Receptor-5 ($S1P_5$) Agonist with Autoimmune Disease-Modifying Activity: Ozanimod: A $S1P_{1,5}$ Receptor Agonist for Autoimmune Disease. *Br. J. Pharmacol.* **2016**, *173* (11), 1778–1792.

(35) Vagner, J.; Handl, H. L.; Monguchi, Y.; Jana, U.; Begay, L. J.; Mash, E. A.; Hruby, V. J.; Gillies, R. J. Rigid Linkers for Bioactive Peptides. *Bioconjug. Chem.* **2006**, *17* (6), 1545–1550.

(36) Chen, X.; Zaro, J. L.; Shen, W.-C. Fusion Protein Linkers: Property, Design and Functionality. *Adv. Drug Deliv. Rev.* **2013**, *65* (10), 1357–1369.

(37) Shinohara, M.; Chang, B. Y.; Buggy, J. J.; Nagai, Y.; Kodama, T.; Asahara, H.; Takayanagi, H. The Orally Available Btk Inhibitor Ibrutinib (PCI-32765) Protects against Osteoclast-Mediated Bone Loss. *Bone* **2014**, *60*, 8–15.

(38) Berglöf, A.; Hamasy, A.; Meinke, S.; Palma, M.; Krstic, A.; Månsson, R.; Kimby, E.; Österborg, A.; Smith, C. I. E. Targets for Ibrutinib Beyond B Cell Malignancies. *Scand. J. Immunol.* **2015**, *82* (3), 208–217.

(39) Andrade, K.; Fornetti, J.; Zhao, L.; Miller, S. C.; Randall, R. L.; Anderson, N.; Waltz, S. E.; McHale, M.; Welm, A. L. RON Kinase: A Target for Treatment of Cancer-Induced Bone Destruction and Osteoporosis. *Sci. Transl. Med.* **2017**, *9* (374), eaai9338.

(40) Zhang, Y. Y.; Cui, Y. Z.; Luan, J.; Zhou, X. Y.; Zhang, G. L.; Han, J. X. Platelet-Derived Growth Factor Receptor Kinase Inhibitor AG-1295 Promotes Osteoblast Differentiation in MC3T3-E1 Cells via the Erk Pathway. *Biosci. Trends* **2012**, *6* (3), 130–135.

CHAPTER 7. CONCLUSIONS AND FUTURE DIRECTIONS

7.1 Conclusions

Bone fractures are causing enormous economic and health burdens across the world, costing tens of billions of dollars to the healthcare systems[1] and substantial lost wages,[2] let alone the pain, anxiety, and depression that can eat away a patient's life quality[3,4]. Unfortunately, therapeutic approaches for fractures have not seen major advancement in decades. Despite the serious problems caused by bone fractures, in our perspective, the awareness for the need of a modern, convenient, and effective therapy to improve fracture repair has remained befuddlingly low. Even patients suffering from fractures need a boost in their awareness: although more women over 55 in America are hospitalized each year for osteoporosis-associated fracture than for heart attacks, breast cancer, or strokes, two-thirds of them still believe those other diseases are more of a concern than fractures.[5–7] We believe that patients with broken bones demand a better therapy, and that bone fractures deserve the same attention from medical researchers as any other diseases. The development of a systemically-administered drug that can potently accelerates bone fracture repair without causing systemic toxicities serves as a good starting point for our endeavor.

In this dissertation, we have demonstrated that DAC, a fracture-targeted version of the Src kinase inhibitor dasatinib,[8,9] promotes osteoblast differentiation and activation *in vitro* and accelerates bone fracture repair *in vivo*. By linking dasatinib to a fracture-homing deca-aspartic acid oligopeptide, the therapeutic efficacy of dasatinib is dramatically improved, enabling a DAC therapy to restore the mechanical strength of a broken femur more than twice as fast without altering normal homeostasis of undamaged bones. Our

studies have pointed out that Src inhibition with dasatinib does not solely display antiresorptive properties as the dogma suggests; instead, it is strongly bone-anabolic without apparent suppression of bone remodeling. Still, improvements on the dosing schedule are required before DAC could be useful for human patients; thus, a wide range of studies have been carried out to optimize the dosing regimen for DAC. An upgraded version of DAC combines a more stable ester linker, an improved therapeutic efficacy, and a dosing schedule that consists of only 6 doses in total (versus 11 total doses in the previous version), without any required dosing during the first week after the fracture. We believe that this upgraded drug is able to benefit fracture patients significantly more not only because of the reduced dosing frequency, but because it works better at accelerating bone fracture repair and is less likely to degrade prematurely in the blood stream, alleviating concerns regarding toxicity or loss of efficacy. The updated dasatinib conjugate makes a more mature drug, and is ready for validation of efficacy in other animal species before further examinations in a human clinical trial.

The successful development of a targeted dasatinib therapy for enhanced fracture repair, however, does not conclude this dissertation. We have implemented a modular synthetic method for the synthesis of DAC, dividing the chemistry in two parts: synthesis of D_{10}-cys on SPPS, and synthesis of dasatinib-maleimide with a PyBOP-assisted esterification. This synthetic route has been proven to be highly adaptable beyond the use with dasatinib, making the screening of other drug warheads, linkers, and targeting ligands easy and convenient. The interchangeability of this route has not only allowed us to test the slow-release linker and the D-aspartic acid targeting ligand with dasatinib, but made possible the highly efficient *in vivo* investigations of four different small molecule bone-

anabolic agents in their targeted forms. Conclusively, this modular synthetic method has enabled a relatively high-throughput workflow in the identification of new bone-anabolic molecules as potential warheads to accelerate bone fracture repair.

With the help of the modular synthetic method, we have verified that Src inhibition does promote osteoblast differentiation and function, with another Src inhibitor E738. In addition to Src inhibition, GSK-3β inhibition and S1PR1 signaling activation have also been recognized as promising mechanisms to promote bone growth. With further optimizations of the dosing regimen and linker property, targeted versions of these molecules could also be useful in speeding up fracture repair. Most importantly, we hope that the work in this dissertation could provide new perspectives and insights into the development of fracture-targeted bone-anabolic agents to help patients bearing bone fractures recover faster and return to a pre-fracture lifestyle earlier.

7.2 Future Directions

Much work remains to be done to better prepare DAC for human clinical trials and to further develop other bone-anabolic agents studied in this dissertation. To begin with, mechanical strength data has been unavailable for *in vivo* studies with many new warheads. Mechanical data for those studies and any future studies should be obtained to provide more precise insights into the effectiveness and optimization routes for each new drug.

Expectedly, more detailed investigations into using non-digestible targeting ligands are in the plan. In our studies, a non-digestible targeting ligand DD_{10} failed to show value over regular D_{10}. However, given the abundance of reports using bisphosphonates as targeting ligands for bone diseases,[10–14] more work is required to uncover possible benefits of using stable ligands. Thus, the rate at which newly-formed bone might bury unreleased

conjugate bound to the fracture site needs to be determined, then the potential benefits and pitfalls of using a non-digestible targeting ligand could be studied more thoroughly.

Currently, D_{10}-E738 can achieve a therapeutic efficacy not far from that of DAC at a dosage less than a third of what DAC is dosed at. As a promising therapeutic agent for bone fractures, D_{10}-E738 demands optimizations of its dosing regimen and/or linker property to further enhance its *in vivo* bone-anabolic capacity. Importantly, as Src inhibitors, dasatinib and E738 represent not only two promising bone-anabolic agents, but the entire category of Src inhibitors. In the future, besides optimizations to D_{10}-E738, more Src inhibitors might be tested with our framework to identify the one with the best efficacy. With the possibility of future Src inhibitors with improved potency and selectivity being designed, our finding has ensured a pathway of finding effective bone-anabolic agents for the enhancement of fracture repair.

Also, additional studies should be planned for a targeted version of ozanimod. Promoting bone formation by binding to and activating the downstream pathway of a cell surface receptor S1PR1, ozanimod is able to function without the need to internalize into cells, which theoretically removes the requirement of a release mechanism. As discussed in Section 6.4, if a non-releasable D_{10}-ozanimod conjugate with the optimal spacer length could be identified, it could have properties that are superior to DAC. Dosage might be significantly reduced, while loss of efficacy associated with non-optimal release rate or release mechanism might be eliminated. To start the exploration with a non-releasable ozanimod conjugate, a modified synthetic route with the hydroxyl group protected during the synthesis is required for the synthesis of a non-releasable D_{10}-ozanimod conjugate with spacers of varying lengths. Should the strategy prove effective, extrapolation to other bone-

anabolic molecules that functions by binding to cell surface receptors can be projected, which is expected to bring even bigger benefit to fracture patients than DAC.

Hopefully, current and future work both in and after this dissertation would be able to bring to the market one systemically-administered small molecule drug to accelerate bone fracture while recognizing many more as potential candidates in the pipeline.

7.3 References

(1) Gu, Q.; Koenig, L.; Mather, R. C.; Tongue, J. Surgery for Hip Fracture Yields Societal Benefits That Exceed the Direct Medical Costs. *Clin. Orthop. Relat. Res.* **2014**, *472* (11), 3536–3546.

(2) Holm, A. G. V.; Lurås, H.; Randsborg, P.-H. The Economic Burden of Outpatient Appointments Following Paediatric Fractures. *Injury* **2016**, *47* (7), 1410–1413.

(3) Keene, G. S.; Parker, M. J.; Pryor, G. A. Mortality and Morbidity after Hip Fractures. *BMJ* **1993**, *307* (6914), 1248–1250.

(4) Adachi, J. D.; Adami, S.; Gehlbach, S.; Anderson, F. A.; Boonen, S.; Chapurlat, R. D.; Compston, J. E.; Cooper, C.; Delmas, P.; Díez-Pérez, A.; et al. Impact of Prevalent Fractures on Quality of Life: Baseline Results from the Global Longitudinal Study of Osteoporosis in Women. *Mayo Clin. Proc.* **2010**, *85* (9), 806–813.

(5) Singer, A.; Exuzides, A.; Spangler, L.; O'Malley, C.; Colby, C.; Johnston, K.; Agodoa, I.; Baker, J.; Kagan, R. Burden of Illness for Osteoporotic Fractures Compared with Other Serious Diseases among Postmenopausal Women in the United States. *Mayo Clin. Proc.* **2015**, *90* (1), 53–62.

(6) Writing Group Members; Mozaffarian, D.; Benjamin, E. J.; Go, A. S.; Arnett, D. K.; Blaha, M. J.; Cushman, M.; Das, S. R.; de Ferranti, S.; Després, J.-P.; et al. Heart Disease and Stroke Statistics-2016 Update: A Report From the American Heart Association. *Circulation* **2016**, *133* (4), e38-360.

(7) Burge, R.; Dawson-Hughes, B.; Solomon, D. H.; Wong, J. B.; King, A.; Tosteson, A. Incidence and Economic Burden of Osteoporosis-Related Fractures in the United States, 2005-2025. *J. Bone Miner. Res. Off. J. Am. Soc. Bone Miner. Res.* **2007**, *22* (3), 465–475.

(8) Imming, P.; Sinning, C.; Meyer, A. Drugs, Their Targets and the Nature and Number of Drug Targets. *Nat. Rev. Drug Discov.* **2006**, *5* (10), 821–834.

(9) Piccaluga, P. P.; Paolini, S.; Martinelli, G. Tyrosine Kinase Inhibitors for the Treatment of Philadelphia Chromosome-Positive Adult Acute Lymphoblastic Leukemia. *Cancer* **2007**, *110* (6), 1178–1186.

(10) Sedghizadeh, P. P.; Sun, S.; Junka, A. F.; Richard, E.; Sadrerafi, K.; Mahabady, S.; Bakhshalian, N.; Tjokro, N.; Bartoszewicz, M.; Oleksy, M.; et al. Design, Synthesis, and Antimicrobial Evaluation of a Novel Bone-Targeting Bisphosphonate-Ciprofloxacin Conjugate for the Treatment of Osteomyelitis Biofilms. *J. Med. Chem.* **2017**, *60* (6), 2326–2343.

(11) Gil, L.; Han, Y.; Opas, E. E.; Rodan, G. A.; Ruel, R.; Seedor, J. G.; Tyler, P. C.; Young, R. N. Prostaglandin E2-Bisphosphonate Conjugates: Potential Agents for Treatment of Osteoporosis. *Bioorg. Med. Chem.* **1999**, *7* (5), 901–919.

(12) Hrubý, M.; Etrych, T.; Kučka, J.; Forsterová, M.; Ulbrich, K. Hydroxybisphosphonate-Containing Polymeric Drug-Delivery Systems Designed for Targeting into Bone Tissue. *J. Appl. Polym. Sci.* **2006**, *101* (5), 3192–3201.

(13) Morioka, M.; Kamizono, A.; Takikawa, H.; Mori, A.; Ueno, H.; Kadowaki, S.; Nakao, Y.; Kato, K.; Umezawa, K. Design, Synthesis, and Biological Evaluation of Novel Estradiol-Bisphosphonate Conjugates as Bone-Specific Estrogens. *Bioorg. Med. Chem.* **2010**, *18* (3), 1143–1148.

(14) Tower, R. J.; Campbell, G. M.; Müller, M.; Will, O.; Glüer, C. C.; Tiwari, S. Binding Kinetics of a Fluorescently Labeled Bisphosphonate as a Tool for Dynamic Monitoring of Bone Mineral Deposition In Vivo: BISPHOSPHONATE BINDING KINETICS TO MONITOR IN VIVO BONE METABOLISM. *J. Bone Miner. Res.* **2014**, *29* (9), 1993–2003.

VITA

Mingding Wang was born in the city of Guiyang in China, where he graduated from high school before enrolling in a special program called “Fundamental Sciences of Chemistry and Biology” in Tsinghua University in Beijing, China. During his undergraduate years, he has taken all required courses in the realms of both chemistry and biology, developing a strong and unique interdisciplinary background. He worked as an undergraduate researcher in Dr. Yen Wei’s lab on immobilizing lipase in mesoporous silica network with a sol-gel process, endowing the enzyme with enhanced stress tolerance without noticeable loss in enzyme activity. After graduating from Tsinghua University, Mingding joined Dr. Philip S. Low’s research group in Purdue University to find better cures for diseases using targeted drug delivery. He began his research work with the attempts to target cancer cells with bombesin receptor subtype-3, and later started to work on targeting bone-anabolic agents to bone fracture to accelerate fracture repair. His work on the targeted delivery of dasatinib has shown promise to be included in a human clinical trial, and has been published and featured on the cover story of Bioconjugate Chemistry. He has presented his research in two international conferences, and earned various awards including American Association of Pharmaceutical Scientists Best Abstract Award, Orthopedic Research Society 3-Minute Thesis Competition Honorable Mention, and several intramural poster competition awards. He has accepted a position at Stanford University under the direction of Dr. Jianghong Rao, where he will develop novel imaging agents and therapeutics for the treatment of cancer and mycobacterial diseases.

PUBLICATION

Bioconjugate Chemistry

Article

Cite This: Bioconjugate Chem. 2018, 29, 3800−3809

pubs.acs.org/bc

Bone-Fracture-Targeted Dasatinib-Oligoaspartic Acid Conjugate Potently Accelerates Fracture Repair

Mingding Wang,[†] Soie Park,[†] Yoonhee Nam,[†] Jeffery Nielsen,[‡] Stewart A. Low,[†] Madduri Srinivasarao,[†] and Philip S. Low*[,†,§]

[†]Department of Chemistry, Purdue University, 560 Oval Drive, West Lafayette, Indiana 47907, United States
[§]Institute for Drug Discovery, Purdue University , 720 Clinic Drive, West Lafayette, Indiana 47907, United States
[‡]College of Pharmacy, Purdue University, 575 Stadium Mall Drive, West Lafayette, Indiana 47907, United States

Supporting Information

ABSTRACT: Approximately 6.3 million bone fractures occur annually in the United States, resulting in considerable morbidity, deterioration in quality of life, loss of productivity and wages, and sometimes death (e.g., hip fractures). Although anabolic and antiresorptive agents have been introduced for treatment of osteoporosis, no systemically administered drug has been developed to accelerate the fracture-healing process. To address this need, we have undertaken to target a bone anabolic agent selectively to fracture surfaces in order to concentrate the drug's healing power directly on the fracture site. We report here that conjugation of dasatinib to a bone fracture-homing oligopeptide via a releasable linker reduces fractured femur healing times in mice by ~60% without causing overt off-target toxicity or remodeling of nontraumatized bones. Thus, achievement of healthy bone density, normal bone volume, and healthy bone mechanical properties at the fracture site is realized after only 3−4 weeks in dasatinib-targeted mice, but it requires ~8 weeks in PBS-treated controls. We conclude that targeting of dasatinib to bone fracture surfaces can significantly accelerate the healing process at dasatinib concentrations that are known to be safe in oncological applications.

INTRODUCTION

Approximately 6 million bone fractures occur each year in the United States,[1] resulting in 3.5 million visits to the emergency room and 887 679 longer-term hospitalizations (data source: National Ambulatory Medical Care Survey and the American Academy of Orthopedic Surgeons). With 61 million older Americans estimated to suffer from osteoporosis,[2] this number of fractures is expected to increase, especially as the population continues to age. Costs associated with hip fracture repairs were estimated at $21 billion in 2009,[3] and lost wages due to fracture-related absence from work have added substantially to these costs.[4] Morbidities deriving from loss of motility, pain, anxiety, and depression can also erode a patient's quality of life.[5,6] Most importantly, many fractures trigger more serious pathologies, with complications deriving from hip fractures leading to 75 000 deaths/year in the United States.[7,8] Clearly, strategies that might accelerate and/or improve bone fracture repair could mitigate many problems facing an aging and physically active population.

Although many treatments for osteoporosis exist,[9] there is surprisingly no systemically administered FDA-approved drug available for acceleration of bone fracture repair. Antiresorptive drugs such as bisphosphonates, estrogens, and anti-RANKL antibodies can be effective in suppressing osteoclasts,[10−13] but do not promote formation of new bone, which is essential for the healing process.[14] Biologics such as abaloparatide, teriparatide, and parathyroid hormone-related protein can activate osteoblasts and thereby induce bone mineralization,[15,16] but their abilities to improve fracture repair in humans have not proven to be statistically significant,[17] even at concentrations that promoted hypercalcemia and the consequent pain, nausea, confusion, and fatigue.[18−20] Although bone morphogenetic proteins can also stimulate bone anabolism,[21] their uses to date have been restricted to topical application onto fracture surfaces, which are only accessible when surgery is required to repair the damaged bone.[22] On the basis of these considerations, a systemically administered bone anabolic agent that would target a fracture surface and accelerate fracture repair locally without promoting systemic growth of healthy bones or toxicities associated with hypercalcemia[19,23] could address many of the aforementioned limitations.

Because the mineral component of bone, hydroxyapatite $[Ca_{10}(PO_4)_6(OH)_2]$, is protected by a periosteum in healthy bone but exposed at a fracture site,[24] we elected to exploit the unique accessibility of hydroxyapatite at fracture surfaces to concentrate an anabolic agent at the fracture site. In the paper

Received: September 17, 2018
Revised: October 27, 2018
Published: October 31, 2018

DOI: 10.1021/acs.bioconjchem.8b00860
Bioconjugate Chem. 2018, 29, 3800−3809

below, we exploit the high affinity of a linear oligoaspartic acid peptide for hydroxyapatite[25−28] to concentrate the Src kinase inhibitor, dasatinib, specifically on a fracture surface. To evaluate the rate and outcome of fracture repair in vivo, we adopted a robust model of bone fracture repair on ND4 Swiss Webster mice.[25,28] We report that administration of a decapeptide of aspartic acid linked to dasatinib significantly accelerates repair of fractured femurs in mice without inducing detectable systemic toxicity or altering the properties of healthy bones.

■ RESULTS

Effect of Dasatinib on Differentiation of a Preosteoblastic Cell Line. Although Src kinase is ubiquitously expressed in human tissues,[29] the only major consequence of Src gene knockout appears to be osteopetrosis,[30,31] suggesting that Src kinase plays a critical role in bone turnover and formation.[32] To evaluate the effect of the Src kinase inhibitor, dasatinib, on osteoblast differentiation and function in vitro, a murine preosteoblastic cell line (MC3T3-E1) was cultured in mineralization media containing different concentrations of dasatinib. Analysis of osteoblast-related gene expression on days 7 and 14 revealed that transcripts required for osteoblast differentiation and function all increased during exposure to dasatinib (Figure 1A−G). Thus, genes required for differentiation of osteoblasts from mesenchymal precursors (e.g., Runt-related transcription factor 2 (RUNX2), and osterix (OSX)), genes involved in production of enzymes and extracellular matrix proteins critical to osteoblast function (e.g., alkaline phosphatase (ALP), type-I collagen alpha 1 (COL1A1), and osteopontin (OPN)), and genes essential to regulation of osteogenesis (e.g., RANKL and osteoprotegerin (OPG)) were all upregulated from 2- to 60-fold in response to Src inhibition. Moreover, the ratio of OPG to RANKL, a measure of the balance between osteoblastogenesis and osteoclastogenesis, was observed to shift toward the former (Figure 1H). When considered together with the increase in ALP activity (a widely used marker for osteoblast differentiation, Figure 1I), the data collectively indicate that treatment of an osteoblast precursor with a Src kinase inhibitor (dasatinib) can reprogram a preosteoblastic cell to express genes involved in bone regenerating processes, in accordance with findings from other studies.[33−35]

Hydroxyapatite-Targeted Dasatinib Enhances Bone Fracture Repair in Vivo. In order to evaluate whether dasatinib might promote bone fracture repair in vivo, a method to systemically target dasatinib specifically to a fracture surface was required. For this purpose, dasatinib was linked to an aspartic acid decapeptide (Scheme 1) similar to other oligoaspartic acids shown to concentrate unrelated molecules on bone fracture surfaces,[17,28,37,38] and administered to ND4 Swiss Webster mice containing broken but stabilized femurs (see Method). As shown in Figure 2A, daily injection of 10 μmol/kg dasatinib-Asp_{10} conjugate (DAC) essentially doubled the bone density at the fracture site relative to vehicle-treated controls. While nontargeted dasatinib also enhanced mineralization by the end of the three-week evaluation period, its impact was less than half that of its targeted counterpart. In terms of total bone volume (Figure 2B), treatment with DAC also exceeded vehicle-treated controls by 82%. Importantly, daily dosage of the free targeting oligopeptide, Asp_{10}, had no impact on either bone density or total bone volume, confirming that the enhanced therapeutic effect of DAC is entirely due to the targeted delivery of dasatinib.

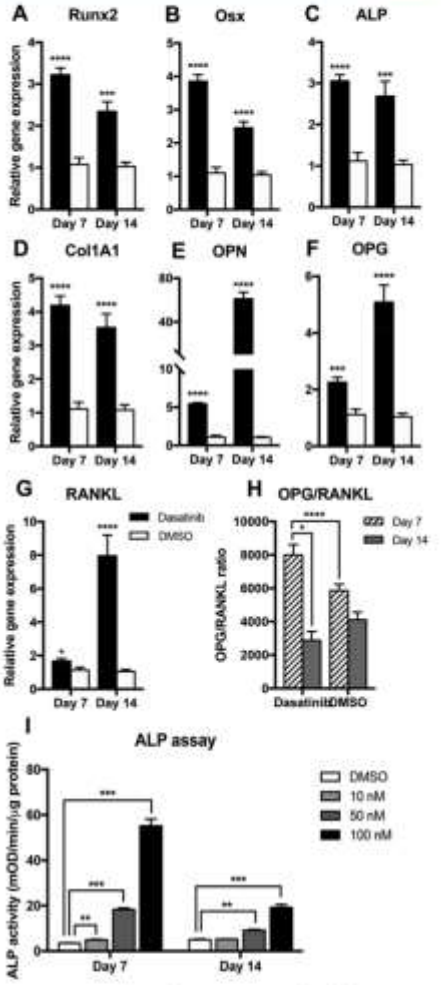

Figure 1. Dasatinib stimulates expression of multiple osteogenic genes. (A)−(G) Mouse preosteoblastic cell line MC3T3-E1 was incubated in mineralization media containing 100 nM dasatinib or DMSO ($n = 3$ for all groups) and expression levels of selected bone remodeling genes were analyzed and normalized to GAPDH. Specifically, (H) shows the ratio of OPG and RANKL expression. (I) MC3T3-E1 cells were cultured in mineralization media containing 10, 50, or 100 nM dasatinib or DMSO only, and the enzymatic activity of intracellular alkaline phosphatase (ALP) was measured. Levels of statistical significance are denoted with asterisks according to the following definition: $^{*}p < 0.05$; $^{**}p < 0.01$; $^{***}p < 0.001$; $^{****}p < 0.0001$.

More detailed analysis of μCT data demonstrated that DAC-treated mice have denser trabecular bone microstructures than

DOI: 10.1021/acs.bioconjchem.8b00603
Bioconjugate Chem. 2018, 29, 3800−3809

Scheme 1. Synthesis of the Dasatinib-Asp_{10} Conjugate (DAC)

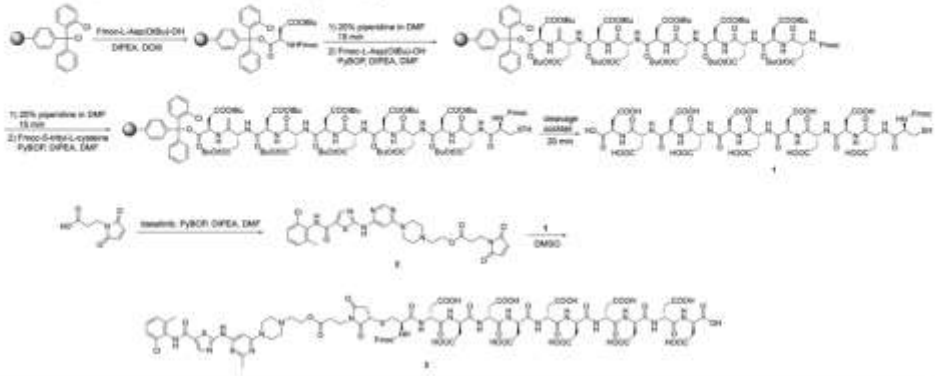

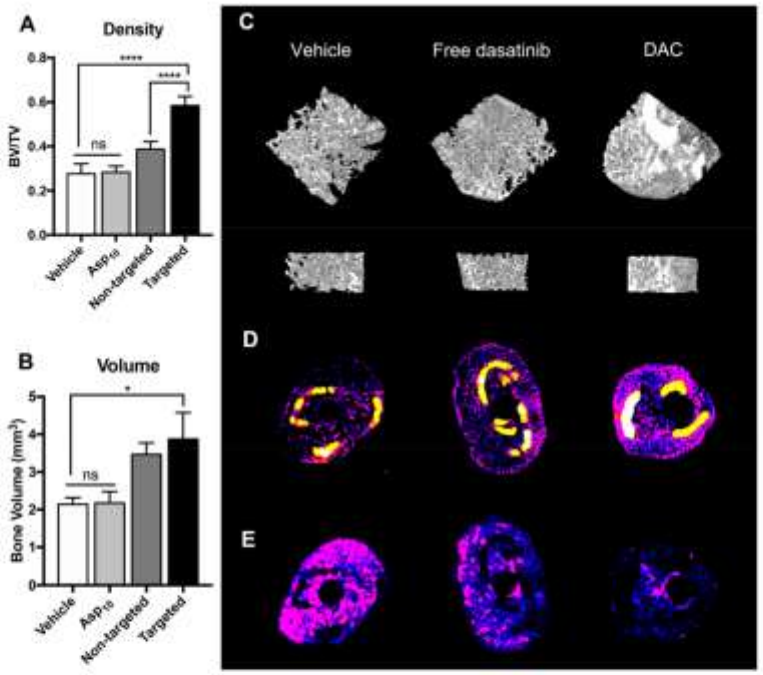

Figure 2. DAC increases bone density and volume while reducing trabecular spacing at the fracture site. Femurs were broken in ND4 Swiss Webster mice and stabilized with an internal rod prior to daily therapy with either vehicle, free targeting ligand Asp_{10} (10 μmol/kg), free dasatinib (10 μmol/kg), or DAC (10 μmol/kg) ($n = 8$ in each group, except for $n = 13$ in DAC group). After 3 weeks mice were euthanized and analyzed for (A) bone density (bone volume/total volume) and (B) bone volume (mineral volume) at the fracture callus site. μCT images at the fracture callus site were also obtained, and representative images of (C) trabecular structure, (D) trabecular thickness (with colors from blue to magenta representing thinner to thicker, and bright yellow indicating cortical bone), and (E) trabecular spacing (with colors from magenta to blue representing the open spacing between trabeculae from larger to smaller, respectively). Complete dark denotes spaces fully filled with trabecular or cortical bone. Levels of statistical significance are denoted with asterisks according to the following definition: $^{*}p < 0.05$; $^{****}p < 0.0001$; ns: no statistical significance.

DOI: 10.1021/acs.bioconjchem.8b00603
Bioconjugate Chem. 2018, 29, 3800−3809

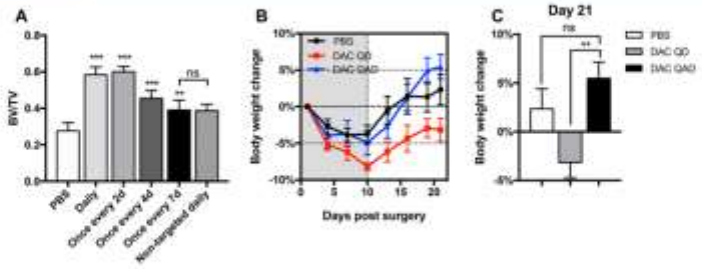

Figure 3. DAC stimulates bone growth at lower dosing frequencies. Mouse femurs were broken and stabilized as in Figure 3, and affected mice were treated with PBS, dasatinib (10 μmol/kg), or DAC (10 μmol/kg) at the indicated dosing frequencies prior to analysis at 3 weeks postfracture. (A) Bone density (bone volume/total volume) at the fracture callus site. (B) Percent body weight change during therapy. (C) Percent body weight on the last day of the study. ($n = 7$ in each group; levels of statistical significance are denoted with asterisks according to the following definition: $^{**}p < 0.01$; $^{***}p < 0.001$.).

either vehicle- or free dasatinib-treated controls (Figure 2C). Fracture calluses from DAC-targeted mice were also characterized by increases in trabecular thickness (Figure 2D) and decreases in trabecular separation (Figure 2E); that is, this evidence further established that the repair process was leading to stronger bone. Because each of these changes occurs much sooner in the DAC-treated than control mice, we conclude that fracture healing process is accelerated in DAC-treated mice.

Evaluation of Optimal DAC Dosing Frequency. To determine whether DAC dosing frequency might be reduced without compromising therapeutic efficacy, similar studies were performed with increasingly longer intervals between DAC administration. As seen in Figure 3A, treatment with DAC every other day for 3 weeks was equally effective as daily injection of DAC, more than doubling the bone density relative to PBS-treated controls. Reducing dosing frequency to every 4 days, however, resulted in a measurable decline in potency (~62% increase over saline controls), and this potency was further diminished when DAC was dosed only weekly (i.e., ~39% increase over saline controls). As expected, analysis of μCT scans of fracture calluses (Figure S1) confirmed this trend toward reduced mineralization with decreasing dosing frequency. However, even the weekly dosing schedule resulted in a callus density that was comparable to that seen in mice treated daily with nontargeted dasatinib, suggesting that dasatinib's potency is dramatically increased by concentrating the drug on the fracture surface.

Assessment of DAC Dosing on Animal Weight Gain. Although the dose of DAC used in these studies (equivalent to 4.9 mg/kg dasatinib) was more than 8-fold lower than free dasatinib's MTD (40 mg/kg[10]), it was still important to obtain a crude measure of the systemic toxicity of the different DAC treatment regimens. Because weight loss constitutes a widely employed metric for whole animal toxicity, we monitored the weight of all animals in each of the studies. As seen in Figure 3B, all animals lost weight over the first 10 days following femur fracturing, presumably due to loss of appetite or discomfort associated with moving to a feeding station. However, persistence of weight loss differed among the treatment groups, with the daily dosed cohort displaying the slowest recovery to normal weight and the alternate day dosed cohort experiencing weight recovery at least as rapid as PBS-treated controls (Figure 3C). Because the alternate day dosing schedule maintained the accelerated rate of fracture repair without inducing overt toxicity, all subsequent studies were performed using every-other-day dosing.

Evaluation of the Time Course of DAC-Induced Bone Fracture Healing. Although it was difficult to quantitate the minimum time for affected mice to return to normal mobility, it was nevertheless possible to accurately compare both the rates of fracture callus remineralization and restoration of mechanical strength among treatment groups. As shown in Figure 4A, DAC-dosed mice showed significantly greater bone density than PBS-treated mice at every time point during the 8-week dosing period (i.e., confirming the accelerated healing process enabled by DAC). Moreover, comparison of the forces required to refracture the healing femurs (maximum sustainable loads) at each time point (Figure 4B) revealed that DAC-treated animals recovered weight-bearing mechanical strength more than twice as fast as their PBS-treated counterparts. Thus, DAC-treated femurs required only 3 weeks to develop the same mechanical strength achieved by PBS-treated controls only after 8 weeks. In addition to this dramatically improved resistance to refracture, DAC-treated femurs were also mechanically more stiff (Figure S2A) and ductile (Figure S2B) than their PBS-treated counterparts, requiring more work to refracture the repaired bones (Figure S2C) at every time point during the healing process than PBS-treated controls. In fact, PBS-treated femurs achieved the same desirable mechanical properties realized by DAC-treated femurs only after 8 weeks of healing (Figure S2A-C).

As expected, differences in bone properties at the fracture site between treated and untreated mice gradually decreased as both cohorts remodeled to form normal bone (i.e., demonstrating that the final repaired bone eventually became similar between treated and untreated groups). Thus, as noted in Figure 4C, trabecular bone eventually remodeled into cortical bone in both groups; however, the cortical bone remained slightly thicker and more voluminous in the DAC- than PBS-treated group (Figure S3A-B), enabling the DAC-remodeled bone to more closely resemble healthy femur than the PBS-treated controls (Figure S3C). Importantly, analysis of body weight changes during the course of these studies revealed no obvious toxicities that were not attributed to the short-term trauma associated with the broken femurs (Figure 4D).

DAC Demonstrates No Off-Target Effects on Healthy Bones. While an absence of body weight loss suggested no obvious systemic toxicity deriving from DAC therapy, a

DOI: 10.1021/acs.bioconjchem.8b00603
Bioconjugate Chem. 2018, 29, 3800−3809

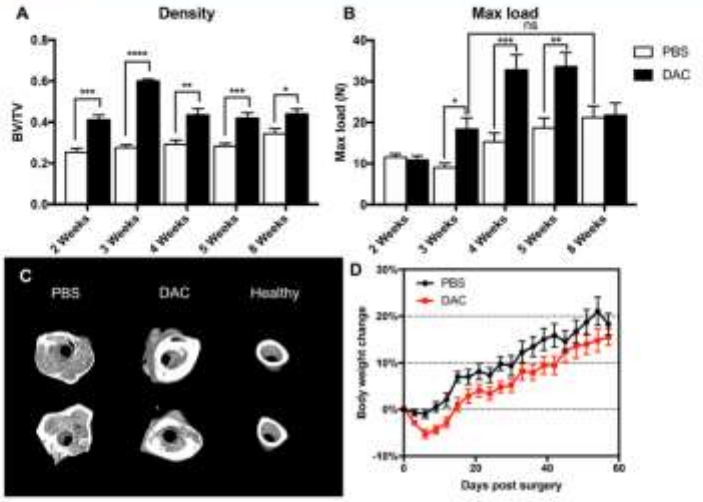

Figure 4. DAC accelerates fracture repair and return to normal mechanical strength. Mouse femurs were broken and stabilized as in Figure 3, and affected mice were treated every other day with either PBS or DAC (10 μmol/kg) for the indicated duration prior to euthania and analysis. (A) Bone density (bone volume/total volume) at the fracture callus site. (B) Maximum load quantitated using a four-point bending apparatus as described in Methods. (C) μCT images of bone microstructure at the fracture callus site after 8 weeks of therapy. (D) Percent change in body weight of mice undergoing the aforementioned treatments. (n = 9 in each group, except n = 8 for DAC and PBS groups in 2-week dosing group; levels of statistical significance are denoted with asterisks according to the following definition: $^{*}p < 0.05$; $^{**}p < 0.01$; $^{***}p < 0.001$; $^{****}p < 0.0001$.)

concern nevertheless remained that systemic administration of a bone anabolic agent might promote unwanted growth of healthy bones. To assess whether DAC might have altered the properties of healthy bones, unbroken femurs from the contralateral legs of both DAC- and PBS-treated mice were analyzed by μCT. Comparison of bone density, trabecular thickness, and trabecular separation at the distal femurs showed no significant differences between PBS- and DAC-treated mice following continuous QAD dosing for 8 weeks. Moreover, comparison of the properties of the healthy femurs following both 2 and 8 weeks of continuous DAC dosing revealed no changes in bone characteristics (Figure 5A); i.e. BV/TV, trabecular thickness, and trabecular separation did not change in healthy femurs during 8 weeks of treatment with DAC. Because nontargeted dasatinib has been shown to increase trabecular bone growth in healthy distal femurs,[33] the absence of impact of the fracture-targeted DAC on healthy femur properties (Figure 5B) reinforces that fracture-specific targeting of dasatinib can avoid unwanted systemic effects that arise when dasatinib is not targeted.

■ DISCUSSION

Although a variety of cytokines, hormones, peptides, and low-molecular-weight drugs have been found to exhibit bone anabolic activity,[40−45] we elected to target dasatinib to fracture surfaces because it was previously reported to potently promote bone formation.[33,35,46] Thus, while the mechanism underpinning dasatinib's acceleration of fracture repair remains uncertain, we speculate that it derives from inhibition of Src kinase, since systemic knockdown of Src in mice has been shown to increase osteoblast number and activity as well as induce excessive bone formation.[30,32] Indeed, analysis of osteoblast mRNA levels that changed in response to dasatinib administration (Figure 1) revealed that transcription of genes involved in (i) differentiation of mesenchymal precursors into osteoblasts, (ii) biosynthesis of enzymes and extracellular matrix proteins critical for osteoblast function, and (iii) bone turnover and remodeling were all amplified considerably. This dramatic reprograming of bone metabolic processes, however, also raised a concern that the plethora of induced osteogenic activities might not be properly balanced, resulting in an abnormal healing process at the fracture site and stimulation of bone growth at healthy/undamaged sites. Fortunately, as shown in Figures 3-5, neither major concern was realized, as the fracture healing chronology seemed to track the normal process, only at an accelerated rate, and since healthy bone elsewhere in the body remained essentially unperturbed.

Although the duration of any bone fracture therapy should ideally last only a few weeks, the fact that nontargeted dasatinib has been administered daily at higher doses for many years to CML patients without significant toxicity suggests that the likelihood of encountering disqualifying toxicities with DAC should be minimal. Thus, as shown in Figure 3, the optimal dosing regimen for DAC was 10 μmol/kg DAC every other day for 3 weeks (i.e., the equivalent of 4.9 mg/kg free dasatinib QAD). Considering that the recommended human dose for advanced CML therapy (180 mg/day; equivalent to 5.2 mg/kg/day in a mouse with the oral bioavailability taken into account[47,48]) is higher, one might anticipate that a lower dasatinib dose that was targeted specifically to a fracture

DOI: 10.1021/acs.bioconjchem.8b00603
Bioconjugate Chem. 2018, 29, 3800−3809

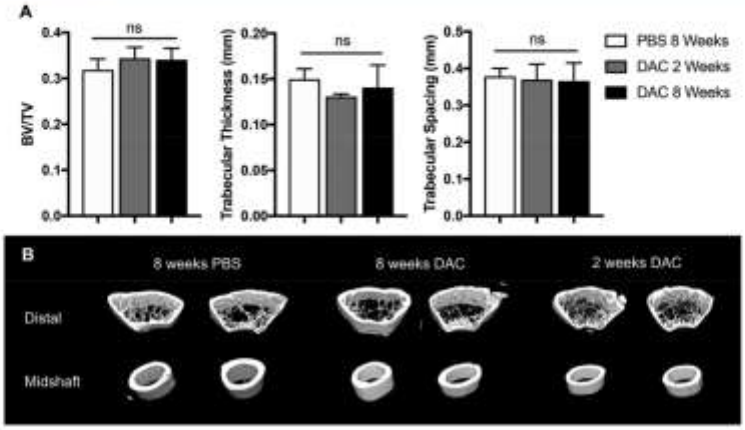

Figure 5. DAC causes no detectable changes in healthy contralateral femurs. (A) Bone volume fraction (bone volume/total volume), trabecular thickness, and trabecular spacing at the distal femur of healthy contralateral femurs in mice after receiving either PBS for 8 weeks, or DAC (10 μmol/kg) therapy q.a.d. for 2 weeks/8 weeks. (B) μCT images of femoral midshaft or distal femur cross sections from healthy contralateral femurs of mice after various durations of therapy with either PBS or DAC (10 μmol/kg) q.a.d. ($n = 9$ in each group, except $n = 8$ for DAC and PBS groups in 2-week dosing group; ns: no statistical significance; ns: no statistical significance.).

surface on alternate days should cause significantly fewer adverse effects.

As noted above, we were initially concerned that the diverse effects of dasatinib on calcium fixation,[35] bone matrix protein biosynthesis,[49] release of bone remodeling hormones,[50] and differentiation of osteoblast and osteoclast precursors,[33] etc. (see also Figure 1) might not be physiologically balanced and thereby result in an altered or functionally inadequate bone structure. For example, reports of reduced osteoclast viability and function following exposure to dasatinib[46,51,52] raised concern that DAC might yield a "healed" fracture comprised of excessive trabecular bone characterized by weaker mechanical properties; i.e. similar to the trabecular bone commonly seen after antiresorptive therapy.[53] However, this concern was soon dismissed when DAC-treated femurs were observed to gradually remodel to a density and morphology approaching that of healthy femurs. Thus, fracture calluses at the 8-week time point consisted almost exclusively of desired cortical bone, implying that a normal remodeling process had been stimulated. More importantly, by the 8-week juncture, DAC-treated femurs displayed similar mechanical properties to PBS-treated controls, confirming that DAC does not alter the final repaired fracture, but simply accelerates its development. These results, combined with the decline in OPG/RANKL ratio during later stages of mineralization (Figure 1H), confirm that DAC therapy differs significantly from antiresorptive therapy in that it more accurately recapitulates normal fracture repair.

Although accelerated fracture repair may seem unimportant when the fracture minimally impedes normal activity, more complicated fractures that significantly limit mobility can lead to serious morbidities and even mortality, especially in the elderly. Thus, when fracture immobilization that prevents ambulation is required, quality of life can decrease, muscle mass and bone density can decline,[54] blood perfusion of internal organs can be compromised, and earned income can be lost.[55] In the case of hip fractures in older individuals, associated complications will lead to death in ~25% of patients.[7,8] Clearly, a safe and effective therapy that accelerates return to normal activity should find application in some patient populations. Although the ~60% reduction in healing time (i.e., time to restoration of normal bone mechanical strength) suggests that DAC might fulfill this need (Figure 4B), several challenges must still be addressed before DAC or a similar molecule can be moved toward a clinical trial. Thus, while every-other-day dosing constitutes an improvement over the initial daily dosing regimen, every-other-day dosing might still be too frequent for widespread compliance. Moreover, although DAC can apparently be administered without injection site reactions, an orally bioavailable formulation would still be preferred by most patients. Finally, while initial data look encouraging for use of DAC in treating long bone fractures, additional studies will be required before DAC should be considered as a potential treatment for nonunion fractures, hip fractures, stress fractures, or spinal fusions, especially when comorbidities such as diabetes, infections, or smoking exist.

In conclusion, we have demonstrated that DAC, a fracture-targeted version of the potent Src kinase inhibitor dasatinib, promotes osteoblast differentiation and activation in vitro and accelerates bone fracture repair in vivo. By linking dasatinib to a fracture-homing deca-aspartic acid oligopeptide, the therapeutic efficacy of dasatinib is dramatically improved without altering normal homeostasis of undamaged bones. With possible improvements in dosing schedule and confirmation of efficacy in other species, a DAC–like molecule could soon be ready for human clinical trials.

■ MATERIALS AND METHODS

Materials. All materials, solvents, and reagents were purchased from commercial sources and used without further purification unless specifically noted. Dimethylformamide (DMF),

DOI: 10.1021/acs.bioconjchem.8b00603
Bioconjugate Chem. 2018, 29, 3800−3809

dimethyl sulfoxide (DMSO), trifluoroacetic acid (TFA), piperidine, triethylamine (TEA), diisopropylethylamine (DIPEA), isopropanol (IPA), methanol (MeOH), dichloromethane (DCM), diethyl ether (Et_2O), and β-glycerophosphate were purchased from Sigma-Aldrich (St. Louis, MO). Fmoc-L-Asp(OtBu)−OH, Fmoc-S-trityl-L-cysteine, triisopropylsilane (TIPS), and ethanedithiol (EDT) were purchased from Chem-Impex International (Wood Dale, IL). Benzotriazol-1-yl-oxytripyrrolidinophosphonium hexafluorophosphate (PyBOP) and dasatinib were obtained from AK Scientific (Union City, CA), while 2-chlorotrityl chloride resin was purchased from ChemPep, Inc. (Wellington, FL). 3-Maleimidopropionic acid was purchased from Combi-Blocks (San Diego, CA). Mass spectra were obtained on Agilent Technologies 1220 series LC-coupled 6130 quadrupole MS. HPLC purifications were performed on an Agilent Technologies 1200 series semipreparatory HPLC. Regular-phase flash column chromatography was performed on Teledyne CombiFlash Rf+ Lumen system. NMR spectra were obtained on a Bruker Avance III 500 HD Spectrometer.

Syntheses. *Synthesis of Asp_{10}-Cys (1).* As shown in Scheme 1, the peptidic portion of the dasatinib-Asp_{10} conjugate was synthesized by standard fluorenylmethoxycarbonyl (Fmoc) solid-phase peptide synthesis. For the initial loading, 2-chlorotrityl chloride resin (0.4 g, 1.4 mmol/g) was swollen in DCM (10 mL/g resin) followed by addition of Fmoc-L-Asp(OtBu)−OH (1.15 g, 2.8 mmol) and DIPEA (1.66 mL, 9.5 mmol) dissolved in DCM (14 mL). The mixture was agitated by bubbling argon for 1 h, after which the solution was drained before 20 mL of capping cocktail (DCM:MeOH:DIPEA = 17:2:1) was added and the solution was again bubbled for 20 min. The resin was then subjected to standard washing procedures which consisted of washes with DMF (3 times), DCM (3 times), and IPA (3 times) following each coupling reaction, and washes with DMF (3 times) following each deprotection. After the initial loading, all subsequent coupling reactions were performed with solutions of Fmoc-L-Asp(OtBu)−OH (1.15 g, 2.8 mmol) or Fmoc-S-trityl-L-cysteine (1.64 g, 2.8 mmol), PyBOP (1.42 g, 2.75 mmol), and DIPEA (1.66 mL, 9.5 mmol) in DMF (14 mL). The 1-h standard coupling time was used for all aspartic acid and cysteine residues. Fmoc-deprotection was done with 20% piperidine solution in DMF for two sessions of 5 and 10 min each. The 11-mer peptidic product was cleaved off the resin using a cleavage cocktail consisting of 90% TFA, 3.3% TIPS, 3.3% water, and 3.3% EDT. Following cleavage, the crude product was concentrated under reduced pressure to remove most TFA, water, TIPS, and EDT, and then washed 3× with Et_2O, dried under reduced pressure for 24 h to give **1** as a white powder (680 mg, 81.3% overall yield, 98.1% average coupling efficiency). LRMS− LC/MS (m/z): $[M - H]^-$ calcd for $C_{58}H_{87}N_{11}O_{34}S$, 1492.4; found, 1492.4 ($[M - H]^-$), 745.7 ($[M\text{-}2]^{2-}/2$).

Synthesis of 2-(4-(6-((5-((2-Chloro-6-methylphenyl)carbamoyl)thiazol-2-yl)amino)-2-methylpyrimidin-4-yl)piperazin-1-yl)ethyl 3-(2,5-dioxo-2,5-dihydro-1H-pyrrol-1-yl)propanoate (2). 3-Maleimidopropionic acid (200 mg, 1.18 mmol) and PyBOP (572 mg, 1.10 mmol) were dissolved in 5 mL of anhydrous DMF in a 50 mL round-bottom flask degassed with argon. The flask was cooled on ice, and diisopropylethylamine (1.03 mL, 5.9 mmol) was added and stirred for 5 min. Dasatinib (360 mg, 0.738 mmol) was dissolved in 2 mL of anhydrous DMF and then added dropwise to the mixture. Then the reaction mixture was warmed slowly to room temperature with stirring over the ensuing 4 h. Ethyl acetate (~50 mL) was added to the reaction flask, and the diluted mixture was washed two times with DI water followed by four washes with saturated aqueous NaCl. The organic phase was then collected, dried over sodium sulfate, and concentrated in vacuo to yield the crude product. The crude product was purified by flash column chromatography on Teledyne CombiFlash Rf+ Lumen (0−25% MeOH in DCM) to give **2** as a pale-yellow powder (320 mg, 68%). LRMS−LC/MS (m/z): $[M + H]^+$ calcd for $C_{34}H_{33}ClN_8O_5S$, 639.2; found, 639.1.

Synthesis of Dasatinib-Asp_{10} Conjugate (DAC) (3). **2** (300 mg, 0.47 mmol) was dissolved in 5.5 mL of anhydrous DMSO in a 25 mL round-bottom flask degassed with argon. Then 640 mg of Asp_{10}-Cys (**1**) (0.43 mmol) was added quickly to the aforementioned solution and stirred until all solid dissolved. The reaction mixture was stirred for 1 h under argon atmosphere before purification using preparatory reverse-phase HPLC. Pure fractions were collected, concentrated in vacuo to remove acetonitrile, frozen, and lyophilized to yield the final product DAC (**3**) as a white solid (228 mg, 32%). LRMS−LC/MS (m/z): $[M - H]^-$ calcd for $C_{87}H_{98}ClN_{19}O_{56}S_2$, 2131.5; found, 1064.8 ($[M - 2]^{2-}/2$), 709.5 ($[M\text{-}3]^{3-}/3$).

Culture of MC3T3-E1 Cells. A murine preosteoblast cell line (MC3T3-E1) was purchased from American Type Culture Collection (ATCC) and cultured in α-MEM without ascorbic acid (Gibco, Thermo Fisher Scientific, Waltham, MA), supplemented with 10% heat-inactivated fetal bovine serum (HI-FBS) (VWR, Chicago, IL) and 1% penicillin/streptomycin (Corning, Corning, NY) as monolayers at 37 °C in a 5% CO_2/95% humidified-air atmosphere. Next 24-well plates were seeded with 0.05 million cells per well, followed by a switch to mineralization media (α-MEM (Gibco, Thermo Fisher Scientific, Waltham, MA) supplemented with 10% HI-FBS, 1% penicillin/streptomycin, and 10 mM β-glycerophosphate) when cells reached confluence, which marked Day 0 of mineralization. Media in each well was switched every 3 days to fresh mineralization media containing the desired concentration of dasatinib (20 mM stock solution dissolved in DMSO). For this purpose, the stock solution was diluted with PBS, sterile-filtered and further diluted in mineralization media to yield media with various concentrations of dasatinib.

Real-Time Quantitative PCR. To determine the mRNA levels of diagnostic markers for osteoblast differentiation and activation, cultured cells (3 wells per dasatinib concentration) were analyzed by real-time quantitative PCR with SYBR Green dye (SensiFAST SYBR No-ROX Kit; Bioline, Taunton, MA). Briefly, total cell RNA from each study group was extracted and purified using a GenCatch Total RNA Extraction Kit (Epoch Life Science, Sugar Land, TX). Approximately 900 ng of RNA was reverse transcribed using High-Capacity cDNA Reverse Transcription Kit (Thermo Fisher Scientific, Waltham, MA) on a Bio-Rad T100 Thermal Cycler. cDNA samples were diluted 7.5× before real-time reactions were performed on a Bio-Rad CFX Connect Real Time System using 40 cycles at 95 °C for 5 s, 60 °C for 10 s, and 72 °C for 20 s. Primers for each target gene and the housekeeping gene (Runx2, Osx, Col1A1, ALP, OPN, OPG, RANKL, GAPDH) were purchased from Integrated DNA Technologies (Coralville, IA). Technical triplicates were performed for each of the three biological replicates in each treatment group to ensure reliability of results. The Cq values obtained were analyzed using the

DOI: 10.1021/acs.bioconjchem.8b00603
Bioconjugate Chem. 2018, 29, 3800−3809

ΔΔCq method and presented as the relative expression level between each target gene and the reference gene (GAPDH). All relative expression levels were normalized against the control (DMSO) value.

Quantitation of Alkaline Phosphatase Activity. Alkaline phosphatase (ALP) activity was quantified with SensoLyte ALP Kit (AnaSpec, Fremont, CA) following the instructions provided by the manufacturer. Briefly, cells in a 24-well plate were washed twice with ice-cold lysis buffer and then lysed in the same buffer supplemented with 0.5% Triton-X 100. Whole cell lysates were collected, centrifuged at 2500*g* for 10 min, then mixed with *p*-nitrophenol phosphate. The absorbance at 405 nM was measured every 5 min for 1 h at 37 °C. The ALP activity was calculated from the rate of absorbance change, using only data with a linear correlation coefficient of $R^2 > 0.99$. Protein content in each whole cell lysate was also determined using QuickStart Bradford Assay Kit (Bio-Rad, Hercules, CA) according to manufacturer's procedures.

Animal Husbandry and Femur Fracture Induction. All animal protocols were reviewed and approved by Purdue's Animal Care and Use Committee (PACUC). Female ND4 Swiss Webster mice (12-week) were purchased from Envigo (Indianapolis, IN) and maintained on a standard 12 h light-dark cycle (5 animals per cage). All mice were acclimated in the housing facility for 1 week before initiation of any studies.

Preparation of a stabilized femoral fracture with intramedullary pin fixation was performed following a modified method described previously.[25] ND4 Swiss Webster mice were anesthetized by isoflurane inhalation, after which the right hind knee was shaved and sanitized first with 10% (w/v) povidone-iodine solution (Fisher Scientific, Pittsburgh, PA) and then with 70% aqueous ethanol. A small incision through the skin was made with surgical scissors followed by the removal of the knee cap to reveal the distal femur. The femur was then stabilized by insertion of a 22-gauge stainless steel pin down the intramedullary cavity of the bone followed by creation of a controlled fracture near the middle of the femur using surgical scissors. Excess pin was removed with a wire cutter, and the wound was closed with sutures. Fracture induction and implant position were confirmed using an X-ray Multispectral Imaging System (IS4000; Kodak, Rochester, NY) after surgery. For pain relief, all mice were injected subcutaneously with 0.1 mg/kg buprenorphine solution at the time of the surgery, followed by two doses per day for 3 days postsurgery.

Drug Formulation and Injection. Vehicle solution (85% Millipore water, 10% ethanol, and 5% Kolliphor EL) for delivery of dasatinib or dasatinib-Asp_{10} conjugate (**3**, DAC) was prepared according to a modified procedure.[97] Dasatinib or DAC was dissolved in DMSO and then diluted with the vehicle solution to yield a final drug and DMSO concentration of 10 μM and 0.1%, respectively. Buprenorphine solution (0.03 mg/mL final) was prepared by dissolving buprenorphine HCl (Sigma-Aldrich, St. Louis, MO) in DMSO (0.1% final) and then diluting to 0.03 mg/mL with phosphate-buffered saline (PBS). All solutions were sterile-filtered before injection. In studies involving only saline or DAC groups, DAC was dissolved in PBS to reach a final concentration of 10 μM. All injections were performed subcutaneously.

All drug solutions were administered to mice subcutaneously above the neck. Initial injections of test articles were always administered immediately after surgery. Subsequent injections were given at frequencies of everyday (QD), every other day (QAD), every 4 days, every 7 days, or every 10 days, depending on the requirement of the study. The injection schedules are specified in each figure legend.

Microcomputed Tomography. Following the desired treatments with DAC, vehicle or PBS, mice were euthanized with CO_2 followed by cervical dislocation to ensure the mice were dead. Both fractured and contralateral femurs were removed, cleaned, wrapped in Kimwipes wetted with PBS, and stored at −20 °C. The diaphysis of broken femurs that contained the fracture calluses or the entire length of healthy femurs were scanned using high-resolution microcomputed tomography (μCT 40; Scanco Medical AG, Brüttisellen, Switzerland) after removal of the stabilization pins from the femurs. Images were acquired at a tube potential of 70 kVp, an X-ray intensity of 113 μA, and 300 ms integration time, with voxel sizes of $8 \times 8 \times 8$ μm^3. Slide images (2048×2048) were analyzed with ImageJ (version 1.51) containing BoneJ plugin (version 1.4.2).[26] One hundred continuous slices with the largest diameter were selected from each image to represent the center portion of the fracture callus. Manual contouring of the fracture callus region was performed on the first, last and middle slices, followed by automated interpolation for all remaining slices. Three-dimentional (3D) image reconstruction of those slices were used to calculate bone density (bone volume/total volume, or BV/TV), trabecular thickness (Tb.Th), and trabecular separation (Tb.Sp) according to Bouxsein, Dempster, and their colleagues.[27,28]

Four-Point Bending Test. Stabilization pins were removed from the femurs prior to mechanical analysis. Quantitation of the mechanical properties associated with bending and refracturing the repaired femurs was also performed using a four-point bending apparatus (ElectroForce TestBench; TA Instruments). The lower supports were set 10 mm apart on the anterior face of the femur in contact with the proximal and distal diaphysis. The upper supports were 4 mm apart and were placed such that they spanned the entire fracture callus on the diaphysis. Force was applied from the posterior face of the femur with a displacement rate of 0.3 mm/sec. Maximum load, stiffness, displacement to yield, and work to fracture data were then generated. Stiffness is defined as the slope of the linear region of the load−displacement curve. Displacement to yield is defined as the displacement to the fracture point after reaching the yield point. Work to fracture is defined as the total area under the load−displacement curve.[29]

Statistical Analyses. All statistical analyses were performed with GraphPad Prism (version 7.0; GraphPad Software, CA). Unpaired two-tailed *t*-tests were carried out with a 95% confidence interval to assess statistical significance. Data are displayed as mean ± standard error of mean (SEM). In the figures, levels of statistical significance are denoted with asterisks according to the following definition: $*p < 0.05$; $**p < 0.01$; $***p < 0.001$; $****p < 0.0001$.

■ ASSOCIATED CONTENT

Supporting Information

The Supporting Information is available free of charge on the ACS Publications website at DOI: 10.1021/acs.bioconjchem.8b00660.

μCT images of trabecular microstructure at the fracture callus site after mice were treated with DAC; stiffness, displacement to yield, and work to fracture data for femurs receiving DAC or PBS treatment (QAD) for 2−8 weeks; and maximum cortical bone thickness, bone volume, and bone density at fracture sites in PBS- and

DOI: 10.1021/acs.bioconjchem.8b00660
Bioconjugate Chem. 2018, 29, 3800−3809

DAC-treated mice after 8 weeks of DAC or PBS treatment (QAD) (PDF)

AUTHOR INFORMATION

Corresponding Author

*E-mail: plow@purdue.edu. Phone: 765-494-5283. Fax: 765-494-5272.

ORCID

Philip S. Low: 0000-0001-9042-5528

Notes

The authors declare no competing financial interest.

ACKNOWLEDGMENTS

This work was supported by funds from an endowed chair to Philip S. Low. Thanks to Pamela Lachcik and Purdue CTSI for providing access and assistance for the μCT. Thanks to Dr. Russel Main for providing access and assistance for the four-point bending device.

ABBREVIATIONS

RANKL: receptor activator of nuclear factor κ−B ligand; DAC: dasatinib-Asp_{10} conjugate; μCT: microcomputed tomography; QD: daily dosage; QAD: every-other-day dosage

REFERENCES

(1) Office of the Surgeon General (US) (2004) *Bone Health and Osteoporosis: A Report of the Surgeon General*, Office of the Surgeon General (US), Rockville (MD).

(2) Bartl, R., Frisch, B., and Bartl, C. (2009) *Osteoporosis: diagnosis, prevention, therapy*, 2nd revised ed., Springer, Berlin.

(3) Gu, Q., Koenig, L., Mather, R. C., and Tongue, J. (2014) Surgery for Hip Fracture Yields Societal Benefits That Exceed the Direct Medical Costs. *Clin. Orthop. Relat. Res. 472*, 3536−3546.

(4) Holm, A. G. V., Lurås, H., and Randsborg, P.-H. (2016) The economic burden of outpatient appointments following paediatric fractures. *Injury 47*, 1410−1413.

(5) Keene, G. S., Parker, M. J., and Pryor, G. A. (1993) Mortality and morbidity after hip fractures. *BMJ. 307*, 1248−1250.

(6) Adachi, J. D., Adami, S., Gehlbach, S., Anderson, F. A., Boonen, S., Chapurlat, R. D., Compston, J. E., Cooper, C., Delmas, P., Diez-Pérez, A., et al. (2010) Impact of prevalent fractures on quality of life: baseline results from the global longitudinal study of osteoporosis in women. *Mayo Clin. Proc. 85*, 806−813.

(7) Bentler, S. E., Liu, L., Obrizan, M., Cook, E. A., Wright, K. B., Geweke, J. F., Chrischilles, E. A., Pavlik, C. E., Wallace, R. B., Ohsfeldt, R. L., et al. (2009) The aftermath of hip fracture: discharge placement, functional status change, and mortality. *Am. J. Epidemiol. 170*, 1290−1299.

(8) Braithwaite, R. S., Col, N. F., and Wong, J. B. (2003) Estimating hip fracture morbidity, mortality and costs. *J. Am. Geriatr. Soc. 51*, 364−370.

(9) Pavone, V., Testa, G., Giardina, S. M. C., Vescio, A., Restivo, D. A., and Sessa, G. (2017) Pharmacological Therapy of Osteoporosis: A Systematic Current Review of Literature. *Front. Pharmacol. 8*, 803.

(10) Lee, D., Heo, D. N., Kim, H.-J., Ko, W.-K., Lee, S. J., Heo, M., Bang, J. B., Lee, J. B., Hwang, D.-S., Do, S. H., and Kwon, I. K. (2016) Inhibition of Osteoclast Differentiation and Bone Resorption by Bisphosphonate-conjugated Gold Nanoparticles. *Sci. Rep. 6*, 27336.

(11) Fitzpatrick, L. A. (2006) Estrogen therapy for postmenopausal osteoporosis. *Arq. Bras. Endocrinol. Metabol. 50*, 705−719.

(12) Deeks, E. D. (2018) Denosumab: A Review in Postmenopausal Osteoporosis. *Drugs Aging 35*, 163−173.

(13) Boyce, B. F., and Xing, L. (2008) Functions of RANKL/RANK/OPG in bone modeling and remodeling. *Arch. Biochem. Biophys. 473*, 139−146.

(14) Weske, S., Vaidya, M., Reese, A., von Wnuck Lipinski, K., Keul, P., Bayer, J. K., Fischer, J. W., Flögel, U., Nelsen, J., Epple, M., et al. (2018) Targeting sphingosine-1-phosphate lyase as an anabolic therapy for bone loss. *Nat. Med. 24*, 667−678.

(15) Krell, M. H. (2000) Parathyroid hormone temporal effects on bone formation and resorption. *Bull. Math. Biol. 62*, 163−188.

(16) Babu, S., Sandiford, N. A., and Vrahas, M. (2015) Use of Teriparatide to improve fracture healing: What is the evidence? *World J. Orthop. 6*, 457−461.

(17) Shi, Z., Zhou, H., Pan, B., Lu, L., Liu, J., Kang, Y., Yan, X., and Feng, S. (2016) Effectiveness of Teriparatide on Fracture Healing: A Systematic Review and Meta-Analysis. *PLoS One 11*, e0168691.

(18) Zhao, W., Byrne, M. H., Boyce, B. F., and Krane, S. M. (1999) Bone resorption induced by parathyroid hormone is strikingly diminished in collagenase-resistant mutant mice. *J. Clin. Invest. 103*, 517−524.

(19) Karatoprak, C., Kayatas, K., Kilicaslan, H., Yolbas, S., Yazimci, N. A., Gümüskemer, T., and Demirtunç, R. (2012) Severe hypercalcemia due to teriparatide. *Indian J. Pharmacol. 44*, 270−271.

(20) Neer, R. M., Arnaud, C. D., Zanchetta, J. R., Prince, R., Gaich, G. A., Reginster, J. Y., Hodsman, A. B., Eriksen, E. F., Ish-Shalom, S., Genant, H. K., et al. (2001) Effect of parathyroid hormone (1−34) on fractures and bone mineral density in postmenopausal women with osteoporosis. *N. Engl. J. Med. 344*, 1434−1441.

(21) Kamiya, N. (2012) The role of BMPs in bone anabolism and their potential targets SOST and DKK1. *Curr. Mol. Pharmacol. 5*, 153−163.

(22) Bishop, G. B., and Einhorn, T. A. (2007) Current and future clinical applications of bone morphogenetic proteins in orthopaedic trauma surgery. *Int. Orthop. 31*, 721−727.

(23) Meehan, A. D., Udumyan, R., Kardell, M., Landén, M., Järhult, J., and Wallin, G. (2018) Lithium-Associated Hypercalcemia: Pathophysiology, Prevalence, Management. *World J. Surg. 42*, 415−424.

(24) (2017) *Bio-Targets and Drug Delivery Approaches* (Maiti, S., and Sen, K. K., Eds.), Taylor & Francis, Boca Raton.

(25) Low, S. A., Galliford, C. V., Yang, J., Low, P. S., and Kopeček, J. (2015) Biodistribution of Fracture-Targeted GSK3β Inhibitor-Loaded Micelles for Improved Fracture Healing. *Biomacromolecules 16*, 3145−3153.

(26) Sekido, T., Sakura, N., Higashi, Y., Miya, K., Nitta, Y., Nomura, M., Sawanishi, H., Morito, K., Masamune, Y., Kasugai, S., et al. (2001) Novel drug delivery system to bone using acidic oligopeptide: pharmacokinetic characteristics and pharmacological potential. *J. Drug Target. 9*, 111−121.

(27) Kasugai, S., Fujisawa, R., Waki, Y., Miyamoto, K., and Ohya, K. (2000) Selective drug delivery system to bone: small peptide (Asp)6 conjugation. *J. Bone Miner. Res. 15*, 936−943.

(28) Low, S. A., Galliford, C. V., Jones-Hall, Y. L., Roy, J., Yang, J., Low, P. S., and Kopeček, J. (2017) Healing efficacy of fracture-targeted GSK3β inhibitor-loaded micelles for improved fracture repair. *Nanomedicine 12*, 185−193.

(29) Peruzzi, B., Rucci, N., and Teti, A. (2012) The Crucial Role of c-Src Tyrosine Kinase in Bone Metabolism. *Protein Kinases* (Da Silva Xavier, G., Ed.) pp 357−380, Chapter 16, InTech, London, U.K.

(30) Soriano, P., Montgomery, C., Geske, R., and Bradley, A. (1991) Targeted disruption of the c-src proto-oncogene leads to osteopetrosis in mice. *Cell 64*, 693−702.

(31) Boyce, B. F., Yoneda, T., Lowe, C., Soriano, P., and Mundy, G. R. (1992) Requirement of pp60c-src expression for osteoclasts to form ruffled borders and resorb bone in mice. *J. Clin. Invest. 90*, 1622−1627.

(32) Marzia, M., Sims, N. A., Voit, S., Migliaccio, S., Taranta, A., Bernardini, S., Faraggiana, T., Yoneda, T., Mundy, G. R., Boyce, B. F., et al. (2000) Decreased c-Src expression enhances osteoblast differentiation and bone formation. *J. Cell Biol. 151*, 311−320.

(33) García-Gomez, A., Ocio, E. M., Crusoe, E., Santamaría, C., Hernández-Campo, P., Blanco, J. F., Sanchez-Guijo, F. M., Hernández-Iglesias, T., Briñón, J. G., Pisac-Herrero, R. M., et al.

DOI: 10.1021/acs.bioconjchem.8b00603
Bioconjugate Chem. 2018, 29, 3800−3809

(2012) Dasatinib as a Bone-Modifying Agent: Anabolic and Anti-Resorptive Effects. *PLoS One 7*, e34914.
(34) Cappariello, A., Loftus, A., Muraca, M., Maurizi, A., Rucci, N., and Teti, A. (2018) Osteoblast-Derived Extracellular Vesicles Are Biological Tools for the Delivery of Active Molecules to Bone. *J. Bone Miner. Res. 33*, 517−533.
(35) Id Boufker, H., Lagneaux, L., Najar, M., Piccart, M., Ghanem, G., Body, J.-J., and Journé, F. The Src inhibitor dasatinib accelerates the differentiation of human bone marrow-derived mesenchymal stromal cells into osteoblasts. *BMC Cancer* (2010) *10*. DOI: 10.1186/1471-2407-10-298
(36) Lee, Y.-C., Huang, C.-F., Murshed, M., Chu, K., Araujo, J. C., Ye, X., deCrombrugghe, B., Yu-Lee, L.-Y., Gallick, G. E., and Lin, S.-H. (2010) Src family kinase/abl inhibitor dasatinib suppresses proliferation and enhances differentiation of osteoblasts. *Oncogene 29*, 3196−3207.
(37) Yokogawa, K., Miya, K., Sekido, T., Higashi, Y., Nomura, M., Fujisawa, R., Morito, K., Masamune, Y., Waki, Y., Kasugai, S., et al. (2001) Selective delivery of estradiol to bone by aspartic acid oligopeptide and its effects on ovariectomized mice. *Endocrinology 142*, 1228−1233.
(38) Ishizaki, J., Waki, Y., Takahashi-Nishioka, T., Yokogawa, K., and Miyamoto, K.-I. (2009) Selective drug delivery to bone using acidic oligopeptides. *J. Bone Miner. Metab. 27*, 1−8.
(39) Dubrovsky, L., Pankov, D., Brea, E. J., Dao, T., Scott, A., Yan, S., O'Reilly, R. J., Liu, C., and Scheinberg, D. A. (2014) A TCR-mimic antibody to WT1 bypasses tyrosine kinase inhibitor resistance in human BCR-ABL+ leukemias. *Blood 123*, 3296−3304.
(40) Zhang, Y., Desai, A., Yang, S. Y., Bae, K. B., Antczak, M. I., Fink, S. P., Tiwari, S., Willis, J. E., Williams, N. S., Dawson, D. M., et al. (2015) Inhibition of the prostaglandin-degrading enzyme 15-PGDH potentiates tissue regeneration. *Science 348*, aaa2340−aaa2340.
(41) Chew, C. K., and Clarke, B. L. (2017) Abaloparatide: Recombinant human PTHrP (1−34) anabolic therapy for osteoporosis. *Maturitas 97*, 53−60.
(42) Amso, Z., Cornish, J., and Brimble, M. A. (2016) Short Anabolic Peptides for Bone Growth: SHORT ANABOLIC PEPTIDES FOR BONE GROWTH. *Med. Res. Rev. 36*, 579−640.
(43) Kim, H.-Y., Choi, S., Yoon, J.-H., Lim, H. J., Lee, H., Choi, J., Ro, E. J., Heo, J.-N., Lee, W., No, K. T., et al. (2016) Small molecule inhibitors of the Dishevelled-CXXC5 interaction are new drug candidates for bone anabolic osteoporosis therapy. *EMBO Mol. Med. 8*, 375−387.
(44) Kulkarni, N. H., Onyia, J. E., Zeng, Q., Tian, X., Liu, M., Halladay, D. L., Frolik, C. A., Engler, T., Wei, T., Kriauciunas, A., et al. (2006) Orally Bioavailable GSK-3α/β Dual Inhibitor Increases Markers of Cellular Differentiation In Vitro and Bone Mass In Vivo. *J. Bone Miner. Res. 21*, 910−920.
(45) Mediero, A., Wilder, T., Perez-Aso, M., and Cronstein, B. N. (2015) Direct or indirect stimulation of adenosine A2A receptors enhances bone regeneration as well as bone morphogenetic protein-2. *FASEB J. 29*, 1577−1590.
(46) Vandyke, K., Dewar, A. L., Diamond, P., Fitter, S., Schultz, C. G., Sims, N. A., and Zannettino, A. C. (2010) The tyrosine kinase inhibitor dasatinib dysregulates bone remodeling through inhibition of osteoclasts in vivo. *J. Bone Miner. Res. 25*, 1759−1770.
(47) Nair, A., and Jacob, S. (2016) A simple practice guide for dose conversion between animals and human. *J. Basic Clin. Pharm. 7*, 27.
(48) Kamath, A. V., Wang, J., Lee, F. Y., and Marathe, P. H. (2008) Preclinical pharmacokinetics and in vitro metabolism of dasatinib (BMS-354825): a potent oral multi-targeted kinase inhibitor against SRC and BCR-ABL. *Cancer Chemother. Pharmacol. 61*, 365−376.
(49) Bortolotto, A., Caldarelli, L., Bencivenga, D., Stampone, E., Perrotta, S., Oliva, A., and Della Ragione, F. (2017) Tyrosine kinase inhibitors and mesenchymal stromal cells: effects on self-renewal, commitment and functions. *Oncotarget 8*, 5540−5565.
(50) Aleman, J. O., Farooki, A., and Girotra, M. (2014) Effects of tyrosine kinase inhibition on bone metabolism: untargeted consequences of targeted therapies. *Endocr.-Relat. Cancer 21*, R247−R259.
(51) Brownlow, N., Mol, C., Hayford, C., Ghaem-Maghami, S., and Dibb, N. J. (2009) Dasatinib is a potent inhibitor of tumour-associated macrophages, osteoclasts and the FMS receptor. *Leukemia 23*, 590−594.
(52) Jönsson, S., Hjorth-Hansen, H., Olsson, B., Wadenvik, H., Sundan, A., and Standal, T. (2010) Second-generation TKI dasatinib inhibits proliferation of mesenchymal stem cells and osteoblast differentiation in vitro. *Leukemia 24*, 1357−1359.
(53) Li, J., and Stocum, D. L. (2014) Fracture Healing. *Basic and Applied Bone Biology*, Elsevier, Amsterdam, pp 205−223.
(54) Dittmer, D. K., and Teasell, R. (1993) Complications of immobilization and bed rest. Part 1: Musculoskeletal and cardiovascular complications. *Can. Fam. Physician Med. Fam. Can. 39*, 1428−1432 1435−1437. .
(55) Arangio, G. A., Lehr, S., and Reed, J. F. (1997) Reemployment of patients with surgical salvage of open, high-energy tibial fractures: an outcome study. *J. Trauma 42*, 942−945.
(56) Doube, M., Kłosowski, M. M., Arganda-Carreras, I., Cordelières, F. P., Dougherty, R. P., Jackson, J. S., Schmid, B., Hutchinson, J. R., and Shefelbine, S. J. (2010) BoneJ: Free and extensible bone image analysis in ImageJ. *Bone 47*, 1076−1079.
(57) Bouxsein, M. L., Boyd, S. K., Christiansen, B. A., Guldberg, R. E., Jepsen, K. J., and Müller, R. (2010) Guidelines for assessment of bone microstructure in rodents using micro-computed tomography. *J. Bone Miner. Res. 25*, 1468−1486.
(58) Dempster, D. W., Compston, J. E., Drezner, M. K., Glorieux, F. H., Kanis, J. A., Malluche, H., Meunier, P. J., Ott, S. M., Recker, R. R., and Parfitt, A. M. (2013) Standardized nomenclature, symbols, and units for bone histomorphometry: A 2012 update of the report of the ASBMR Histomorphometry Nomenclature Committee. *J. Bone Miner. Res. 28*, 2−17.
(59) Jepsen, K. J., Silva, M. J., Vashishth, D., Guo, X. E., and van der Meulen, M. C. H. (2015) Establishing biomechanical mechanisms in mouse models: practical guidelines for systematically evaluating phenotypic changes in the diaphyses of long bones. *J. Bone Miner. Res. 30*, 951−966.

DOI: 10.1021/acs.bioconjchem.8b00603
Bioconjugate Chem. 2018, 29, 3800−3809